(19) DANMARK

(10) **DK/EP 4249456 T3**

(12) Oversættelse af europæisk patentskrift

Patent- og Varemærkestyrelsen

(51) Int.Cl.: ***A 61 P 35/00 (2006.01)*** ***A 61 K 51/04 (2006.01)*** ***A 61 K 51/10 (2006.01)*** ***C 07 B 59/00 (2006.01)***

(45) Oversættelsen bekendtgjort den: **2024-12-02**

(80) Dato for Den Europæiske Patentmyndigheds bekendtgørelse om meddelelse af patentet: **2024-09-04**

(86) Europæisk ansøgning nr.: **23167668.5**

(86) Europæisk indleveringsdag: **2020-01-30**

(87) Den europæiske ansøgnings publiceringsdag: **2023-09-27**

(30) Prioritet: **2019-01-30 EP 19154500**

(62) Stamansøgningsnr: **20702636.0**

(84) Designerede stater: **AL AT BE BG CH CY CZ DE DK EE ES FI FR GB GR HR HU IE IS IT LI LT LU LV MC MK MT NL NO PL PT RO RS SE SI SK SM TR**

(73) Patenthaver: **Technische Universität München, Arcistr. 21, 80333 München, Tyskland**
Technische Universität München - Klinikum Rechts der Isar, Ismaningerstrasse 22, 81675 München, Tyskland

(72) Opfinder: **WURZER, Alexander Josef, , 81673 München, Tyskland**
WESTER, Hans-Jürgen, , 85304 Dinkelweg, Tyskland
EIBER, Matthias Johannes, , 85591 Vaterstetten, Tyskland

(74) Fuldmægtig i Danmark: **RWS Group, Europa House, Chiltern Park, Chiltern Hill, Chalfont St Peter, Bucks SL9 9FG, Storbritannien**

(54) Benævnelse: **PSMA-BINDENDE DOBBELTFUNGERENDE RADIOAKTIVT SPORSTOF OG TERAPEUTIKUM**

(56) Fremdragne publikationer:
S. LITAU ET AL: "Next Generation of SiFA lin -Based TATE Derivatives for PET Imaging of SSTR-Positive Tumors: Influence of Molecular Design on In Vitro SSTR Binding and In Vivo Pharmacokinetics", BIOCONJUGATE CHEMISTRY, vol. 26, no. 12, 16 December 2015 (2015-12-16), US, pages 2350 - 2359, XP055452403, ISSN: 1043-1802, DOI: 10.1021/acs.bioconjchem.5b00510

DESCRIPTION

Description

[0001] The present invention relates to the compound:

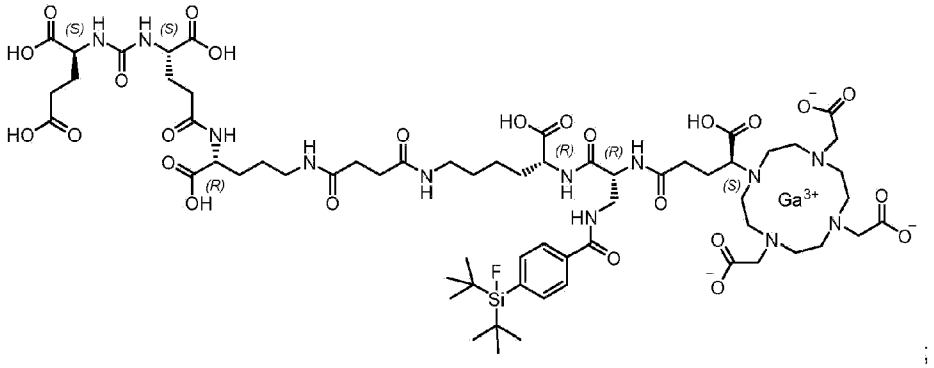

;

or a pharmaceutically acceptable salt thereof, wherein F is either ^{18}F or ^{19}F.

Prostate cancer

[0002] Prostate Cancer (PCa) remained over the last decades the most common malignant disease in men with high incidence for poor survival rates. Due to its overexpression in prostate cancer, prostate-specific membrane antigen (PSMA) or glutamate carboxypeptidase II (GCP II) proved its eligibility as excellent target for the development of highly sensitive radiolabelled agents for endoradiotherapy and imaging of PCa. Prostate-specific membrane antigen is an extracellular hydrolase whose catalytic center comprises two zinc(II) ions with a bridging hydroxido ligand. It is highly upregulated in metastatic and hormone-refractory prostate carcinomas, but its physiologic expression has also been reported in kidneys, salivary glands, small intestine, brain and, to a low extent, also in healthy prostate tissue. In the intestine, PSMA facilitates absorption of folate by conversion of pteroylpoly-γ-glutamate to pteroylglutamate (folate). In the brain, it hydrolyses N-acetyl-Laspartyl-L-glutamate (NAAG) to N-acetyl-L-aspartate and glutamate.

Prostate-specific membrane antigen (PSMA)

[0003] Prostate-specific membrane antigen (PSMA) is a type II transmembrane glycoprotein that is highly overexpressed on prostate cancer epithelial cells. Despite its name, PSMA is also expressed, to varying degrees, in the neovasculature of a wide variety of nonprostate cancers. Among the most common nonprostate cancers to demonstrate PSMA expression include breast, lung, colorectal, and renal cell carcinoma.

[0004] The general necessary structures of PSMA targeting molecules comprise a binding unit that encompasses a zinc-binding group (such as urea, phosphinate or phosphoramidate) connected to a P1' glutamate moiety, which warrants high affinity and specificity to PSMA and is typically further connected to an effector functionality. The effector part is more flexible and to some extent tolerant towards structural modifications. The entrance tunnel accommodates two other prominent structural features, which are important for ligand binding. The first one is an arginine patch, a positively charged area at the wall of the entrance funnel and the mechanistic explanation for the preference of negatively charged functionalities at the P1 position of PSMA. This appears to be the reason for the preferable incorporation of negative charged residues within the ligand-scaffold. An in-depth analysis about the effect of positive charges on PSMA ligands has been, to our knowledge, so far not conducted. Upon binding, the concerted repositioning of the arginine side chains can lead to the opening of an S1 hydrophobic accessory pocket, the second important structure that has been shown to accommodate an iodo-benzyl group of several urea based inhibitors, thus contributing to their high affinity for PSMA.

[0005] Zhang et al. discovered a remote binding site of PSMA, which can be employed for bidentate binding mode (Zhang et al., Journal of the American Chemical Society 132, 12711-12716 (2010)). The so called arene-binding site is a simple structural motif shaped by the side chains of Arg463, Arg511 and Trp541, and is part of the GCPII entrance lid. The engagement of the arene binding site by a distal inhibitor moiety can result in a substantial increase in the inhibitor affinity for PSMA due to avidity effects. PSMA I&T was developed with the intention to interact this way with PSMA, albeit no crystal structure analysis of binding mode is available. A necessary feature according to Zhang et al. is a linker unit (Suberic acid in the case of PSMA I&T) which facilitates an open conformation of the entrance lid of GCPII and thereby enabling the accessibility of the arene-binding site. It was further shown that the structural composition of the linker has a significant impact on the tumor-targeting and biologic activity as well as on imaging contrast and pharmacokinetics (Liu et al., Bioorganic & medicinal chemistry letters 21, 7013-7016 (2011)), properties which are crucial for both high imaging quality and efficient targeted endoradiotherapy.

[0006] Two categories of PSMA targeting inhibitors are currently used in clinical settings. On the one side there are tracers with chelating units for radionuclide complexation such as PSMA I&T or related compounds. On the other side there are small molecules, comprising a targeting unit and effector molecules.

[0007] The most often used agents for selective PSMA imaging are PSMA HBED-CC, PSMA-617 and PSMA I&T, which are predominantly labelled with ^{68}Ga (88.9% β^+, $E_{\beta+,\,max}$ = 1.89 MeV, $t_{½}$ = 68 min). Among these ^{68}Ga-PSMA-HBED-CC (also known as ^{68}Ga-PSMA-11), is so far considered as the golden standard for PET imaging of PCa.

^{18}F labelling

[0008] Recently, several groups have focused on the development of novel ^{18}F-labelled urea-based inhibitors for PCa diagnosis. In contrast to the radiometal ^{68}Ga, which can be obtained from commercially distributed ^{68}Ge/^{68}Ga radionuclide generators (^{68}Ge; $t_{½}$ = 270.8 d), the radioisotope ^{18}F-fluoride (96.7% β^+, $E_{\beta+,\,max}$ = 634 keV) requires an on-site cyclotron for its production. Despite this limitation, ^{18}F offers due to its longer half-live ($t_{½}$ = 109.8 min) and its lower positron energy, significant advantages in terms of routine-handling and image quality. Additionally, there is the possibility for largescale production in a cyclotron, which would be beneficial for a higher patient throughput and reduction of production costs.The ^{18}F-labelled urea-based PSMA inhibitor ^{18}F-DCFPyl demonstrated promising results in the detection of primary and metastatic PCa (Rowe et al., Molecular Imaging and Biology, 1-9 (2016)) and superiority to ^{68}Ga-PSMA-HBED-CC in a comparative study (Dietlein et al., Molecular Imaging and Biology 17, 575-584 (2015)). Based on the structure of PSMA-617, the ^{18}F-labelled analogue PSMA-1007 was recently developed, which showed comparable tumor-to-organ ratios (Cardinale et al., Journal of nuclear medicine: official publication, Society of Nuclear Medicine 58, 425-431 (2017); Giesel et al., European journal of nuclear medicine and molecular imaging 43, 1929-1930 (2016)). A comparative study with ^{68}Ga-PSMA-HBED-CC revealed similar diagnostic accuracy of both tracers and a reduced urinary clearance of ^{18}F-PSMA-1007, enabling a better assessment of the prostate (Giesel et al., European journal of nuclear medicine and molecular imaging 44, 678-688 (2017)).

[0009] An attractive approach for introducing ^{18}F labels is the use of silicon fluoride acceptors (SIFA). Silicon fluoride acceptors are described, for example, in Lindner et al., Bioconjugate Chemistry 25, 738-749 (2014). In order to preserve the silicon-fluoride bond, the use of silicon fluoride acceptors introduces the necessity of sterically demanding groups around the silicone atom. This in turn renders silicon fluoride acceptors highly hydrophobic. In terms of binding to the target molecule, in particular to the target molecule which is PSMA, the hydrophobic moiety provided by the silicone fluoride acceptor may be exploited for the purpose of establishing interactions of the radio-diagnostic or -therapeutic compound with the hydrophobic pocket described in Zhang et al., Journal of the American Chemical Society 132, 12711-12716 (2010). Yet, prior to binding, the higher degree of lipophilicity introduced into the molecule poses a severe problem with respect to the development of radiopharmaceuticals with suitable in vivo biodistribution, i.e. low unspecific binding in non-target tissue.

Failure to solve the hydrophobicity problem

[0010] Despite many attempts, the hydrophobicity problem caused by silicon fluoride acceptors has not been satisfactorily solved in the prior art.

[0011] To explain further, Schirrmacher E. et al. (Bioconjugate Chem. 2007, 18, 2085-2089) synthesized different ^{18}F-labelled peptides using the highly effective labelling synthon p-(di-tert-butylfluorosilyl) benzaldehyde ([^{18}F]SIFA-A), which is one example of a silicon fluoride acceptor. The SIFA technique resulted in an unexpectedly efficient isotopic ^{19}F-^{18}F exchange and yielded the ^{18}F-synthon in almost quantitative yields in high specific activities between 225 and 680 GBq/pmol (6081-18 378 Ci/mmol) without applying HPLC purification. [^{18}F]SIFA-benzaldehyde was finally used to label the N-terminal amino-oxy (N-AO) derivatized peptides AO-Tyr3 -octreotate (AO-TATE), cyclo(fK(AO-N)RGD) and N-AO-PEG_2-[D-Tyr-Gln-Trp-Ala-Val-Ala-His-Thi-Nle-NH_2] (AO-BZH3, a bombesin derivative) in high radiochemical yields. Nevertheless, the labelled peptides are highly lipophilic (as can be taken from the HPLC retention times using the conditions described in this paper) and thus are unsuitable for further evaluation in animal models or humans.

[0012] In Wängler C. et al. (Bioconjugate Chem., 2009, 20 (2), pp 317-321), the first SIFA-based Kit-like radio-fluorination of a protein (rat serum albumin, RSA) has been described. As a labelling agent, 4-(di-tert-butyl[^{18}F]fluorosilyl)benzenethiol (Si[^{18}F]FA-SH) was produced by simple isotopic exchange in 40-60% radiochemical yield (RCY) and coupled the product directly to maleimide derivatized serum albumin in an overall RCY of 12% within 20-30 min. The technically simple labelling procedure does not require any elaborated purification procedures and is a straightforward example of a successful application of Si-18F chemistry for in vivo imaging with PET. The time-activity cureves and µPET images of mice showed that most of the activity was localized in the liver, thus demonstrating that the labelling agent is too lipophilic and directs the in vivo probe to hepatobiliary excretion and extensive hepatic metabolism.

[0013] Wängler C. et al. (see Bioconjug Chem. 2010 Dec 15;21(12):2289-96) subsequently tried to overcome the major drawback of the SIFA technology, the high lipophilicity of the resulting radiopharmaceuticals, by synthesizing and evaluating new SIFA-octreotate analogues (SIFA-Tyr3-octreotate, SIFA-Asn(AcNH-β-Glc)-Tyr3-octreotate and SIFA-Asn(AcNH-β-Glc)-PEG-Tyr3-octreotate). In these compounds, hydrophilic linkers and pharmacokinetic modifiers were introduced between the peptide and the SIFA-moiety, i.e. a carbohydrate and a PEG linker plus a carbohydrate. As a measure of lipophilicity of the conjugates, the log P(ow) was determined and found to be 0.96 for SIFA-Asn(AcNH-β-Glc)-PEG-Tyr^3-octreotate and 1.23 for SIFA-Asn(AcNH-p-Glc)-Tyr^3-octreotate. These results show that the high lipophilicity of the SIFA moiety can only be marginally compensated by applying hydrophilic moieties. A first imaging study demonstrated excessive hepatic clearance /liver uptake and thus has never been transferred into a first human study.

[0014] Bernard-Gauthier et al. (Biomed Res Int. 2014;2014:454503) reviews a great plethora of different SIFA species that have been reported in the literature ranging from small prosthetic groups and other compounds of low molecular weight to labelled peptides and most recently affibody molecules. Based on these data the problem of lipophilicity of SIFA-based prosthetric

groups has not been solved sofar; i.e. a methodology that reduces the overall lipophilicity of a SIFA conjugated peptide to a log D lower than approx -2,0 has not been described.

[0015] In Lindner S. et al. (Bioconjug Chem. 2014 Apr 16;25(4):738-49) it is described that PEGylated bombesin (PESIN) derivatives as specific GRP receptor ligands and RGD (one-letter codes for arginine-glycine-aspartic acid) peptides as specific αvβ3 binders were synthesized and tagged with a silicon-fluorine-acceptor (SIFA) moiety. To compensate the high lipophilicity of the SIFA moiety various hydrophilic structure modifications were introduced leading to reduced logD values. SIFA-Asn(AcNH-β-Glc)-PESIN, SIFA-Ser(β-Lac)-PESIN, SIFA-Cya-PESIN, SIFA-LysMe3-PESIN, SIFA-γ-carboxy-d-Glu-PESIN, SIFA-Cya2-PESIN, SIFA-LysMe3-γ-carboxy-d-Glu-PESIN, SIFA-(γ-carboxy-d-Glu)2-PESIN, SIFA-RGD, SIFA-γ-carboxy-d-Glu-RGD, SIFA-(γ-carboxy-d-Glu)2-RGD, SIFA-LysMe3-γ-carboxy-d-Glu-RGD. All of these peptides - already improved and derivatized with the aim to reduce the lipophilicity - showed a logD value in the range between +2 and -1.22.

[0016] In Niedermoser S. et al. (J Nucl Med. 2015 Jul;56(7):1100-5), newly developed ^{18}F-SIFA- and ^{18}F-SIFAlin- (SIFA = silicon-fluoride acceptor) modified TATE derivatives were compared with the current clinical gold standard ^{68}Ga-DOTATATE for high-quality imaging of somatostatin receptor-bearing tumors. For this purpose, ^{18}F-SIFA-TATE and two quite complex analogues, ^{18}F-SIFA-Glc-PEG1-TATE, ^{18}F-SIFAlin-Glc-Asp2-PEG1-TATE were developed. None of the agents showed a logD <-1.5. S. Litau et al. (Bioconjugate Chem. 2015, 26, 2350-2359) discloses SIFAlin-based TATE derivatives for PET imaging of SSTR-positive tumors.

[0017] In view of the above, the technical problem underlying the present invention can be seen in providing radio-diagnostics and radio-therapeutics which contain a silicone fluoride acceptor and which are, at the same time, characterized by favourable in-vivo properties.

[0018] As will be become apparent in the following, a proof-of-principle has been established using specific conjugates which bind with high affinity to prostate-specific antigen (PSMA) as target. Accordingly, a further technical problem underlying the present invention can be seen in providing improved radio-therapeutics and -diagnostics for the medical indication which is cancer, preferably prostate cancer.

[0019] WO2019/020831 discloses a genus of PSMA binding compounds. Disclosed herein is an advantageous subset of the compounds from the earlier application. The application herein is a selection of advantageous features not appreciated by the inventors at the time of filing WO2019/020831.

[0020] These technical problems are solved by the subject-matter of the claims. The invention is set out in the appended claims. All described embodiments which fall outside the scope of the appended claims do not represent the invention.

[0021] The present invention relates to the compound:

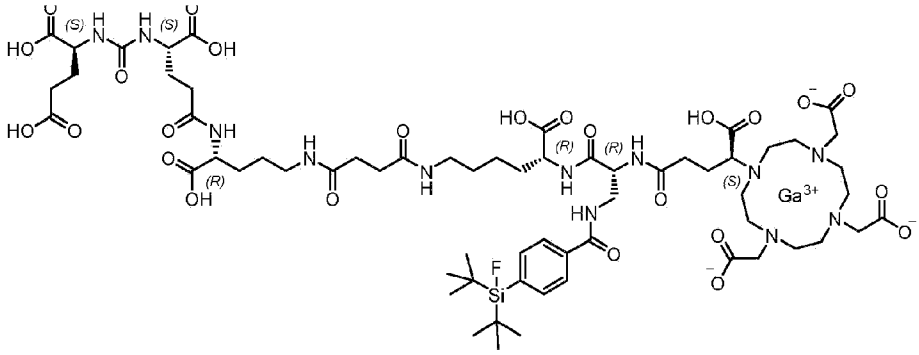

;

or a pharmaceutically acceptable salt thereof, wherein F is either ^{18}F or ^{19}F.

[0022] The present disclosure also provides a compound according to formula (V):

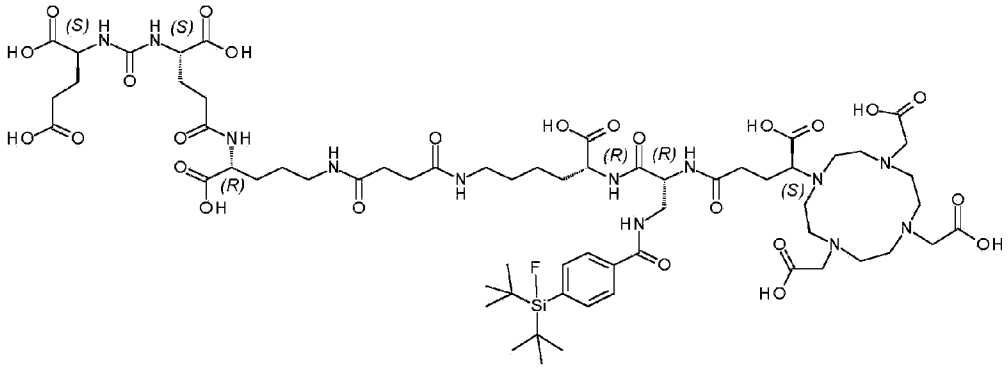

(V)

or a pharmaceutically acceptable salt thereof, containing either a chelated radioactive cation or wherein F is optionally ^{18}F.

[0023] Compounds disclosed can be in the form of salts. The present disclosure also relates to compounds of formula (Va):

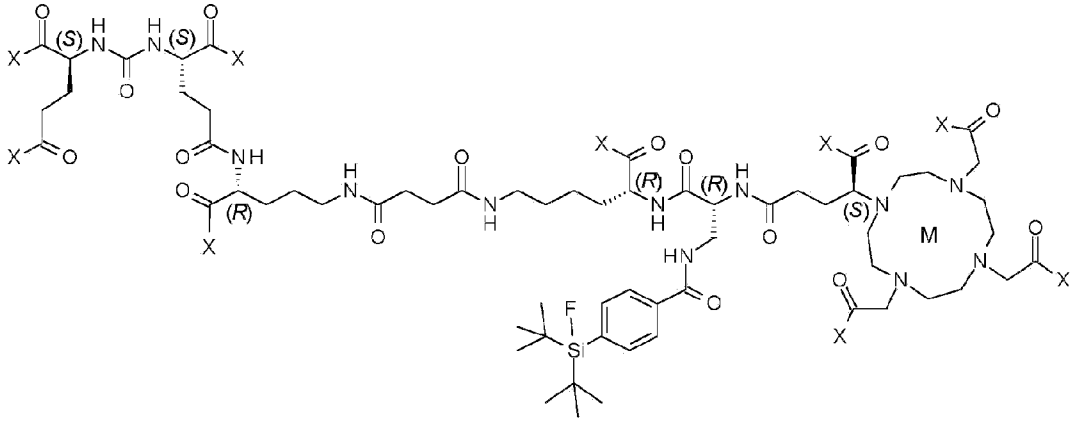

(Va)

or a pharmaceutically acceptable salt thereof, wherein;

each X is independently OH or O^-;

M is either a chelated radioactive cation or is absent;

and F is optionally ^{18}F.

[0024] In addition, the combination of the use of a chelator and an isotopic exchange on SIFA by means of ^{18}F-fluoride also results in "paired" diagnostic tracers that can either be used as [^{18}F][^{nat}Ion]tracers at centers with onsite cyclotron or centers that obtain ^{18}F-fluoride by shipment from cyclotron centers, whereas in centers, that do not have access to ^{18}F-fluoride but have access to radioisotope generators, such as a Ge-68/Ga-68 generator, the corresponding versions, e.g. [^{nat}F][^{68}Ga]tracers can be used.

[0025] Importantly, in both cases, the chemically identical radiopharmaceutical is injected, and thus no differences in the *in vivo* behavior are expected. Whereas currently, due to chemical differences, the clinical data of a ^{18}F-labelled compound provided by a patient cohort at one site cannot be directly compared with the clinical data of a ^{68}Ga-analogue provided by another group at another site, radiopharmaceuticals and/or diagnostics according to the disclosure can be directly compared and thus will allow to link such data (e.g. data from a center in Europe working with F-18 and another center in India working with Ga-68).

[0026] Furthermore, when suitably selected, the chelate can also be used for labelling with a therapeutic isotope, such as the beta-emitting isotopes Lu-177, Y-90, or the alpha emitting isotope Ac-225, thus allowing to expand the concept of "paired" tracers to bridge diagnostic ([^{18}F][^{nat}Lu]tracers) and therapeutic radiopharmaceuticals ([^{nat}F][^{177}Lu],

[0027] A further advantage of the compounds, especially of PSMA targeted compounds of the present disclosure is their surprisingly low accumulation in the kidneys of mice when compared to other PSMA targeted radiopharmaceuticals, such as PSMA I&T. Without wishing to be bound by a particular theory, it seems to be the combination of the structural element SIFA with a chelator which provides for the unexpected reduction of accumulation in the kidneys.

[0028] In terms of lipophilicity/hydrophilicity, the logP value (sometimes also referred to as logD value) is an art-established measure.

[0029] The term "lipophilicity" relates to the strength of being dissolved in, or be absorbed in lipid solutions, or being adsorbed at a lipid-like surface or matrix. It denotes a preference for lipids (literal meaning) or for organic or apolar liquids or for liquids, solutions or surfaces with a small dipole moment as compared to water. The term "hydrophobicity" is used with equivalent meaning herein. The adjectives lipophilic and hydrophobic are used with corresponding meaning to the substantives described above.

[0030] The mass flux of a molecule at the interface of two immiscible or substantially immiscible solvents is governed by its lipophilicity. The more lipophilic a molecule is, the more soluble it is in the lipophilic organic phase. The partition coefficient of a molecule that is

observed between water and n-octanol has been adopted as the standard measure of lipophilicity. The partition coefficient P of a species A is defined as the ratio $P = [A]_{n\text{-}octanol} / [A]_{water}$. A figure commonly reported is the logP value, which is the logarithm of the partition coefficient. In case a molecule is ionizable, a plurality of distinct microspecies (ionized and not ionized forms of the molecule) will in principle be present in both phases. The quantity describing the overall lipophilicity of an ionizable species is the distribution coefficient D, defined as the ratio D = [sum of the concentrations of all microspecies]$_{n\text{-}octanol}$ / [sum of the concentrations of all microspecies] $_{water}$. Analogous to logP, frequently the logarithm of the distribution coefficient, logD, is reported. Often, a buffer system, such as phosphate buffered saline is used as alternative to water in the above described determination of logP.

[0031] If the lipophilic character of a substituent on a first molecule is to be assessed and/or to be determined quantitatively, one may assess a second molecule corresponding to that substituent, wherein said second molecule is obtained, for example, by breaking the bond connecting said substituent to the remainder of the first molecule and connecting (the) free valence(s) obtained thereby to hydrogen(s).

[0032] Alternatively, the contribution of the substituent to the logP of a molecule may be determined. The contribution π_{Xx} of a substituent X to the logP of a molecule R-X is defined as $\pi_{Xx} = logP_{R\text{-}X} - logP_{R\text{-}H}$, wherein R-H is the unsubstituted parent compound.

[0033] Values of P and D greater than one as well as logP, logD and π_{Xx} values greater than zero indicate lipophilic/hydrophobic character, whereas values of P and D smaller than one as well as logP, logD and $\pi_{X\ x}$ values smaller than zero indicate hydrophilic character of the respective molecules or substituents.

[0034] The above described parameters characterizing the lipophilicity of the lipophilic group or the entire molecule according to the disclosure can be determined by experimental means and/or predicted by computational methods known in the art (see for example Sangster, Octanol-water Partition Coefficients: fundamentals and physical chemistry, John Wiley & Sons, Chichester. (1997)).

[0035] In a preferred embodiment, the logP value of the compounds of the disclosure is between -5 and -1.5. It is particularly preferred that the logP value is between -3.5 and -2.0.

[0036] In a preferred embodiment the chelating group comprises a chelated cation which is radioactive. More preferred is a chelated radioactive metal isotope.

[0037] Preferred examples of cations that may be chelated by the chelating group are the cations of ^{43}SC, ^{44}Sc, ^{47}Sc, ^{51}Cr, ^{52m}Mn, ^{58}Co, ^{52}Fe, ^{56}Ni, ^{57}Ni, ^{62}Cu, ^{64}Cu, ^{67}Cu, ^{66}Ga, ^{67}Ga ^{68}Ga, ^{89}Zr, ^{90}Y, ^{89}Y, <Tc, ^{99m}Tc, ^{97}Ru, ^{105}Rh, ^{109}Pd, ^{111}Ag,^{110m}In, ^{111}In ^{113m}In, ^{114m}In, ^{117m}Sn, ^{121}Sn, ^{127}Te, ^{142}Pr, ^{143}Pr, ^{149}Pm, ^{151}Pm, ^{149}Tb, ^{152}Tb, ^{155}Tb, ^{161}Tb, ^{153}Sm, ^{157}Gd, ^{161}Tb,

^{166}Ho, ^{165}Dy, ^{169}Er, ^{169}Yb, ^{175}Yb, ^{172}Tm, ^{177}Lu, ^{186}Re, ^{188}Re, ^{191}Pt, ^{197}Hg, ^{198}Au, ^{199}Au, ^{212}Pb, ^{203}Pb, ^{211}At, ^{212}Bi, ^{213}Bi, ^{223}Ra, ^{225}Ac, ^{227}Th, a cationic molecule comprising ^{18}F or a cation such as ^{18}F-$[AlF]^{2+}$; more preferably the cations of ^{44}Sc, ^{47}Sc, ^{64}Cu, ^{67}Cu, ^{68}Ga, ^{90}Y, ^{111}In, ^{161}Tb, ^{166}Ho, ^{177}Lu, ^{188}Re, ^{212}Pb, ^{212}Bi, ^{213}Bi, ^{225}Ac, and ^{227}Th or a cationic molecule comprising ^{18}F. Cations may be selected from Lu-177, Y-90, or Ac-225.

[0038] In a further aspect, provided is a pharmaceutical composition comprising or consisting of one or more compounds as disclosed herein above.

[0039] In a further aspect, provided is a diagnostic composition comprising or consisting of one or more compounds as disclosed herein above.

[0040] In a further aspect, provided is a therapeutic composition comprising or consisting of one or more compounds as disclosed herein above.

[0041] The pharmaceutical composition may further comprise pharmaceutically acceptable carriers, excipients and/or diluents. Examples of suitable pharmaceutical carriers, excipients and/or diluents are well known in the art and include phosphate buffered saline solutions, water, emulsions, such as oil/water emulsions, various types of wetting agents, sterile solutions etc. Compositions comprising such carriers can be formulated by well known conventional methods. These pharmaceutical compositions can be administered to the subject at a suitable dose. Administration of the suitable compositions may be effected by different ways, e.g., by intravenous, intraperitoneal, subcutaneous, intramuscular, topical, intradermal, intranasal or intrabronchial administration. It is particularly preferred that said administration is carried out by injection and/or delivery, e.g., to a site in the pancreas or into a brain artery or directly into brain tissue. The compositions may also be administered directly to the target site, e.g., by biolistic delivery to an external or internal target site, like the pancreas or brain. The dosage regimen will be determined by the attending physician and clinical factors. As is well known in the medical arts, dosages for any one patient depends upon many factors, including the patient's size, body surface area, age, the particular compound to be administered, sex, time and route of administration, general health, and other drugs being administered concurrently. Pharmaceutically active matter may be present in amounts between 0,1 ng and 10 mg/kg body weight per dose; however, doses below or above this exemplary range are envisioned, especially considering the aforementioned factors.

[0042] In a further aspect, provided is one or more compounds as disclosed herein above for use in medicine.

[0043] Preferred uses in medicine are in nuclear medicine such as nuclear diagnostic imaging, also named nuclear molecular imaging, and/or targeted radiotherapy of diseases associated with an overexpression, preferably of PSMA on the diseased tissue.

[0044] In a further aspect, provided is a compound as defined herein above for use in a

method of diagnosing and/or staging cancer, preferably prostate cancer. Prostate cancer is not the only cancer to express PSMA. Nonprostate cancers known to demonstrate PSMA expression include breast, lung, colorectal, and renal cell carcinoma. Thus any compound described herein having a PSMA binding moiety can be used in the diagnosis, imaging or treatment of a cancer having PSMA expression.

[0045] Preferred indications are the detection or staging of cancer, such as, but not limited high grade gliomas, lung cancer and especially prostate cancer and metastasized prostate cancer, the detection of metastatic disease in patients with primary prostate cancer of intermediate-risk to high-risk, and the detection of metastatic sites, even at low serum PSA values in patients with biochemically recurrent prostate cancer. Another preferred indication is the imaging and visualization of neoangiogensis.

[0046] In terms of medical indications to be subjected to therapy, especially radiotherapy, cancer is a preferred indication. Prostate cancer is a particularly preferred indication.

[0047] In a further aspect, provided is a compound as defined herein above for use in a method of diagnosing and/or staging cancer, preferably prostate cancer.

[0048] The present disclosure furthermore relates to the following items.

[0049] The compound according to formula (V):

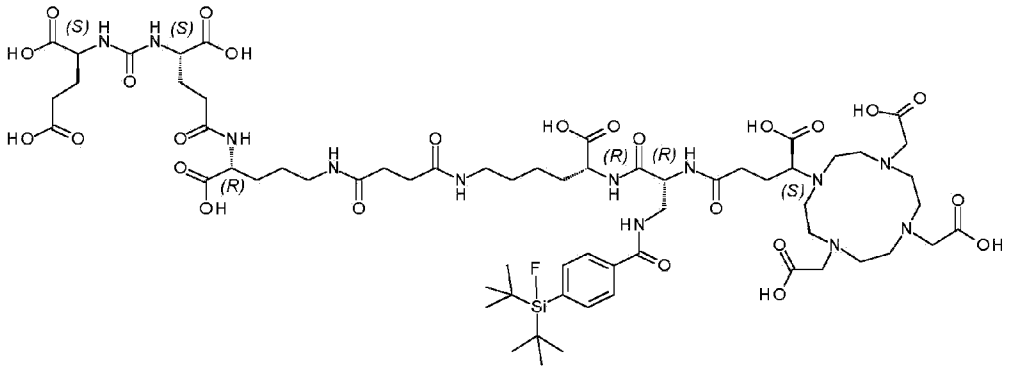

(V)

or a pharmaceutically acceptable salt thereof, containing either a chelated radioactive cation or wherein F is optionally ^{18}F.

[0050] The compound may contain a chelated cation selected from the cations of Sc, Cu, Ga, Y, In, Tb, Ho, Lu, Re, Pb, Bi, Ac, Er and Th. The chelated cation may be radioactive. The chelated radioactive cation may be any radioactive isotope(s) of Gallium, Erbium, copper, scandium, Lutetium or Yttrium.

[0051] The compound of formula (Va):

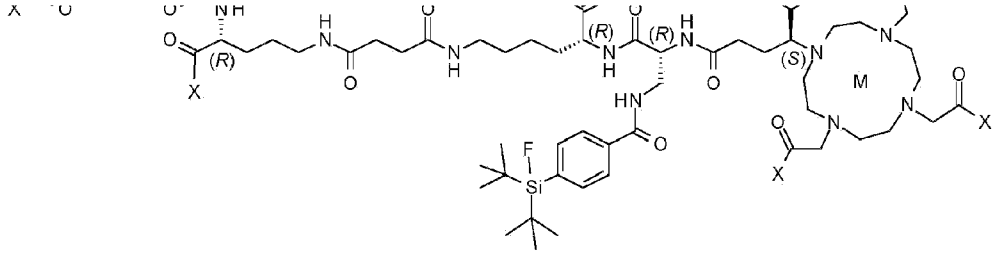

(Va)

or a pharmaceutically acceptable salt thereof, wherein;

each X is independently OH or O^-;

M is a chelated radioactive cation or is absent;

and F is optionally ^{18}F.

[0052] In the compound of formula (Va), X may be OH. X may be O^-. One or more of groups X may be chelated to M when M is present.

[0053] In the compound of formula (Va), M may be a chelated radioactive cation. M may be absent. M may be a radioactive cation chelated to one or more X groups. M may be a radioactive cation chelated to one or more N atoms. M may be a radioactive cation chelated to one or more N atoms or one or more X groups. M may be a radioactive cation chelated to one or more N atoms and one or more X groups.

[0054] In the compound of formula (V) or (Va), F may be ^{18}F. F may be ^{19}F.

[0055] In the compound of formula (V) or (Va), the chelated radioactive cation may be selected from the cations of ^{43}Sc, ^{44}Sc, ^{47}Sc, ^{51}Cr, ^{52m}Mn, ^{58}Co, ^{52}Fe, ^{56}Ni, ^{57}Ni, ^{62}Cu, ^{64}Cu, ^{67}Cu, ^{66}Ga, ^{67}Ga ^{68}Ga, ^{89}Zr, ^{90}Y, ^{89}Y, <Tc, ^{99m}Tc, ^{97}Ru, ^{105}Rh, ^{109}Pd, ^{111}Ag,^{110m}In, ^{111}In, ^{113m}In, ^{114m}In, ^{117m}Sn, ^{121}Sn, ^{127}Te, ^{142}Pr, ^{143}Pr, ^{149}Pm, ^{151}Pm, ^{149}Tb, ^{152}Tb, ^{155}Tb, ^{161}Tb, ^{153}Sm, ^{157}Gd, ^{161}Tb, ^{166}Ho, ^{165}Dy, ^{169}Er, ^{169}Yb, ^{175}Yb, ^{172}Tm, ^{177}Lu, ^{186}Re, ^{188}Re, ^{191}Pt, ^{197}Hg, ^{198}Au, ^{199}Au, ^{212}Pb, ^{203}Pb, ^{211}At, ^{212}Bi, ^{213}Bi, ^{223}Ra, ^{225}Ac, ^{227}Th, a cationic molecule comprising ^{18}F or a cation such as ^{18}F-$[AlF]^{2+}$; more preferably the cations of ^{44}Sc, ^{47}Sc, ^{64}Cu, ^{67}Cu, ^{68}Ga, ^{90}Y, ^{111}In, ^{161}Tb, ^{166}Ho, ^{177}Lu, ^{188}Re, ^{212}Pb, ^{212}Bi, ^{213}Bi, ^{225}Ac, and ^{227}Th or a cationic molecule comprising ^{18}F. The chelated radioactive cation may be selected from the cations of Sc, Cu, Ga, Y, In, Tb, Ho, Lu, Re, Pb, Bi, Ac, Er and Th. The chelated radioactive cation may be Ga. The chelated radioactive cation may be Lu-177, Y-90, or Ac-225.

[0056] In the compound of formula (Va), M may be selected from the cations of ^{43}Sc, ^{44}Sc,

^{47}Sc, ^{51}Cr, ^{52m}Mn, ^{58}Co, ^{52}Fe, ^{56}Ni, ^{57}Ni, ^{62}Cu, ^{64}Cu, ^{67}Cu, ^{66}Ga, ^{67}Ga ^{68}Ga, ^{89}Zr, ^{90}Y, ^{89}Y, <Tc, ^{99m}Tc, ^{97}Ru, ^{105}Rh, ^{109}Pd, ^{111}Ag,^{110m}In, ^{111}In ^{113m}In, ^{114m}In, ^{117m}Sn, ^{121}Sn, ^{127}Te, ^{142}Pr, ^{143}Pr, ^{149}Pm, ^{151}Pm, ^{149}Tb, ^{152}Tb, ^{155}Tb, ^{161}Tb, ^{153}Sm, ^{157}Gd, ^{161}Tb, ^{166}Ho, ^{165}Dy, ^{169}Er, ^{169}Yb, ^{175}Yb, ^{172}Tm, ^{177}Lu, ^{186}Re, ^{188}Re, ^{191}Pt, ^{197}Hg, ^{198}Au, ^{199}Au, ^{212}Pb, ^{203}Pb, ^{211}At, ^{212}Bi, ^{213}Bi, ^{223}Ra, ^{225}Ac, ^{227}Th, a cationic molecule comprising ^{18}F or a cation such as ^{18}F-$[AlF]^{2+}$; more preferably the cations of ^{44}Sc, ^{47}Sc, ^{64}Cu, ^{67}Cu, ^{68}Ga, ^{90}Y, ^{111}In, ^{161}Tb, ^{166}Ho, ^{177}Lu, ^{188}Re, ^{212}Pb, ^{212}Bi, ^{213}Bi, ^{225}Ac, and ^{227}Th or a cationic molecule comprising ^{18}F. M may be selected from the cations of Sc, Cu, Ga, Y, In, Tb, Ho, Lu, Re, Pb, Bi, Ac, Er and Th. M may be Ga. M may be Lu-177, Y-90, or Ac-225.

[0057] It is advantageous to synthesise compounds with as few isomers as possible. Whilst the isomers can be separated, only a single isomer is used in-vivo and hence the wrong isomer is simply discarded and not used. Thus conditions which minimise racemisation or inversion of any of the defined chiral centres are ideally avoided.

[0058] Also described is a method producing the compound comprising the steps of:

1. a) reacting a compound of formula (I):

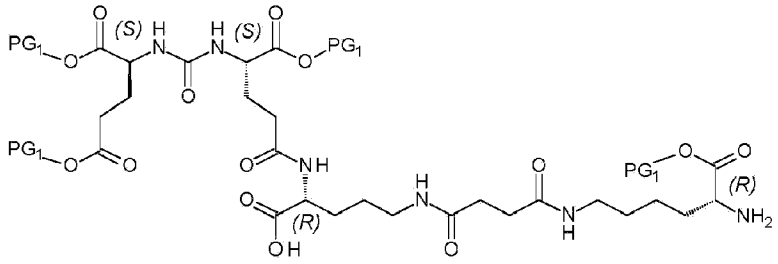

(I)

with a compound of formula (II):

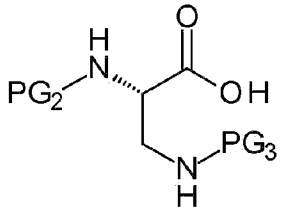

(II)

to form a compound of formula (III):

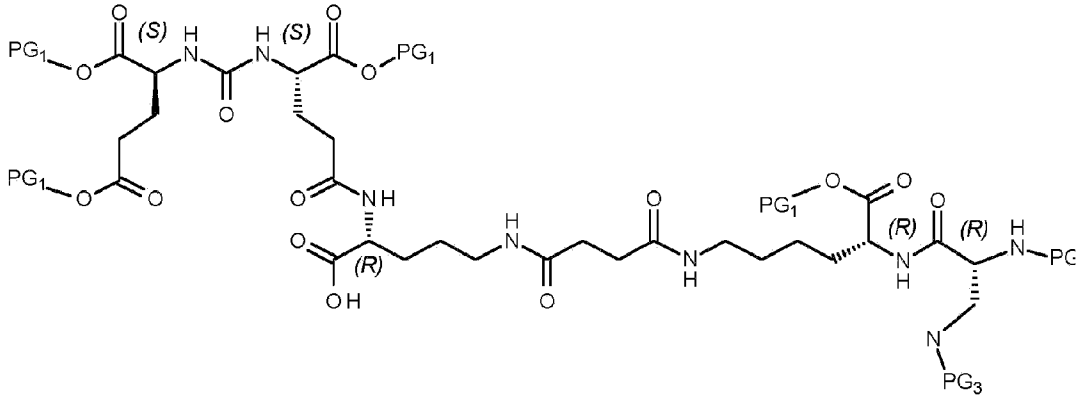

(III)

wherein PG_1 is tBu, PG_2 is Fmoc and PG_3 is Dde;

and the reaction conditions involve the use of a base, wherein the base is 2,4,6-collidine or 2,6-dimethylpyridine;

2. b) reacting the compound of formula (III) under conditions suitable for forming a compound of formula (IV):

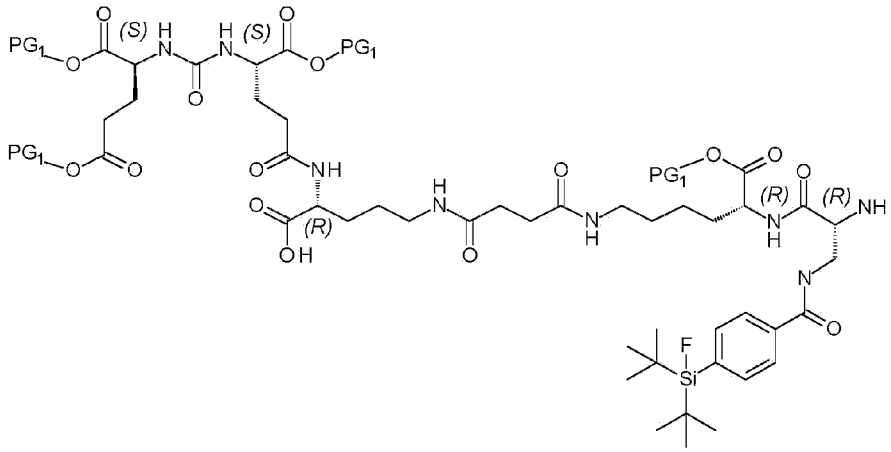

(IV)

and

3. c) reacting the compound of formula (IV) under conditions suitable for forming compound (V):

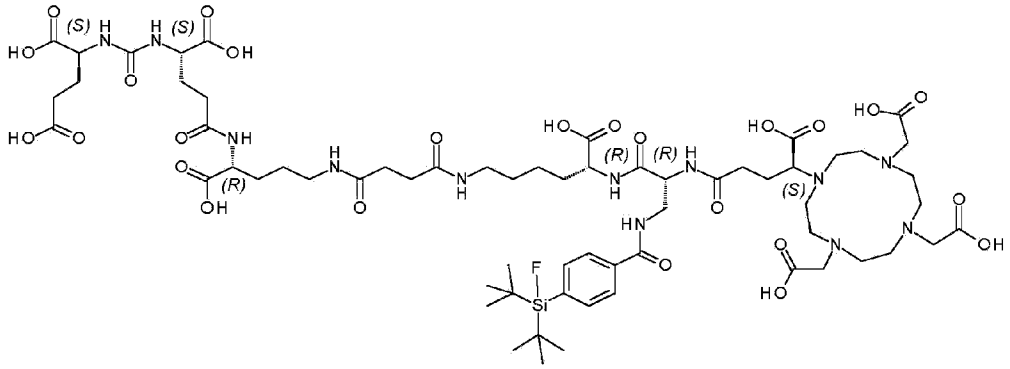

(V)

[0059] The method above includes a method wherein compound (II) is preactivated by reaction with 2-(1H-Benzotriazole-1-yl)-1,1,3,3-tetramethylaminium tetrafluoroborate (TBTU), 1-Hydroxy-7-azabenzotriazole (HOAt) and 2,4,6-collidine prior to reaction with compound (I). The preactivation takes place for 5 minutes or less.

[0060] The use of 2,4,6-collidine or 2,6-dimethylpyridine as base, along with the short activation time helps to minimise racemisation of the activated chiral compound (II) when compared to other nitrogenous bases such as DIPEA. The more sterically hindered base does not extract the acidic proton on the chiral centre of the acid, hence lowering racemisation before coupling to the amine.

[0061] Disclosed herein is the compound according to formula (VI)

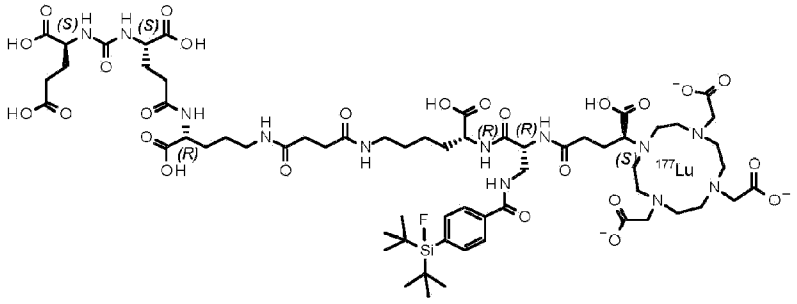

(VI)

or a pharmaceutically acceptable salt thereof.

[0062] Where the chelated metal is shown, the acid groups to which it is chelated are merely representatively shown as COO^-, the equivalent fourth acid may also be partly chelated and hence may not literally be COOH.

[0063] Disclosed herein is the compound according to formula (VII)

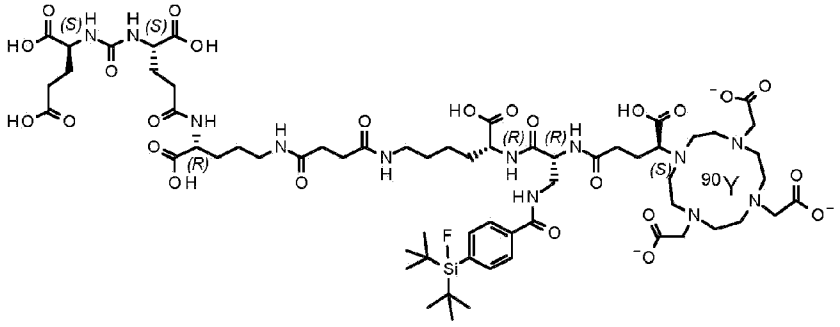

(VII)

or a pharmaceutically acceptable salt thereof.

[0064] Disclosed herein is a pharmaceutical or diagnostic composition comprising the compound of formula (V) or (VI). The conjugate, compound or composition may be used as a cancer diagnostic or imaging agent.

[0065] Disclosed is a method of imaging and/or diagnosing cancer comprising administering a conjugate, compound or composition according to formula (V) or (VI) to a patient in need thereof.

[0066] Disclosed is a conjugate, compound or composition according to formula (V) or (VI) for use in the treatment of cancer.

[0067] Disclosed is a conjugate, compound or composition according to formula (V) or (VI) for use in the diagnosis, imaging or prevention of neoangiogenesis/angiogenesis.

[0068] Disclosed is a conjugate, compound or composition according to formula (V) or (VI) for use as a cancer diagnostic or imaging agent or for use in the treatment of cancer wherein the cancer is prostate, breast, lung, colorectal or renal cell carcinoma.

[0069] The Figures illustrate:

Figure 1:

Exemplary correlation of determination of the nine reference substances in OriginPro 2016G.

Figure 2a:

Quality Control of [19F][natGa]-rhPSMA7-rac ([19F][natGa]D/L-Dap-R/S-DOTAGA-rhPSMA-7-rac), (batch 10, precursor for the production of ([18F][natGa]D/L-Dap-R/S-DOTAGA-rhPSMA-7 at the Department of Nuclear Medicine, TUM). HPLC-conditions: Solvent A: H20 + 0.1% TFA; Solvent B: MeCN + 0.1% TFA. Gradient: 25 - 35 % B 0-40 min, 95 - 95 % B 40-45 min, 35 - 35 % B 45-50 min; flow: 1 mL/min, column: Nucleosil 100-5 C18, 125 × 4.6 mm, Sample: 1 mM (DMSO), 10 µL.

Figure 2b:

Peak assignment: D-Dap-R-DOTAGA-rhPSMA-7.1; rhPSM7-rac from Fig.2a coinjected with enantiopure D-Dap-R-DOTAGA-rhPSMA-7.1. HPLC-conditions: Solvent A: H20 + 0.1% TFA; Solvent B: MeCN + 0.1% TFA. Gradient: 25 - 35 % B 0-40 min, 95 - 95 % B 40-45 min, 35 - 35 % B 45-50 min; flow: 1 mL/min, column: Nucleosil 100-5 C18, 125 × 4.6 mm, Sample: 1 mM (DMSO), 10 µL.

Figure 2c:

HPLC profile of D-Dap-R-DOTAGA-rhPSMA-7.1; HPLC-conditions: Solvent A: H20 + 0.1% TFA; Solvent B: MeCN + 0.1% TFA. Gradient: 25 - 35 % B 0-40 min, 95 - 95 % B 40-45 min, 35 - 35 % B 45-50 min; flow: 1 mL/min, column: Nucleosil 100-5 C18, 125 × 4.6 mm, Sample: 1 mM (DMSO), 10 µL.

Figure 3a:

Peak assignment: L-Dap-R-DOTAGA-rhPSMA-7.2; rhPSM7-rac from Fig.2a coinjected with enantiopure L-Dap-R-DOTAGA-rhPSMA-7.2. HPLC-conditions: Solvent A: H20 + 0.1% TFA; Solvent B: MeCN + 0.1% TFA. Gradient: 25 - 35 % B 0-40 min, 95 - 95 % B 40-45 min, 35 - 35 % B 45-50 min; flow: 1 mL/min, column: Nucleosil 100-5 C18, 125 × 4.6 mm, Sample: 1 mM (DMSO), 10 µL.

Figure 3b:

HPLC profile of L-Dap-R-DOTAGA-rhPSMA-7.2; HPLC-conditions: Solvent A: H20 + 0.1% TFA; Solvent B: MeCN + 0.1% TFA. Gradient: 25 - 35 % B 0-40 min, 95 - 95 % B 40-45 min, 35 - 35 % B 45-50 min; flow: 1 mL/min, column: Nucleosil 100-5 C18, 125 × 4.6 mm, Sample: 1 mM (DMSO), 10 µL.

Figure 4a:

Peak assignment: D-Dap-S-DOTAGA-rhPSMA-7.3; rhPSM7-rac from Fig.2a coinjected with enantiopure D-Dap-S-DOTAGA-rhPSMA-7.3. HPLC-conditions: Solvent A: H20 + 0.1% TFA; Solvent B: MeCN + 0.1% TFA. Gradient: 25 - 35 % B 0-40 min, 95 - 95 % B 40-45 min, 35 - 35 % B 45-50 min; flow: 1 mL/min, column: Nucleosil 100-5 C18, 125 × 4.6 mm, Sample: 1 mM (DMSO), 10 µL.

Figure 4b:

HPLC profile of D-Dap-D-DOTAGA-rhPSMA-7.3; HPLC-conditions: Solvent A: H20 + 0.1% TFA; Solvent B: MeCN + 0.1% TFA. Gradient: 25 - 35 % B 0-40 min, 95 - 95 % B 40-45 min, 35 - 35 % B 45-50 min; flow: 1 mL/min, column: Nucleosil 100-5 C18, 125 ×

4.6 mm, Sample: 1 mM (DMSO), 10 µL.

Figure 5a:

Peak assignment: L-Dap-S-DOTAGA-rhPSMA-7.4; rhPSM7-rac from Fig.2a coinjected with enantiopure D-Dap-S-DOTAGA-rhPSMA-7.3. HPLC-conditions: Solvent A: H20 + 0.1% TFA; Solvent B: MeCN + 0.1% TFA. Gradient: 25 - 35 % B 0-40 min, 95 - 95 % B 40-45 min, 35 - 35 % B 45-50 min; flow: 1 mL/min, column: Nucleosil 100-5 C18, 125 × 4.6 mm, Sample: 1 mM (DMSO), 10 µL.

Figure 5b:

HPLC profile of L-Dap-D-DOTAGA-rhPSMA-7.4; HPLC-conditions: Solvent A: H20 + 0.1% TFA; Solvent B: MeCN + 0.1% TFA. Gradient: 25 - 35 % B 0-40 min, 95 - 95 % B 40-45 min, 35 - 35 % B 45-50 min; flow: 1 mL/min, column: Nucleosil 100-5 C18, 125 × 4.6 mm, Sample: 1 mM (DMSO), 10 µL.

Figure 6a:

Binding affinities (IC50 [nM]) of rhPSMA7.1 and 7.2 to PSMA. Affinities were determined using LNCaP cells (150000 cells/well) and ((4-[125I]iodobenzoyl)KuE ([125I]IB-KuE; c = 0.2 nM) as the radioligand (1 h, 4 °C, HBSS + 1% BSA). Data are expressed as mean ± SD (n = 3, in 3 different experiments).

Figure 6b:

Determination of the binding affinities [nM] of the rhPSMA7 isomers to PSMA. Each of the four column shows the individual affinity measurements for rhPSAM7.1 (left) to rhPSMA7.4 (right). Conditions as described in the legend to Fig 6a.

Figure 7:

Depiction of the individual IC50 [nM] measurements shown in Fig 6a and 6b. Value No 5 of rhPSMA7.1 was deleted Conditions as described in the legend to Fig 6a

Figure 8:

Depiction of the individual internalization measurements [% of [^{125}I]IB-KuE]. Internalized activity (c = 0.5 nM) at 1 hour as % of the reference ligand ([^{125}I]I-BA)KuE (c = 0.2 nM), determined on LNCaP cells (37 °C, DMEM F12 + 5% BSA, 125000 cells/well). Data is corrected for non-specific binding (10 µmol PMPA) and expressed as mean ± SD (n = 3).

Figure 9:

Depiction of the individual measurements of the logP's of the rhPSMA isomers.

Figure 10:

Biodistribution (in %ID/g) of ^{18}F-labeled rhPSMA tracers at 1 h p.i in LNCaP tumor-bearing SCID mice. Data are expressed as mean ± SD (n=4 for rhPSMA7.1, n=5 for 7.2, n=4 for 7.3, n=5 for 7.4 and n=3 for 7-rac).

Figure 11:

Biodistribution [%ID/g] of ^{18}F-rhPSMAs co-injected with PMPA (8 mg/kg) at 1 h p.i in LNCaP tumor-bearing SCID mice. Data are expressed as mean ± SD (n=3).

Figure 12:

Possible species generated by metabolic cleavage of amide bonds. iL: cleavage forms a species with increased lipophilicity; DF: defluorination; nd: not detectable, since not radioactive.

Figure 13:

Left: Graphical analysis of overlapping peaks 1 (rhPSMA7.2) and 2 (rhPSMA7.3); right: deconvolution and integration of peak profiles by Systat PeakFit Software); top: experimental data fitted, bottom: deconvoluted single peaks.

Figure 14a:

Quantification of relative changes (in % change of injected racemic mixture) to evaluate the reproducibility of classical integration (by HPLC program) and deconvolution (by 'PeakFit') of peak 4 (rhPSMA7.1). Both methods demonstrate similar performance for this peak.

Figure 14b:

Quantification of relative changes (in % change of injected racemic mixture) to evaluate the reproducibility of classical integration (by HPLC program) and deconvolution (by 'PeakFit') of peak 3 (rhPSMA7.4). Both methods demonstrate similar performance for this peak.

Figure 15:

Percentage change of each rhPSAM7.1-7.4 isomer in blood, liver, kidney, tumor and urine with respect to its proportion the injected solution ([^{18}F][^{nat}Ga]rhPSMA7-rac. Data expressed as mean values ± SD (n=4; see also Fig 16).

Figure 16:

Percentage change of each rhPSAM7.1-7.4 isomer for each sample and experiment) in blood, liver, kidney, tumor and urine with respect to its proportion in the injected solution ([^{18}F][^{nat}Ga]rhPSMA7-rac). Analyses were carried out with Systat PeakFit.

Figure 17:

Left: TLC scanner profile of a TLC plate with liver sample (30.07.2018, overall cts: 142 cts). Due to their bad statistics and limited validity dataset with cts<200 were removed. Right: Phophoimage of a TLC plate with liver sample: long tailing of the moving tracer.

Figure 18:

Left: TLC scanner profile of a TLC plate with a quality control sample (01.08.2018, overall cts: 384). Right: Exemplay phophoimage of a TLC plate with Urine, kidney, liver, tumor, blood and QK sample.

Figure 19:

Radio-TLC of [F-18]rhPSMA7-rac (30.07.2018) as part of the Quality Control in the Department of Nuclear Medicine prior to clinical application of the tracer. Note that a tailing of the tracer is even observed in the formulation buffer (and thus in the absence of proteins).

Figure 20:

Quantification of free [F-18]Fluoride and 'intact' [F-18]rhPSMA7-rac by radio-TLC of a urine sample (30.07.2018).

Figure 21:

Left: Radio-HPLC analysis of urine collected and pooled from 4 normal mice injected with the respective [F-18]rhPSAM-7.x tracer.

Right: Radio-HPLC analysis of 'cold' urine spiked with the respective [F-18]rhPSAM-7.x tracer for a period of 1h (7.1., 7.2.), 0.5h (7.3.) and 2h (7.4.).

HPLC-conditions: Solvent A: H20 + 0.1% TFA; Solvent B: MeCN + 0.1% TFA; Gradient: 5% isocratic 0-3 min, 25 - 35 % B 3-43 min, 95 - 95 % B 43-48 min; flow: 1 mL/min, column: Nucleosil 100-5 C18, 125 × 4.6 mm.

Figure 22:

Separation of radioactive species in urine by cartridge fixation and TLC.

Top: Radio-HPLC analysis of urine 30min p.i. of [F-18]rhPSMA7.3 in mice showing a small proportion at 1.6 min and intact tracer at ca. 34.5 min.

Bottom (left): urine of mice, 30min p.i. of [F-18]rhPSMA7.3, was diluted and subjected to STRATA-X cartridge fixation. The cartridge was washed and eluted with MeCN/water (60/40 v/v +1% TFA); only intact tracer was detected.

Bottom (right): both the breakthrough from the cartridge fixation (non-retained components) and the fraction finally eluted MeCN/water from the cartridge were analysed by TLC (bottom, right). Whereas 96.1% [F-18]rhPSMA7.3 and only 3.9% [F-18]fluoride were found in the eluate of the cartridge, the reverse ratio was found in the breakthrough of the cartridge (3.4% [F-18]rhPSMA7.3 and only 96.6% [F-18]fluoride).

Figure 23:

To fresh and nonradioactive urine of mice [F-18]rhPSMA7.3 was added, followed by 0.5µmol cold F-19-fluoride; incubation for 2h.
Radioactivity was completely (98.5%) converted to a very hydrophilic fraction representing [F-18]fluoride (peak at 1.6 min). Note: peak at 1.6 min was subsequently immobilized on a QMA cartridge and eluted with with NaCl (1M) (=fluoride).

Figure 24:

Clinical biodistribution and uptake in tumor lesions of 18F-rhPSMA-7 (left) and 18F-rhPSMA-7.3 (right) as demonstrated by SUVmax. Data are expressed as mean ± SD.

Figure 25:

Clinical biodistribution and uptake in tumor lesions of ^{18}F-rhPSMA-7 (left) and ^{18}F-rhPSMA-7.3 (right) as demonstrated by SUVmean. Data are expressed as mean ± SD.

Figure 26.

Clinical biodistribution and uptake in tumor lesions of ^{18}F-rhPSMA-7 (left) and ^{18}F-rhPSMA-7.3 (right) as demonstrated by the ratio SUVmax to background. Data are expressed as mean ± SD.

Figure 27:

Clinical biodistribution and uptake in tumor lesions of ^{18}F-rhPSMA-7 (left) and ^{18}F-rhPSMA-7.3 (right) as demonstrated by the ratio SUVmean to background. Data are expressed as mean ± SD.

Figure 28:

Two clinical case examples of ^{18}F-rhPSMA-7.3 PET-imaging.

Example 1: Material and Methods

[0070] The Fmoc-(9-fluorenylmethoxycarbonyl-) and all other protected amino acid analogs were purchased from Bachem (Bubendorf, Switzerland) or Iris Biotech (Marktredwitz, Germany). The tritylchloride polystyrene (TCP) resin was obtained from PepChem (Tübingen, Germany). Chematech (Dijon, France) delivered the chelators DOTAGA-anhydride, (*R*)-DOTA-GA(*t*Bu)$_4$ and (S)-DOTAGA(*t*Bu)$_4$. All necessary solvents and other organic reagents were purchased from either, Alfa Aesar (Karlsruhe, Germany), Sigma-Aldrich (Munich, Germany) or VWR (Darmstadt, Germany). Solid phase synthesis of the peptides was carried out by manual operation using an Intelli-Mixer syringe shaker (Neolab, Heidelberg, Germany). Analytical and preparative reversed-phase high pressure chromatography (RP-HPLC) were performed using Shimadzu gradient systems (Shimadzu Deutschland GmbH, Neufahrn, Germany), each equipped with a SPD-20A UV/Vis detector (220 nm, 254 nm). A Nucleosil 100 C18 (125 × 4.6 mm, 5 µm particle size) column (CS GmbH, Langerwehe, Germany) was used for analytical measurements at a flow rate of 1 mL/min. Both specific gradients and the corresponding retention times t_R are cited in the text. Preparative HPLC purification was done with a Multospher 100 RP 18 (250 × 10 mm, 5 µm particle size) column (CS GmbH, Langerwehe, Germany) at a constant flow rate of 5 mL/min. Analytical and preparative radio RP-HPLC was performed using a Nucleosil 100 C18 (5 µm, 125 × 4.0 mm) column (CS GmbH, Langerwehe, Germany). Eluents for all HPLC operations were water (solvent A) and acetonitrile (solvent B), both containing 0.1% trifluoroacetic acid. Electrospray ionization-mass spectra for characterization of the substances were acquired on an expression^L CMS mass spectrometer (Advion Ltd., Harlow, UK). NMR spectra were recorded on Bruker AVHD-300 or AVHD-400 spectrometers at 300 K. pH values were measured with a Seven Easy pH-meter (Mettler Toledo, Gießen, Germany).

Synthesis protocols

1) Solid-phase peptide synthesis following the Fmoc-strategy

TCP-resin loading (GP1)

[0071] Loading of the tritylchloride polystyrene (TCP) resin with a Fmoc-protected amino acid (AA) was carried out by stirring a solution of the TCP-resin (1.95 mmol/g) and Fmoc-AA-OH (1.5 eq.) in anhydrous DCM with DIPEA (4.5 eq.) at room temperature for 2 h. Remaining tritylchloride was capped by the addition of methanol (2 mL/g resin) for 15 min. Subsequently the resin was filtered and washed with DCM (2 × 5 mL/g resin), DMF (2 × 5 mL/g resin), methanol (5 mL/g resin) and dried *in vacuo.* Final loading *l* of Fmoc-AA-OH was determined by

the following equation:

$$l\left[\frac{mmol}{g}\right] = \frac{(m_2 - m_1) \times 1000}{(M_W - M_{HCl})\, m_2}$$

m_2 = mass of loaded resin [g]

m_1 = mass of unloaded resin [g]

M_W = molecular weight of AA [g/mol]

M_{HCl} = molecular weight of HCl [g/mol]

On-resin amide bond formation (GP2)

[0072] For conjugation of a building block to the resin bound peptide, a mixture of TBTU and HOBT is used for pre-activation with DIPEA or 2,4,6-trimethylpyridine as a base in DMF (10 mL/g resin) for 5 min. The exact stoichiometry and reaction time for each conjugation step is given in the synthesis protocol. After reaction, the resin was washed with DMF (6 × 5 mL/g resin).

On-resin Fmoc-deprotection (GP3)

[0073] The resin-bound Fmoc-peptide was treated with 20% piperidine in DMF (v/v, 8 mL/g resin) for 5 min and subsequently for 15 min. Afterwards, the resin was washed thoroughly with DMF (8 × 5 mL/g resin).

On-resin Dde-deprotection (GP4)

[0074] The Dde-protected peptide (1.0 eq.) was dissolved in a solution of 2% hydrazine monohydrate in DMF (v/v, 5 mL/g resin) and shaken for 20 min (GP4a). In the case of present Fmoc-groups, Dde-deprotection was performed by adding a solution of imidazole (0.92 g/g resin), hydroxylamine hydrochloride (1.26 g/g reisn) in NMP (5.0 mL) and DMF (1.0 mL) for 3 h at room temperature (GP4b). After deprotection the resin was washed with DMF (8 × 5 mL/g resin).

Peptide cleavage from the resin with simultaneous deprotection of acid labile protecting groups (GP 5)

[0075] The fully protected resin-bound peptide was dissolved in a mixture of TFA/TIPS/water (v/v/v; 95/2.5/2.5) and shaken for 30 min. The solution was filtered off and the resin was treated in the same way for another 30 min. Both filtrates were combined, stirred for additional 5 h and concentrated under a stream of nitrogen. After dissolving the residue in a mixture of tert-butanol and water and subsequent lyophilisation the crude peptide was obtained.

^{nat}Ga-complexation (GP6)

[0076] For ^{nat}Ga-complexation, the peptide (1.0 eq.) was dissolved in a 3:1 *(v/v)* mixture of tBuOH in H_2O and an aqueous solution of $Ga(NO_3)_3$ (3.5 eq.) was added. After heating the resulting mixture for 30 min at 75°C the peptide was purified by RP-HPLC.

2) Synthesis of the PSMA binding motif

Glu-urea-Glu ((tBuO)EuE(OtBu)2)

[0077]

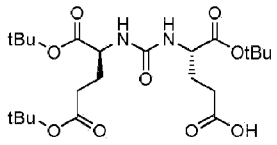

[0078] The tBu-protected Glu-urea-Glu binding motif (EuE) was synthesized according to a previously published procedure (scheme 1) for tBu-protected Glu-urea-Lys (EuK).

Di-tert-butyl (1H-imidazole-1-carbonyl)-L-glutamate (i)

[0079] A solution of DCM containing 2.0 g (7.71 mmol, 1.0 eq.) l-di-*tert*-butyl-L-glutamate·HCl was cooled on ice for 30 min and afterwards treated with 2.69 mL TEA (19.28 mmol, 2.5 eq.) and 3.3 mg (0.3 mmol, 0.04 eq.) DMAP. After additional stirring for 5 min, 1.38 g (8.84 mmol, 1.1 eq.) of 1,1'-carbonyldiimidazole (CDI) dissolved in DCM were slowly added over a period of 30 min. The reaction mixture was further stirred overnight and enabled to warm to RT. The reaction was stopped using 8 mL saturated $NaHCO_3$ with concomitant washing steps of water (2 ×) and brine (2 ×) and dried over Na_2SO_4. The remaining solvent was removed *in vacuo* and the crude product (S)-Di-*tert*-butyl 2-(1H-imidazole-1-carboxamido)pentanedioate (i) was used without further purification.

5-benzyl 1-(tert-butyl) (((S)-1,5-di-tert-butoxy-1,5-dioxopentan-2-yl)carbamoyl)-L-

glutamate (ii)

[0080] 2.72 g (7.71 mmol, 1.0 eq.) of the crude product (S)-Di-tert-butyl-2-(1H-imidazole-1-carboxamido) pentanedioate (i) were dissolved in 1,2-dichloroethane (DCE) and cooled on ice for 30 min. To this solution were added 2.15 mL (15.42 mmol, 2.0 eq.) TEA and 2.54 g (7.71 mmol, 1.0 eq.) H-L-Glu(OBzl)-O*t*Bu·HCl and the solution was stirred overnight at 40 °C. The remaining solvent was evaporated and the crude product purified using silica gel flash-chromatography with an eluent mixture containing ethyl acetate/hexane/TEA (500:500:0.8 ; v/v/v). After removal of the solvent, 5-benzyl-1-(tert-butyl)-(((S)-1,5-di-tert-butoxy-1,5-dioxopentan-2-yl)carbamoyl)-L-glutamate (ii) was obtained as a colorless oil.

(tBuO)EuE(OtBu)$_2$ (iii)

[0081] To synthesize (*t*BuO)EuE(O*t*Bu)$_2$, 3.17 g (5.47 mmol, 1.0 eq.) of 5-benzyl-1-(tert-butyl)-(((S)-1,5-di-tert-butoxy-1,5-dioxopentan-2-yl)carbamoyl)-L-glutamate (ii) were dissolved in 75 mL EtOH and 0.34 g (0.57 mmol, 0.1 eq.) palladium on activated charcoal (10%) were given to this solution. The flask containing the reaction mixture was initially purged with H_2 and the solution was stirred over night at room temperature under light H_2-pressure (balloon). The crude product was purified through celite and the solvent evaporated *in vacuo.* The product (iii) was obtained as a hygroscopic solid (84%). HPLC (10% to 90% B in 15 min): t_R = 11.3 min. Calculated monoisotopic mass ($C_{23}H_{49}N_2O_9$): 488.3; found: m/z = 489.4 $[M+H]^+$, 516.4 $[M+Na]^+$.

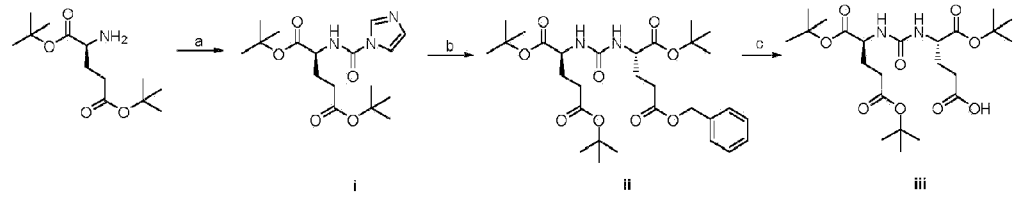

Scheme 1 Synthesis of (*t*BuO)EuE(O*t*Bu)$_2$: a) DCI, TEA, DMAP (DCM); b) H-L-Glu(OBzl)-O*t*Bu·HCl, TEA (DCE); c) Pd/C (10%), H_2 (EtOH).

3) Synthesis of the silicon-fluoride acceptor

4-(Di-tert-butylfluorosilyl)benzoic acid (SiFA-BA)

[0082]

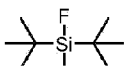

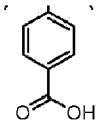

[0083] SiFA-BA was synthesized according to a previously published procedure (scheme 2). All reactions were carried out in dried reaction vessels under argon using a vacuum gas manifold.

((4-bromobenzyl)oxy)(tert-butyl)dimethylsilane (i)

[0084] To a stirred solution of 4-bromobenzylalcohol (4.68 g, 25.0 mmol, 1.0 eq.) in anhydrous DMF (70 mL) imidazole (2.04 g, 30.0 mmol, 1.2 eq.) and TBDMSCl (4.52 g, 30.0 mmol, 1.2 eq.) were added and the resulting mixture was stirred at room temperature for 16 h. The mixture was then poured into ice-cold H_2O (250 mL) and extracted with Et_2O (5 × 50 mL). The combined organic fractions were washed with sat. aq. $NaHCO_a$ (2 ×100 mL) and brine (100 mL), dried, filtered and concentrated *in vacuo* to give the crude product which was purified by flash column chromatography (silica, 5% EtOAc/petrol) to give i as a colourless oil (7.18 g, 95%). ^{1}H NMR (400 MHz, CDCl3): δ [ppm] = 0.10 (6H, s, Si*Me*$_2$t-Bu), 0.95 (9H, s, SiMe$_2$t*Bu*), 4.69 (2H, s, C*H*$_2$OSi), 7.21 (2H, d), 7.46 (2H, d). HPLC (50 to 100% B in 15 min): t_R = 15 min.

Di-tert-butyl{4-[(tert-butyldimethylsilyloxy)methyl]phenyl}fluorosilane (ii)

[0085] At -78 °C under magnetic stirring, a solution of tBuLi in pentane (7.29 mL, 1.7 mol/L, 12.4 mmol 2.4 eq.) was added to a solution of ((4-bromobenzyl)oxy)(tert-butyl)dimethylsilane (i) (1.56 g, 5.18 mmol, 1.0 eq.) in dry THF (15 mL). After the reaction mixture had been stirred for 30 min at -78 °C, the suspension obtained was added dropwise over a period of 30 min to a cooled (-78 °C) solution of di-tert-butyldifluorosilane (1.12 g, 6.23 mmol, 1.2 eq.) in dry THF (10 mL). The reaction mixture was allowed to warm to room temperature over a period of 12 h and then hydrolyzed with saturated aqueous NaCl solution (100 mL). The organic layer was separated and the aqueous layer was extracted with diethyl ether (3 × 50 mL). The combined organic layers were dried over magnesium sulfate and filtered. The filtrate was concentrated *in vacuo* to afford ii as a yellowish oil (1.88 g, 95%). It was used for subsequent reactions without further purification. NMR spectra were in accordance with the data reported in the literature[2]. HPLC (50 to 100% B in 20 min): t_R = 19 min.

4-(Di-tert-butylfluorosilanyl)benzyl alcohol (iii)

[0086] A catalytic amount of concentrated aqueous HCl (0.5 mL) was added to a suspension

of ii (1.88 g, 4.92 mmol, 1.0 eq.) in methanol (50 mL). The reaction mixture was stirred for 18 h at room temperature and then the solvent and the volatiles were removed under reduced pressure. The residue was redissolved in diethyl ether (40 mL) and the solution was washed with saturated aqueous $NaHCO_3$ solution. The aqueous layer was extracted with diethyl ether (3 × 50 mL). The combined organic layers were dried over magnesium sulfate and filtered. The filtrate was concentrated *in vacuo* to afford iii as a yellowish oil (1.29 g, 98%) that solidified. The product was used without further purification. NMR spectra were in accordance with the data reported in the literature[2]. HPLC (50 to 100% B in 15 min): t_R = 8.2 min.

4-(Di-tert-butylfluorosilyl)benzaldehyde (iv)

[0087] A solution of the alcohol iii (1.37 g, 5.10 mmol, 1.0 eq.) in dry dichloromethane (20 mL) was added dropwise to a stirred ice-cooled suspension of pyridinium chlorochromate (2.75 g, 12.8 mmol, 2.5 eq.) in dry dichloromethane (60 mL). After the reaction mixture had been stirred for 30 min at 0°C and for 2.5 h at room temperature, anhydrous diethyl ether (40 mL) was added and the supernatant solution was decanted from the black gum-like material. The insoluble material was washed thoroughly with diethyl ether and the combined organic phases were passed through a short pad of silica gel (10 cm per g crude product) for filtration. The solvents were removed *in vacuo* to yield aldehyde **iv** as a yellowish oil (1.31 g, 96%). NMR spectra were in accordance with the data reported in the literature[2]. HPLC (50 to 100% B in 15 min): t_R = 10.5 min.

4-(Di-tert-butylfluorosilyl)benzoic acid (v)

[0088] At room temperature, 1 M aqueous $KMnO_4$ (30 mL) was added to a mixture of iv (1.31 g, 4.92 mmol, 1.0 eq.), tert-butanol (30 mL), dichloromethane (3.3 mL), and 1.25 M $NaH_2PO_4 \cdot H_2O$ buffer (20 mL) at pH 4.0-4.5. After the mixture had been stirred for 25 min, it was cooled to 5 °C, whereupon excess $KMnO_4$ (0.78 g, 4.92 mmol, 1.0 eq.) was added. The reaction was then quenched by the addition of saturated aqueous Na_2SO_3 solution (50 mL). Upon addition of 2 M aqueous HCl, all of the MnO_2 dissolved. The resulting solution was extracted with diethyl ether (3 × 100 mL). The combined organic layers were washed with saturated aqueous $NaHCO_3$ solution, dried over $MgSO_4$, filtered, and concentrated under reduced pressure to provide a white solid, which was purified by recrystallization from Et_2O/n-hexane (1:3, for 12 h) to give v (0.84 g, 60%). NMR spectra were in accordance with the data reported in the literature[2]. HPLC (50 to 100% B in 15 min): t_R = 8.5 min.

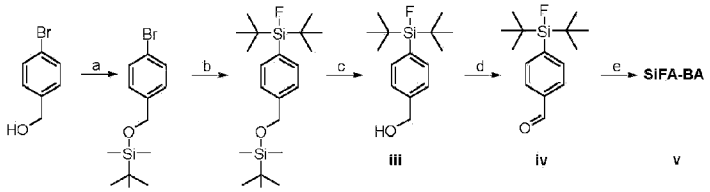

i ii

Scheme 2 Synthesis of SiFA-BA: a) TBDMSCl, imidazole (DMF); b) *t*BuLi, di-tert-butyldifluorosilane (THF); c) HCl (MeOH); d) pyridinium chlorochromate (DCM); e) $KMnO_4$ (DCM, *tert*-butanol, NaH_2PO_4 buffer).

4) Synthesis of rhPSMA-7.1 - 7.4

[0089] The first synthetic steps for preparation of the four different isomers of rhPSMA-7 are identical and carried out together, applying the standard Fmoc-SPPS protocol described above, starting from resin bound Fmoc-D-Orn(Dde)-OH. After cleavage of the Fmoc group with 20% piperidine in DMF (GP3), (*t*BuO)EuE(O*t*Bu)$_2$ (2.0 eq.) was conjugated with HOAt (2.0 eq.), TBTU (2.0 eq.) and DIPEA (6.0 eq.) in DMF for 4.5 h. After cleavage of the Dde-group with a mixture of 2% hydrazine in DMF (GP4a), a solution of succinic anhydride (7.0 eq.) and DIPEA (7.0 eq.) in DMF was added and left to react for 2.5 h. Conjugation of Fmoc-D-Lys(O*t*Bu)·HCl (2.0 eq.) was achieved by adding a mixture of HOAt (2.0 eq.), TBTU (2.0 eq.) and DIPEA (6.0 eq.) in DMF to the resin. After pre-activation for 5 min, Fmoc-D-Lys(O*t*Bu)·HCl (2.0 eq.) dissolved in DMF was added and left to react for 2.5 h (GP2). Subsequent cleavage of the Fmoc-group was performed, by adding a mixture of 20% piperidine in DMF (GP3). Finally, the resin was split in order to synthesize rhPSMA-7.1-7.4 (scheme 3).

rhPSMA-7.1 (D-Dap-(R)-DOTA-GA):

[0090]

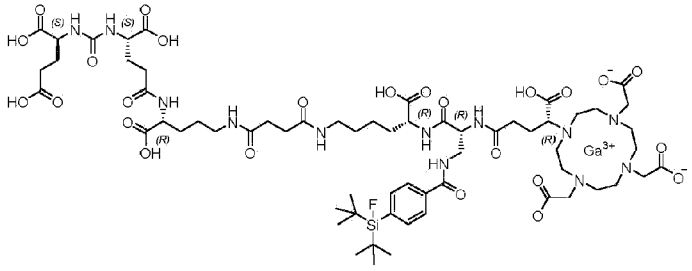

[0091] Fmoc-D-Dap(Dde)-OH (2.0 eq.) was pre-activated in a mixture of HOAt (2.0 eq.), TBTU (2.0 eq.) and 2,4,6-trimethylpyridine (6.7 eq.) in DMF and added to the resin-bound peptide for 2.5 h. Following orthogonal Dde-deprotection was done using imidazole and hydroxylamine hydrochloride dissolved in a mixture of NMP and DMF for 3 h. SiFA-BA (1.5 eq.) was reacted with the free amine of the side chain with HOAt (1.5 eq.), TBTU (1.5 eq.) and DIPEA (4.5 eq.), as activation reagents in DMF for 2 h. After Fmoc-deprotection with piperidine (GP3), (*R*)-DOTA-GA(*t*Bu)$_4$ (2.0 eq.) was conjugated with HOAT (2.0 eq.), TBTU (2.0 eq.) and 2,4,6-trimethylpyridine (6.7 eq.) in DMF for 2.5 h. Cleavage from the resin with simultaneous

deprotection of acid labile protecting groups was performed in TFA, according to GP5. ^{nat}Ga-complexation of the peptide was carried out, as described in GP6.

rhPSMA-7.2 (L-Dap-(R)-DOTA-GA):

[0092]

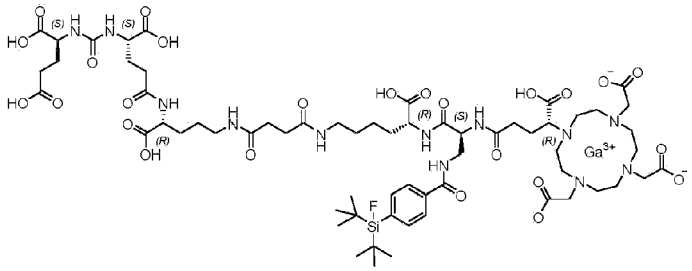

[0093] Fmoc-L-Dap(Dde)-OH (2.0 eq.) was pre-activated in a mixture of HOAt (2.0 eq.), TBTU (2.0 eq.) and 2,4,6-trimethylpyridine (6.7 eq.) in DMF for 2.5 h. Following orthogonal Dde-deprotection, conjugation of SiFA-BA and Fmoc-cleavage was carried out as described for rhPSMA-7.1. (R)-DOTAGA(tBu)$_4$ (2.0 eq.) was conjugated with HOAT (2.0 eq.), TBTU (2.0 eq.) and 2,4,6-trimethylpyridine (6.7 eq.) in DMF for 2.5 h. Cleavage from the resin with simultaneous deprotection of acid labile protecting groups was performed in TFA according to GP5. ^{nat}Ga-complexation of the peptide was carried out, as described in GP6.

rhPSMA-7.3 (D-Dap-(S)-DOTA-GA):

[0094]

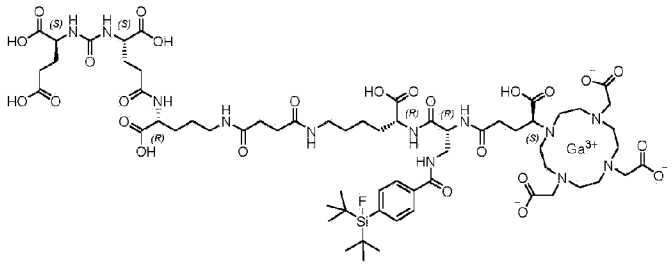

[0095] Fmoc-D-Dap(Dde)-OH (2.0 eq.) was pre-activated in a mixture of HOAt (2.0 eq.), TBTU (2.0 eq.) and 2,4,6-trimethylpyridine (6.7 eq.) in DMF for 2.5 h. Following orthogonal Dde-deprotection, conjugation of SiFA-BA and Fmoc-cleavage was carried out as described for rhPSMA-7.1. (S)-DOTAGA(tBu)$_4$ (2.0 eq.) was conjugated with HOAT (2.0 eq.), TBTU (2.0 eq.) and 2,4,6-trimethylpyridine (6.7 eq.) in DMF for 2.5 h. Cleavage from the resin with simultaneous deprotection of acid labile protecting groups was performed in TFA according to GP5. ^{nat}Ga-complexation of the peptide was carried out, as described in GP6.

rhPSMA-7.4 (L-Dap-(S)-DOTA-GA):

[0096]

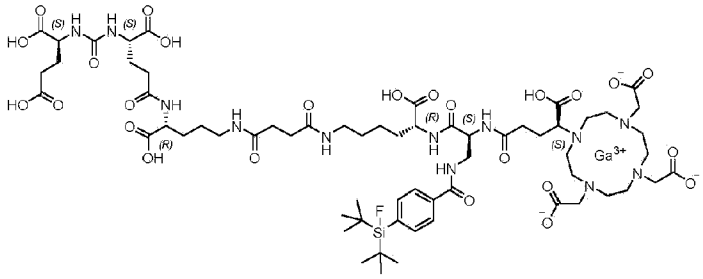

[0097] Fmoc-L-Dap(Dde)-OH (2.0 eq.) was pre-activated in a mixture of HOAt (2.0 eq.), TBTU (2.0 eq.) and 2,4,6-trimethylpyridine (6.7 eq.) in DMF for 2.5 h. Following orthogonal Dde-deprotection, conjugation of SiFA-BA and Fmoc-cleavage was carried out as described for rhPSMA-7.1. (S)-DOTAGA(*t*Bu)$_4$ (2.0 eq.) was conjugated with HOAT (2.0 eq.), TBTU (2.0 eq.) and 2,4,6-trimethylpyridine (6.7 eq.) in DMF for 2.5 h. Cleavage from the resin with simultaneous deprotection of acid labile protecting groups was performed in TFA according to GP5. ^{nat}Ga-complexation of the peptide was carried out, as described in GP6.

rhPSMA-7.1:

[0098]

HPLC (10 to 70% B in 15 min): t_R = 10.5 min.

HPLC (25 to 35%B in 40 min): t_R = 31.4 min.

rhPSMA-7.2:

[0099]

HPLC (10 to 70% B in 15 min): t_R = 10.4 min.

HPLC (25 to 35%B in 40 min): t_R = 27.9 min.

rhPSMA-7.3:

[0100]

HPLC (10 to 70% B in 15 min): t_R = 10.4 min.

HPLC (25 to 35%B in 40 min): t_R = 28.1 min.

rhPSMA-7.4:

[0101]

HPLC (10 to 70% B in 15 min): t_R = 10.5 min.

HPLC (25 to 35%B in 40 min): t_R = 29.1 min.

rhPSMA-7.1-7.4:

[0102] Calculated monoisotopic mass (C63H96FGaN12O25Si): 1536.6 found: m/z = 1539.4 [M+H]+, 770.3 $[M+2H]2^+$.

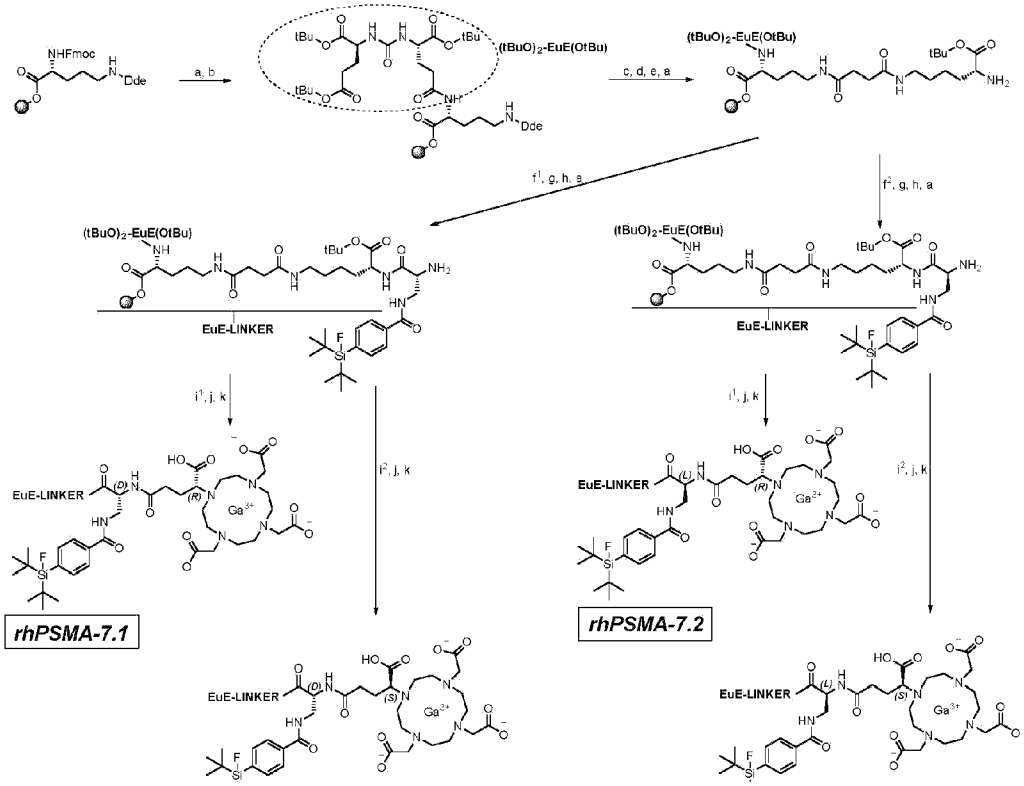

Scheme 3 Synthesis of rhPSMA-7.1–7.4: a) 20% piperidine, (DMF); b) (tBuO)EuE(OtBu)2, HOAt, TBTU, DIPEA, (DMF); c) 2% hydrazine (DMF); d) succinic anhydride, DIPEA, (DMF); e) Fmoc-D-Lys(OtBu)·HCl, HOAt, TBTU, DIPEA, (DMF); f^1) Fmoc-D-Dap(Dde)-OH, HOAt, TBTU, 2,4,6-collidine, (DMF); f^2) Fmoc-L-Dap(Dde)-OH, HOAt, TBTU, 2,4,6-collidine, (DMF); g) imidazole, hydroxylamine hydrochloride, (NMP, DMF); h) SiFA-BA, HOAt, TBTU, DIPEA (DMF); i^1) (R)-DOTA-GA(tBu)$_4$, HOAt, TBTU, 2,4,6-collidine (DMF); i^2) (S)-DOTA-GA(tBu)4, HOAt, TBTU, 2,4,6-collidine (DMF); j) cleavage and deprotection: TFA, TIPS, H_2O; k) $Ga(NO_3)_3$, (tBuOH, H_2O).

5) ^{18}F-labelling

[0103] For ^{18}F-labelling a previously published procedure was applied, which was slightly modified. Briefly, aqueous $^{18}F^-$ was passed through a SAX cartridge (Sep-Pak Accell Plus QMA Carbonate light), which was preconditioned with 10 mL of water. After drying with 10 mL of air, water was removed, by rinsing the cartridge with 10 mL of anhydrous acetonitrile followed by 20 mL of air. ^{18}F was eluted with 100 µmol of $[K^+\subset 2.2.2]OH^-$ dissolved in 500 µL of anhydrous acetonitrile. Before labelling, 30 µmol of oxalic acid in anhydrous acetonitrile (1 M, 30 µL) were added. This mixture was used as a whole or aliquot for fluorination of 10-25 nmol of PSMA-SiFA (1 mM in anhydrous DMSO). The resulting reaction mixture was incubated for 5 minutes at room temperature. For purification of the tracer, a Sep-Pak C18 light cartridge, preconditioned with 10 mL EtOH, followed by 10 mL of H_2O was used. The labelling mixture was diluted with 9 mL PBS (pH 3) and passed through the cartridge followed by 10 mL of H_2O. The peptide was eluted with 500 µL of a 4:1 mixture (v/v) of EtOH in water. Radiochemical purity of the labelled compound was determined by radio RP-HPLC and radio-TLC (Silica gel 60 RP-18 F_{254}s, mobile phase: 3:2 mixture *(v/v)* of MeCN in H_2O supplemented with 10% of 2 M aqueous NaOAc and 1% of TFA).

6) ^{125}I-labelling

[0104] The reference ligand for in vitro studies ([^{125}I]I-BA)KuE was prepared according to a previously published procedure. Briefly, 0.1 mg of the stannylated precursor ($SnBu_3$-BA)(OtBu)KuE$(OtBu)_2$ was dissolved in a solution containing 20 µL peracetic acid, 5.0 µL (21 MBq) [^{125}I]NaI (74 TBq/mmol, 3.1 GBq/mL, 40 mM NaOH, Hartmann Analytic, Braunschweig, Germany), 20 µL MeCN and 10 µL acetic acid. The reaction solution was incubated for 10 min

at RT, loaded on a cartridge and rinsed with 10 mL water (C18 Sep Pak Plus cartridge, preconditioned with 10 mL MeOH and 10 mL water). After elution with 2.0 mL of a 1:1 mix (v/v) of EtOH/MeCN, the radioactive solution was evaporated to dryness under a gentle nitrogen stream and treated with 200 µL TFA for 30 min with subsequent evaporation of TFA. The crude product of ([^{125}I]I-BA)KuE was purified by RP-HPLC (20% to 40% B in 20 min): t_R = 13.0 min.

In vitro experiments

1) Determination of IC_{50}

[0105] The PSMA-posivite LNCaP cells were grown in Dublecco modified Eagle medium/Nutrition Mixture F-12 with Glutamax-I (1:1) (Invitrigon), supplemented with 10% fetal calf serum and maintained at 37 °C in a humidified 5% CO_2 atmosphere. For determination of the PSMA affinity (IC_{50}), cells were harvested 24 ± 2 hours before the experiment and seeded in 24-well plates (1.5 × 10^5 cells in 1 mL/well). After removal of the culture medium, the cells were treated once with 500 µL of HBSS (Hank's balanced salt solution, Biochrom, Berlin, Germany, with addition of 1% bovine serum albumin (BSA)) and left 15 min on ice for equilibration in 200 µL HBSS (1% BSA). Next, 25 µL per well of solutions, containing either HBSS (1% BSA, control) or the respective ligand in increasing concentration (10^{-10} - 10^{-4} M in HBSS, were added with subsequent addition of 25 µL of ([^{125}I]I-BA)KuE (2.0 nM) in HBSS (1% BSA). All experiments were performed at least three times for each concentration. After 60 min incubation on ice, the experiment was terminated by removal of the medium and consecutive rinsing with 200 µL of HBSS. The media of both steps were combined in one fraction and represent the amount of free radioligand. Afterwards, the cells were lysed with 250 µL of 1 M NaOH and united with the 200 µL HBSS of the following wash step. Quantification of bound and free radioligand was accomplished in a γ-counter.

2) Internalization

[0106] For internalization studies, LNCaP cells were harvested 24 ± 2 hours before the experiment and seeded in 24-well plates (1.25 × 10^5 cells in 1 mL/well). Subsequent to the removal of the culture medium, the cells were washed once with 500 µL DMEM-F12 (5% BSA) and left to equilibrate for at least 15 min at 37 °C in 200 µL DMEM-F12 (5% BSA). Each well was treated with either 25 µL of either DMEM-F12 (5% BSA) or a 100 µM PMPA solution for blockade. Next, 25 µL of the ^{68}Ga/^{18}F-labeled PSMA inhibitor (5.0 nM) was added and the cells incubated at 37 °C for 60 min. The experiment was terminated by placing the 24-well plate on ice for 3 min and consecutive removal of the medium. Each well was rinsed with 250 µL HBSS

and the fractions from these first two steps combined, representing the amount of free radioligand. Removal of surface bound activity was accomplished by incubation of the cells with 250 µL of ice-cold PMPA (10 µM in PBS) solution for 5 min and rinsed again with another 250 µL of ice-cold PBS. The internalized activity was determined by incubation of the cells in 250 µL 1 M NaOH and the combination with the fraction of a subsequent wash step with 250 µL 1.0 M NaOH. Each experiment (control and bloackde) was performed in triplicate. Free, surface bound and internalized activity was quantified in a γ-counter. All internalization studies were accompanied by reference studies using ([^{125}I]I-BA)KuE (c = 0.2 nM), which were performed analogously. Data were corrected for non-specific internalization and normalized to the specific-internalization observed for the radioiodinated reference compound.

3) Octanol-water partition coefficient

[0107] Approximately 1 MBq of the labeled tracer was dissolved in 1 mL of a 1:1 mixture (by volumes) of phosphate buffered saline (PBS, pH 7.4) and n-octanol in an Eppendorf tube. After vigorous mixing of the suspension for 3 minutes at room temperature, the vial was centrifuged at 15000 g for 3 minutes (Biofuge 15, Heraus Sepatech, Osterode, Germany) and 100 µL aliquots of both layers were measured in a gamma counter. The experiment was repeated at least six times.

4) HSA binding

[0108] For the determination of HSA binding, a Chiralpak HSA column (50 × 3 mm, 5 µm, H13H-2433) was used at a constant flow rate of 0.5 mL/min. The mobile phase (A: NH_4OAc, 50 mM in water, pH 7 and B: isopropanol) was freshly prepared for each experiment and only used for one day. The column was kept at room temperature and each run was stopped after detection of the signal to reduce the acquisition time. All substances were dissolved in a 0.5 mg/ml concentration in 50% 2-propanol and 50% 50 mM pH 6.9 ammonium acetate buffer. The chosen reference substances display a range of HSA binding from 13% to 99% since a broad variety of albumin binding regarding the peptides was assumed. All nine reference substances were injected consecutively to establish a non-linear regression with OriginPro 2016G.

Table 1: Reference substances used for the calibration of the HSA-column.

Reference	t_R	**Log t_R**	**Lit. HSA%**	**Log *K* HSA**
p-benzylalcohol	2.40	0.38	13.15	-0.82
Aniline	2.72	0.43	14.06	-0.79
Phenol	3.28	0.52	20.69	-0.59
Benzoic Acid	4.08	0.61	34.27	-0.29
Carbamazepine	4.15	0.62	75.00	0.46

Reference	t_R	Log t_R	Lit. HSA%	Log *K* HSA
p-nitrophenol	5.62	0.75	77.65	0.52
Estradiol	8.15	0.91	94.81	1.19
Probenecid	8.84	0.95	95.00	1.20
Glibenclamide	29.18	1.47	99.00	1.69
The retention time is shown exemplary for a conducted experiment; t_R retention time; Lit. HSA literature value of human serum albumin binding in [%]; \Log K HAS logarithmic K of human serum albumin binding.				

In vivo experiments

[0109] All animal experiments were conducted in accordance with general animal welfare regulations in Germany and the institutional guidelines for the care and use of animals. To establish tumor xenografts, LNCaP cells (10^7 cells / 200 µL) were suspended in a 1:1 mixture (v/v) of Dulbecco modified Eagle medium / Nutrition Mixture F-12 with Glutamax-I (1:1) and Matrigel (BD Biosciences, Germany), and inoculated subcutaneously onto the right shoulder of 6-8 weeks old CB17-SCID mice (Charles River, Sulzfeld, Germany). Mice were used for when tumors had grown to a diameter of 5-8 mm (3-4 weeks after inoculation).

1) Biodistribution

[0110] Approximately 1-2 MBq (< 0.2 nmol) of the ^{18}F-labeled PSMA inhibitor was injected into the tail vein of LNCaP tumor-bearing male CB-17 SCID mice and sacrificed after 1 h post injection (n = 4-5). Selected organs were removed, weighted and measured in a γ-counter

2J Metabolism studies

a) Analytical set-up

[0111] Analytical reversed-phase high pressure chromatography (RP-HPLC) were performed using Shimadzu gradient systems (Shimadzu Deutschland GmbH, Neufahrn, Germany), equipped with a SPD-20A UV/Vis detector (220 nm, 254 nm). A Multospher 100 RP18 (125 × 4.6 mm, 5 µm particle size) column (CS GmbH, Langerwehe, Germany) was used for analytical measurements at a flow rate of 1 mL/min. Eluents for all HPLC operations were water (solvent A) and acetonitrile (solvent B), both containing 0.1% trifluoroacetic acid. Radioactivity was detected through connection of the outlet of the UV-photometer to a HERM

LB 500 detector (Berthold Technologies GmbH, Bad Wildbad, Germany). The gradient for all HPLC operations was: 5% B isocratic 0-3 min, 25 - 35 % B 3-43 min, 95 - 95 % B 43-48 min.

[0112] For radio-thin-layer chromatography, aluminum sheets coated with silica gel 60 RP-18 F_{254}s were used with a mobile phase consisting of a 3:2 mixture *(v/v)* of MeCN in H_2O supplemented with 10% of 2 M aqueous NaOAc and 1% of TFA. Analysis was performed using either a Scan-RAM radio-TLC detector (LabLogic Systems Ltd., Sheffield, United Kingdom) or a CR 35 BIO phosphorimager (Duerr Medical GmbH, Bietigheim-Bissingen, Germany).

b) Determination of metabolic stability of rhPSMA-7.1 - 7.4

[0113] For *in vivo* μmetabolism studies, 8 - 12 MBq (< 0.6 nmol) of the respective ^{18}F-labeled ligand (rhPSMA-7.1 - 7.4) was injected into the tail vein of female healthy CB17-SCID mice (n=4). Mice were left under anesthesia for 30 min and the urine was collected using a bladder catheter. Urine samples were pooled and centrifuged for 5 min at 9000 rpm to remove suspended solids. The supernatant was directly used for radio-HPLC analysis with the above mentioned conditions. In order to demonstrate that isotopic exchange of ^{19}F with peptide-bound ^{18}F is taking place in urine, each compound was incubated for certain time intervals with urine samples of female healthy CB-17-SCID mice, which where analysed by radio-HPLC and/or radio-TLC. Additionally, this experiment was carried out with the addition of excess $Na^{19}F$ (0.5 μmol) and incubation for 2 h with ^{18}F-labeled rhPSMA-7.3.

c) Determination of in vivo distribution of rhPSMA-7.1 - 7.4

[0114] In order to quantify the relative uptake of each isomer (rhPSMA-7.1 - 7.4), a tumor-bearing male CB-17-SCID mouse was injected with the racemic mixture of rhPSMA-7 (180-280 MBq, S_A = 247-349 GBq/μmol, produced at the Klinikum rechts der Isar in a fully automated procedure). The animal was left under anesthesia for 30 min and sacrificed. Urine, blood, liver, kidneys and tumor were collected and processed to the hereafter described procedures. The urine sample was centrifuged for 5 min at 9000 rpm to yield a clear solution and directly subjected to radio-HPLC analysis. Blood was diluted to 1 mL with H_2O and centrifuged twice at 13000 g for 5 min. The supernatant was collected and loaded on a Strata X cartridge (33 μm Polymeric Reversed Phase 500 mg, pre-conditioned with 5 mL MeOH, followed by 5 mL H_2O). After washing with 5 mL H_2O, the cartridge was eluted with a 6:4 mixture (*v/v*) of MeCN in H_2O, supplemented with 1% TFA. The eluate was diluted with water and analysed by radio-HPLC. Tumour, kidneys and liver were homogenised using either a Potter-Elvehjem tissue grinder (Kontes Glass Co, Vineland, USA) or a MM-400 ball mill (Retsch GmbH, Haan, Germany).

I) Potter-Elvehjem tissue grinder

[0115] Tumour and kidneys were separately homogenised in the tissue homogeniser with 1 mL of extraction buffer (850 µL 1 M HEPES pH7.4, 100 µL 20 mM PMPA and 100 µL 1M NaCl) for 30 min. The resulting homogenate was collected and centrifuged at 13000 g for 5 min. Subsequently the supernatant was collected, centrifuged again (13000 g, 5 min) and loaded on a Strata X cartridge (33 µm Polymeric Reversed Phase 500 mg, pre-conditioned with 5 mL MeOH, followed by 5 mL H_2O). After washing with 5 mL H_2O, the cartridge was eluted with a 6:4 mixture *(v/v)* of MeCN in H_2O, supplemented with 1% TFA. The eluate of each organ was diluted with water and analysed by radio-HPLC.

II) MM-400 ball mill

[0116] The organs (tumour, kidney, liver) were separately homogenised in a 2 mL tube together with 3 grinding balls (3 mm diameter) and 1 mL of extraction buffer (850 µL 1 M HEPES pH7.4, 100 µL 20 mM PMPA and 100 µL 1M NaCl) for 10 min at 30 Hz. The homogenate was centrifuged at 13000 g for 5 min and the supernatant was collected. Subsequently, the pellet was suspended in 1 mL of extraction buffer and homogenized again with the ball mill for 10 min at 30 Hz. After centrifugation (13000 g, 5 min), both supernatants were combined and loaded on a Strata X cartridge (33 µm Polymeric Reversed Phase 500 mg, pre-conditioned with 5 mL MeOH, followed by 5 mL H_2O). After washing with 5 mL H_2O, the cartridge was eluted with a 6:4 mixture (*v/v*) of MeCN in H_2O, supplemented with 1% TFA. The eluate of each organ was diluted with water and analysed by radio-HPLC. In order to demonstrate that the breakthrough during cartridge loading, is not a result of unbound F-18, the supernatant was also examined by radio-TLC after centrifugation.

[0117] Finally the ratios of the individual isomers were determined from the HPLC profiles of the extracted samples and compared to the ratios of the isomers from the quality control of the racemic mixture of rhPSMA-7. The decay corrected extraction- and cartridge loading-efficiency, as well as the overall extracted activity of the examined samples are given in table 2. The cartridge elution-efficiency was >99% for all experiments.

Example 2: Results

Chromatographic Peak assignment

[0118] The chromatographic peak assignment was carried out by comparison of the UV profiles of

1. a) the rhPSMA7-rac micture with

2. b) the rhPSMA7-rac micture coninjected with each enantiopure rhPSMA7 compound.

[0119] *The following names are used for the different isomers:*

rhPSMA-rac:	[^{19}F][^{nat}Ga]D/L-Dap-R/S-DOTAGA-rhPSMA7
rhPSMA-7-1:	[^{19}F][^{nat}Ga]***D***-Dap-***R***-DOTAGA-rhPSMA7
rhPSMA-7-2:	[^{19}F][^{nat}Ga]***L***-Dap-***R***-DOTAGA-rhPSMA7
rhPSMA-7-3:	[^{19}F][^{nat}Ga]***D***-Dap-***S***-DOTAGA-rhPSMA7
rhPSMA-7-4:	[^{19}F][^{nat}Ga]***L***-Dap-***S***-DOTAGA-rhPSMA7

Table 2: Assignment of the different isomers, names, typical retention times (HPLC conditions are given in Fig. 2a-4b, and percentage of each isomer on a typical rhPSAM7-rac mixture. The exact amount can vary for each isomer.

ligand	**Name**	**t_R [min]**	**typical percentage of whole mixture**
[^{19}F][^{nat}Ga]D-Dap-R-DOTAGA-rhPSMA7	rhPSMA-7-1	31.6	21
[^{19}F][^{nat}Ga]L-Dap-R-DOTAGA-rhPSMA7	rhPSMA-7-2	28.3	22
[^{19}F][^{nat}Ga]D-Dap-S-DOTAGA-rhPSMA7	rhPSMA-7-3	28.9	37
[^{19}F][^{nat}Ga]L-Dap-S-DOTAGA-rhPSMA7	rhPSMA-7-4	30.1	20

Binding Affinities

[0120] The first set of values (rhPSMA-7.1 and rhPSMA-7.2; Fig 6a) were determined by using for the dilution series a solution directly obtained after ^{nat}Ga-complexation of the respective ligand. In the second data set (Fig 6b), the complexed ligands were purified by RP-HPLC in order to separate uncomplexed ^{nat}Ga-salts. Since there were no significant differences observed, both series were merged and used for the calculation of the mean values (±SD).

Table 3: Depiction of the individual IC_{50} [nM] measurements (as shown in Fig 6a and 6b). Conditions as described in the legend to Fig 6a.

No	**rhPSMA7.1**	**rhPSMA7.2**	**rhPSMA7.3**	**rhPSMA7.4**
1	8.74	3.17	nd	nd
2	6.91	2.97	nd	nd
3	7.27	3.36	nd	nd

No	rhPSMA7.1	rhPSMA7.2	rhPSMA7.3	rhPSMA7.4
4	5.04	2.64	3.17	3.4
5		2.76	2.91	3.56
6	7.11	3.94	5.35	2.79
7	8.31	5.8	5.74	4.57
8	4.97	4.31	4.59	3.78
9	6.44	4.32	4.45	nd
Mean	**6.85**	**3.70**	**4.37**	**3.62**
SD	1.36	1.01	1.14	0.65
* Value no 5 of the rhPSMA7.1 series was deleted (statistical outlier).				

Table 4: Binding affinities (IC_{50} [nM]) of other selected PSMA inhibitors (*).

No	Inhibitor	IC_{50} [nM]
1	(I-BA)KuE	7.1 ± 2.4 nM
2	DCFPyL	12.3 ± 1.2 nM
3	DKFZ1007	4.2 ± 0.5 nM
* carried out in our lab using the identical binding assay (Robu et al. EJNMMI Research 2018; 8:30).		

Internalization studies

[0121]

Table 5: Depiction of the individual internalization rates [% of [^{125}I]IB-KuE].

	rhPSMA7.1	rhPSMA7.2	rhPSMA7.3	rhPSMA7.4
1	61,8	188,7	156,6	209,6
1	70,6	182,7	156,0	202,6
1	68,0	169,5	171,7	209,8
1	67,9	205,3	-	-
1	71,5	212,6	-	-
1	77,5	192,3	-	-
Mean	**69,55**	**191,83**	**161,41**	**207,33**
SD	**5,19**	**15,54**	**8,88**	**4,06**

Table 6: Internalization values [% of [^{125}I]IB-KuE] of other selected PSMA inhibitors (*).

No	Inhibitor	internalization [%]
1	PSMA-1007	118 ± 4

No	Inhibitor	internalization [%]
2	DCFPyL	118 ± 5
* carried out in our lab using the identical binding assay (Robu et al. EJNMMI Research 2018; 8:30).		

Lipophilicities *(Octanol-water partition coefficient)*

[0122] Determianation of the logP values was carried out in phosphate buffered saline (PBS, pH 7.4) and n-octanol (= $logP_{oct/PBS}$).

Table 7: Individual log P measurements for rhPSMA7-isomers 7.1-7.4 isomers, determined in octanol / $PBS_{7.4}$ mixtures.

	rhPSMA7.1	rhPSMA7.2	rhPSMA7.3	rhPSMA7.4	rhPSMA7-rac
1	-2,79	-3,00	-3,03	-3,09	-3,23
2	-2,82	-3,01	-3,08	-3,12	-3,15
3	-2,80	-3,00	-3,07	-3,06	-3,17
4	-2,84	-3,00	-3,02	-3,07	-3,10
5	-2,88	-3,03	-3,06	-3,10	-3,17
6	-2,90	-2,96	-3,07	-3,04	-3,24
7	-2,85	-2,94	-3,06	-2,99	-3,80
8	-2,86	-2,89	-2,86	-2,97	-3,60
9	-3,14	-3,02	-3,39	-3,37	-3,87
10	-3,29	-3,02	-3,33	-3,43	-3,61
11	-3,26	-3,06	-3,34	-3,29	-3,76
12	-3,02	-3,02	-3,34	-3,48	-3,65
13	-3,15	-2,99	-3,20	-3,52	-3,67
14	-3,57	-3,02	-3,39	-3,50	-
15	-3,40	-3,06	-3,40	-3,44	-
16	-3,32	-3,14	-3,41	-3,41	-
17	-3,64	-3,40	-3,48	-3,56	-
18	-3,92	-3,50	-3,49	-3,61	-
19	-	-3,45	-3,32	-3,58	-
20	-	-3,45	-3,45	-3,54	-
21	-	-3,53	-3,53	-3,42	-
22	-	-3,48	-3,43	-3,57	-

	rhPSMA7.1	rhPSMA7.2	rhPSMA7.3	rhPSMA7.4	rhPSMA7-rac
23	-	-	-3,56	-3,67	-
Mean	**-3,14**	**-3,13**	**-3,26**	**-3,33**	**-3,46**
SD	**0,34**	**0,22**	**0,19**	**0,22**	**0,29**

Table 8: log P values of PSMA-1007, DCFPYL, rhPSMA7-rac and rhPSAM7.1-7.4 isomers; (n = 6), octanol/$PBS_{7.4}$.

Inhibitor	log P
PSMA-1007	-1.6
DCFPyL	-3.4
^{nat}Ga-^{18}F-rhPSMA 7-rac, ^{68}Ga-^{nat}F-rhPSMA7-rac	- 3.46 ± 0.29
^{nat}Ga-^{18}F-rhPSMA7.1	- 3.14 ± 0.34
^{nat}Ga-^{18}F-rhPSMA7.2	- 3.13 ± 0.22
^{nat}Ga-^{18}F-rhPSMA7.3	- 3.26 ± 0-19
^{nat}Ga-^{18}F-rhPSMA7.4	- 3.33 ± 0.22

Binding of PSMA inhibitors to Human Plasma Protein

[0123]

Table 9: HSA binding of of PSMA-1007, DCFPYL, rhPSMA7-rac and rhPSAM7.1-7.4 isomers; (n = 6). Determined on a Chiralpak HSA column (50 × 3 mm, 5 µm, H13H-2433).

Inhibitor	HSA Binding [%]
PSMA-1007	97.8
DCFPyL	14.3
^{68}Ga-^{nat}F-rhPSMA7-rac	96.7
^{nat}Ga-^{18}F-rhPSMA7.1	97.7
^{nat}Ga-^{18}F-rhPSMA7.2	97.8
^{nat}Ga-^{18}F-rhPSMA.3	96.9
^{nat}Ga-^{18}F-rhPSMA7.4	96.6

Biodistribution of [^{18}F][^{nat}Ga]rhPSMA7.1-7.4 at 1h pi

[0124]

Table 10: Biodistribution (in %ID/g) of ^{18}F-rhPSMAs at 1 h p.i in LNCaP tumor-bearing SCID mice. Data are expressed as mean ± SD (n=4 for rhPSMA7.1, n=5 for 7.2, n=4 for 7.3, n=5 for 7.4 and n=3 for 7-rac).

	[^{18}F][^{nat}Ga]-rhPSMA-7-1	[^{18}F][^{nat}Ga]-rhPSMA-7-2	[^{18}F][^{nat}Ga]-rhPSMA-7-3	[^{18}F][^{nat}Ga]-rhPSMA-7-4	[^{18}F][^{nat}Ga]-rhPSMA-rac
blood	0.53 ± 0.13	0.56 ± 0.20	0.96 ± 0.24	1.15 ± 0.30	1.1 ± 0.03
heart	0.53 ± 0.03	0.32 ± 0.13	0.87 ± 0.17	0.71 ± 0.26	0.69 ± 0.07
lung	1.1 ± 0.21	0.89 ± 0.38	2.2 ± 0.35	1.59 ± 0.61	1.4 ± 0.17
liver	0.75 ± 0.62	0.35 ± 0.08	0.69 ± 0.13	0.69 ± 0.20	0.67 ± 0.07
spleen	20.0 ± 4.2	10.1 ± 6.3	16.6 ± 2.6	18.4 ± 9.77	11.1 ± 2.3
pancreas	0.45 ± 0.12	0.21 ± 0.08	0.63 ± 0.44	0.50 ± 0.30	0.60 ± 0.10
stomach	0.28 ± 0.17	0.19 ± 0.08	0.44 ± 0.23	0.25 ± 0.06	0.49 ± 0.07
intestine	0.30 ± 0.16	0.18 ± 0.07	0.35 ± 0.07	0.37 ± 0.09	0.60 ± 0.27
kidneys	220 ± 24.8	87.6 ± 28.8	292 ± 45.1	153 ± 80.3	71.3 ± 13.3
adrenals	2.0 ± 0.25	1.3 ± 0.8	2.2 ± 0.83	3.57 ± 2.38	3.0 ± 0.45
muscle	0.32 ± 0.30	0.13 ± 0.07	0.33 ± 0.15	0.31 ± 0.08	0.36 ± 0.06
bone	0.50 ± 0.31	0.31 ± 0.24	0.38 ± 0.32	0.62 ± 0.30	0.91 ± 0.11
tumor	14.1 ± 4.1	6.5 ± 2.3	18.3 ± 7.2	18.9 ± 3.27	10.4 ± 0.67

Biodistribution of [^{18}F][^{nat}Ga]rhPSMA7.1-7.4 at 1h pi with competition

[0125]

Table 11: Biodistribution [%ID/g] of ^{18}F-labeled rhPSMA tracers co-injected with PMPA (8 mg/kg) at 1 h p.i in LNCaP tumor-bearing SCID mice. Data are expressed as mean ± SD (n=3).

	[^{18}F][^{nat}Ga]-rhPSMA-7-1	[^{18}F][^{nat}Ga]-rhPSMA-7-2	[^{18}F][^{nat}Ga]-rhPSMA-7-3	[^{18}F][^{nat}Ga]-rhPSMA-7-4
blood	0.86 ± 0.40	1.1 ± 0.31	0.55 ± 0.14	0.82 ± 0.17
heart	0.37 ± 0.16	0.47 ± 0.09	0.26 ± 0.04	0.37 ± 0.05
lung	0.85 ± 0.29	1.1 ± 0.32	0.69 ± 0.10	0.74 ± 0.14
liver	0.43 ± 0.07	0.46 ± 0.07	0.46 ± 0.14	0.48 ± 0.14
spleen	0.21 ± 0.08	0.26 ± 0.07	0.35 ± 0.02	0.28 ± 0.15
pancreas	0.16 ± 0.10	0.12 ± 0.05	0.11 ± 0.02	0.18 ± 0.09
stomach	0.97 ± 0.81	0.21 ± 0.06	0.76 ± 0.74	0.20 ± 0.07
intestine	0.66 ± 0.32	0.33 ± 0.10	0.94 ± 0.97	0.36 ± 0.08

	[^{18}F][^{nat}Ga]-rhPSMA-7-1	[^{18}F][^{nat}Ga]-rhPSMA-7-2	[^{18}F][^{nat}Ga]-rhPSMA-7-3	[^{18}F][^{nat}Ga]-rhPSMA-7-4
kidneys	10.9 ± 2.5	10.9 ± 1.0	15.5 ± 2.2	7.2 ± 2.4
adrenals	0.003 ± 0.004	0.07 ± 0.10	0.07 ± 0.09	0.03 ± 0.04
muscle	0.17 ± 0.15	0.09 ± 0.03	0.09 ± 0.02	0.20 ± 0.05
bone	0.33 ± 0.24	0.57 ± 0.39	0.34 ± 0.22	1.0 ± 0.8
tumor	0.94 ± 0.22	1.0 ± 0.13	1.5 ± 0.4	0.99 ± 0.19

Quantification of Relative Changes of the amount of each rhPSMA7.x isomer in Blood, Kindey, Liver, Urine and Tumor after application of [^{18}F]rhPSMA7-rac

[0126] With the aim to quantify the relative changes of each rhPSMA7 isomer in blood, liver, kidney, urine and tumor 30 min after injection of [^{18}F]rhPSMA7-rac into a LNCaP tumor bearing mouse, two different homogenization methods (a potter and a ball mill) were used to extract the tracer from kidney, liver and tumor tissue (see Materials and Methods).

[0127] Table 12 summarizes the observed efficiencies for both homogenization methods and the efficancy of the subsequent solid phase extraction procedure (to separate the tracer from the protein fraction).

Table 12: Determination of the decay corrected extracted activities from the examined tissue samples via the Potter-Elvehjem tissue grinder (n=1) and the MM-400 ball mill (n=3).

Potter-Elvehjem tissue grinder (n = 1):			
	EFFICIENCY [%]		
	Sample extraction	SPE cartridge-loading	overall
blood	93	93	86
kidney	91	66	60
tumor	90	59	53
MM-400 ball mill (n = 3):			
	EFFICIENCY [%]		
	Sample extraction	SPE cartridge-loading	overall
blood	98 ± 2	94 ± 2	92 ± 3
liver	97	89 ± 2	86 ± 2
kidney	63 ± 5	68 ± 8	43 ± 8
tumor	64 ± 18	65 ± 3	42 ± 14

[0128] Whereas the extraction of activity from the samples using the potter was quite efficient, the use of the ball mill was disappointing. Nevertheless, even with the ball mill >60% extraction efficiency was reached.

[0129] Taking into account the possible species that could be formed by metabolic cleavage of amide bonds of rhPSMA7, only a) species with significantly increase lipophilicity of b) F18-fluoride seem probable. Thus in principle it seem possible that "iL" species depicted in Fig.12 are not extracted from tissue sample (aqueous extraction) and thus do not appear in the final analysis. However, it should be noted that such species would appear in vivo in the liver and intestine (hepatobiliary excretion of lipophilic compounds) or should be bound to plasma proteins (resulting in high activity levels for the blood, which on the other hand showed excellent extraction efficiency).

[0130] For quantification of each isomer in the racemic mixture and especially for the poorly separated first and second peak (rhPSMA 7.2 and rhPSMA7.3) a graphical approximation was initially used. This approach was based on the assumption that a) each isomer is eluted from the HPLC column with an identical peak shape and b) the different peak heights can be used as first approximation to calculate by means of linear factors less separated peaks (i.e. rhPSMA 7.2 and rhPSMA7.3).

[0131] Based on these assumptions, the first analysis was performed by using one LNCaP tumor bearing mice coinjected with [^{18}F][^{nat}Ga]rhPSMA7-rac. With the aim to validate these experiments by means of three additional experiments and to improve the graphical analyses by a more valid procedure, the Systat softare package 'PeakFit' was used. PeakFit allows for automated nonlinear separation, analysis and quantification of HPLC elution profiles by deconvolution procedures that uses a Gaussian response function with a Fourier deconvolution / filtering algorithm (https://systatsoftware.com/products/peakfit/).

[0132] A comparison of the graphical analysis of the first experiments revealed that the graphical analysis overestimated the second peak (rhPSMA7.3), whereas the first peak was underestimated. Consequently, all data sets were reanalyzed and quantified by means of PeakFit.

HPLC-Analyses of 4 independent experiments in tumor bearing mice 30min p.i.

1. Evaluation of Peak 3 and 4 (rhPSMA7.4 and rhPSMA 7.1) by radio-HPLC

[0133] It was first examined, whether the deconvolution technique shows similar data for the last two peaks (rhPSMA7.4 and 7.1) that have a good separation (although they are not baseline separated).

2. Evaluation of all peaks (rhPSMA7.1, 7.2, 7.3 and 7.4) by radio-HPLC

[0134] Figures 14a and 14b summarise the percentage change of each rhPSAM7.n isomer in a given sample with respect to its percentage in the injected solution ([^{18}F][^{nat}Ga]rhPSMA7-rac); the results for the individual experiment are shown in Fig 14. The proportion of each isomer was quantified by analysis of the HPLC elution profile by Systat 'PeakFit'. Subsequently, the percentage change of each isomer in a given sample with repect to its percentage in the injected solution was calculated.

3. Discussion of the HPLC Data

[0135] The radio-HPLC analyses of the radioactivity extracted from the homogenized (kidney, liver, tumor) or diluted (blood) tissues and subsequently immobilized on and eluted from the solid phase extraction cartridge did show no signs of metabolic instability. Thus, no lipophilic metabolic fragments were observed. It should be noted that F-18-fluoride cannot be accurately detected by HPLC under the conditions used for sample preparation (see TLC analysis).

[0136] Although there is a clear trend towards the D-Dap-derivative rhPSMA7.1 and 7.3, the overall changes are low (max 15%). It is also important to stress in this context, that Fig. 15 and 16 show "relative changes" without taking the absolute uptake values into account.

[0137] Although rhPSMA7.1 has the weakest affinity and internalization of all rhPSMA7 compounds, it shows the largest positive percentage change in blood liver, kidney and tumor.

[0138] Although the reason for this result is unclear, one can speculate that homogenization of the tissue samples, even with the ball mill, did not resulted in a quantitative cell disruption. Thus, the rhPSMA7 tracers with the highest internalization (rhPSMA7.2: 191.83% ± 15.54%, rhPSMA7.4: 207.33 ± 4.06% and rhPSMA7.3: 161.41% ± 8.88%) might have been extracted in a less efficient manner, whereas rhPSMA7.1 with its low internalization of only 69.55% ± 5.29% was efficiently extracted and is consequently overestimated in the HPLC analysis.

[0139] In addition, it seems that the rhPSMA compounds 7.2 and 7.4 are somewhat more rapidly excreted (see values for urine). These compounds show generally negative changes in solid tissues and blood, although both compounds exhibit higher affinities and internalization rates when compared with rhPSMA7.1. Whether this might be caused by metabolic degradation of 7.2 and 7.4 (both are L-Dap derivative) is unclear, since no metabolites, i.e. lyophilic metabolites have been detected. It might however be possible, that such metabolites (see Fig. 11), due to their high logP value, are not extractable in aqueous buffer solutions. In this case, they should appear in the liver (see biodistribution) and perhaps in blood samples (high probability for high serum protein binding). Since no elevated activity accumulation has been observed for liver tissue in the course of the biodistribution studies and the activity

extraction from blood was highly efficient (see table 3), we assume that no significant degradation for rhPSMA7.2 and 7.4 occurred. This assumption is supported by unsuspicious SUV-values for liver tissue (gall bladder, intestine) in the context of the clinical use of [^{18}F]rhpsma-rac in humans.

TLC-Analysis in tumor bearing mice 30min p.i.

[0140] Radio-TLC Analysis was carried out a) on urine samples by directly subjecting a small volume onto a TLC strip, b) by analysis of a small volume of the non-immobilized activity during the SPE process (the 'breakthrough fraction'), and c) by analysis of a small volume of the cartridge eluates.

Table 13: TLC analysis of blood, organ and urine samples

Date	Sample	TLC Scanner		Phosphoimager		Comment *
		Intact tracer [%]	^{18}F-Fluoride [%]	Intact tracer [%]	^{18}F-Fluoride [%]	TLC signal intensity [cts] (overall very low-low)
30.07.2018	QK			*Methodological problems*		
	Blood					
	Liver					
	Kidney	94,04	5,96			369
	Urine	82,51	17,49			726
	Tumor					
01.08.2018	QK	94,27	5,73	96,02	3,98	384
	Blood					
	Liver			93,92#	6,08#	
	Kidney	94,58	5,42			572
	Urine	96,2	3,80	98,55	1,55	395
	Tumor					
02.08.2016	QK	*Activity level too low for TLC*		97,43	2,57	
	Blood			96,80	3,20	
	Liver			74,15#	25,85#	
	Kidney			96,48	3,52	
	Urine			95,85	4,15	
	Tumor			96,47	4,15	

(*) due to the low activity level, the TLC measurements with signal intensity <200cts have been deleted.

Discussion of the TLC Data

[0141] Since it is very difficult to detect n.c.a. ^{18}F-fluoride by means of RP-18 chromatography (due to free Si-OH groups of the matrix that interact with nca fluoride), thin layer chromatography was performed to investigate to quantify F-18-Fluoride in the extracted solutions.

[0142] Since none of the reagents and salts normally used for protein precipitation are tested for cold fluoride and to avoid possible liberation of F-18-fluoride from the tracer by isotopic exchange, protein precipitation was not implemented in the sample preparation process - although such protein load often result in limited peak separation, peak tailing and activity that sticks at the start line. The solutions obtained after tissue extraction (or blood centrifugation) were directly used for TLC analysis.

[0143] Although the activity available for analysis was quite low in all samples, the TLC results reveal that the overall content of F-18-fluride was below approx. 6% in the tissue investigated, except:

- the urine sample obtained on July 30, 2018 (17.49% free fluoride),
- the liver sample obtained on August 02, 2018 (25.85% free fluoride).

[0144] Whereas the analysis of the urine by TLC is regarded as valid result (see Profile in the Fig. 20), the result obtained with the liver sample is caused by extensive tailing of the peak representing the intact tracer (see Fig 18). In addition it can be concluded that the above mentioned max. 6% free fluoride represent an overestimation, since peak tailing, even obtained during the QK and release of [F-18]rhPSMA7-rac in PBS (Fig. 18) for clinical application show a tailing of the product peak. As demonstrated by the phosphoimages, this tailing is observed in almost every TLC analysis and contributes to the integrated area of F-18-fluoride.

[0145] It need to be noted that neither the biodistribution studies, nor the clinical PET scans in humans (status July 2018: approx 1400 scans with [F-18]rhPSMA7-rac) resulted in any suspicious or identifiable F-18-acculuation in bone by liberated F-18-fluoride. To further investigate the liberation of F-18 fluoride from [F-18]rhPSMA7-rac (as observed in one urine sample) we investigated the occurrence of F-18-Fluoride in further urine samples (normal mice) by means of RP-18 HPLC (new RP-18 end-capped column) and TLC analyses.

Radio-TLC-Analysis of the formation of F-18-fluoride in normal mice 30min p.i.

[0146] For this purpose normal mice were used. Urine samples were collected by means of a catheter over a period of 30 min. The urine was centrifuged and directly subjected to HPLC and TLC.

[0147] As shown in Fig 21, left column, free F-18-fluoride was found in urine samples of all isomers and is also formed when fresh urine is "incubated with [F-18]rhPSMA7.4. (right column). Identification of F-18-fluoride was performed by demonstrating that a) this species is retained on QMA cartridges (data not shown), b) is eluted in the dead volume of RP-18 columns and c) can not be retained or mobilized on RP-18 columns or RP-18 TLC plates, respectively, irrespective of the mobile phases used.

[0148] Due to the fact that such high amounts of F-18 fluoride were not detected in the HPLC analyses of blood or organs, such as kidneys, tumor, liver etc., that no elevated activity uptake in bone was observed in the biodistribution studies in mice and no elevated activity uptake in bone was observed during the clinical PET scans with the [F-18]rhPSMA7-rac compound since [F-18]rhPSMA7-rac has been established for clinical scanning end of 2017 at the TUM (status end July, 2018: approx. 1400 PET scans in patients with prostate cancer) we concluded that [F-18]fluoride might be formed downstream from glomerular filtration of the tracer, resulting in the formation and subsequent excretion of [F-18]fluoride WITHOUT detectable uptake of F-18-fluoride in blood, organs or bones.

[0149] This assumption is supported by the literature on the toxicology of fluoride that describes relevant amounts of fluoride in KIDNEYS AND URINE. Normal urinary fluoride levels of 0.3ppm were observed in mice (Bouaziz H et al., Fluoride 2005;38(1):23-31). In another publication, the average fluoride concentration in the urine of normal mice was determined to be 0.13-0.14µg/mL (Poesina ND et al. Rom J Morphol Embryol 2014, 55(2):343-349), and Inkielewicz I. et al. found that the fluoride content in the serum of rats is about 5% of the concentration of fluoride in the kidneys (serum: 0.051 µg/mL, kidneys: 0.942 µg/mL) (Fluoride; 36 (4); 263-266). Taken into account that most of the tracer is specifically taken up into and also physiologically cleared by the kidneys, an elevated fluoride level in the kidney, combined with a body temperature of 36.6°C, might result in a continuous elimination of F-18-fluoride from the rhPSMA-compounds in kidneys.

[0150] Consequently, fresh and nonradioactive urine samples collected from normal mice were incubated with [F-18]rhPSMA7.x for various time periods (see legend to Fig. 21). Fig 22, right column, clearly demonstrate that incubation of urine with [F-18]rhPSMA7.x EX VIVO result in the formation of free [F-18]fluoride to various degrees, promoted by the different concentrations of cold F-19-Fluoride in the urine samples and increasing over time.

[0151] To further support the hypothesis, 500 nmol cold F-19-fluoride was added to fresh and

nonradioactive urine of mice, followed by the addition of [F-18]rhPSMA7.3 and incubation for 2h. According to the hypothesis, the high concentration of [F-19]fluoride should result in the formation of a significant amount of [F-18]fluoride. Fig. 23 shows that under these conditions 98.5 % of the radioactivity is exchanged and forms [F-18]fluoride within 2h (Fig 23).

[0152] Since isotopic exchange rates are depending on the concentration of the four relevant species in the equilibrium ([F-18]Fluoride, [F-19]fluoride, [F-18]rhPSMA7.3 and [F-19]rhPSMA7.3), it was also investigated, whether the addition of [F-18]fluoride to fresh and radioactive urine (20,6% [F-18]Fluoride, 79,4% [F-18]rhpsma7.3) followed by the addition of cold [F-19]rhPSMA7.3 tracer also result in the labelling of the radiopharmaceutical [F-18]rhPSMA7-3. Unexpectedly, even a small amount of 5 nmol [F-19]rhPSMA7-3 to the urine above resulted in an increase of [F-18]rhPSMA7.3 from 79.4% to 85.8% (F-18]Fluoride decreased from 20.6% to 14.2%) at room temperature.

[0153] The results obtained by isotopic exchange in urine are considered representative for all tracers conjugated with the 4-(di-tert-butyl[(18)F]fluorosilyl)-benzyl)oxy moiety and thus for all rhPSAM7 isomers.

Preclinical dosimetry, human biodistribution and uptake in tumor lesions

[0154] Please note that in the following 18F-rhPSMA-7 refers to ^{nat}Ga-^{18}F-rhPSMA7-rac and 18F-rhPSMA-7.3 to ^{nat}Ga-^{18}F-rhPSMA7.3

A) Preclinical dosimetry of 18F-rhPSMA-7 and 18F-rhPSMA-7.3 in Mice

[0155] Aim was to assess the distribution and excretion of ^{18}F-rhPSMA-7 and ^{18}F-rhPSMA-7.3 at different time-points up to 300 minutes following a single intravenous administration in mice and to perform calculations for internal dosimetry.

Methods

[0156] 3-5 mice were injected per timepoint with a mean 25.6 ± 3.6 MBq of 18F-rhPSMA-7 and 28.5 ± 4.8 MBq of 18F-rhPSMA-7.3, respectively. Mice, *severe combined immunodeficiency* (SCID) were used for the experiments. All animal experiments were conducted in accordance with general animal welfare regulations in Germany and the institutional guidelines for the care and use of animals.

[0157] Mice were sacrificed at the following timepoints:

^{18}F-rhPSMA-7: 10, 20, 40, 60, 120 and 180 minutes after administration.

^{18}F-rhPSMA-7.3: 10, 60, 120, 180 and 300 minutes after administration.

Please note that based on initial experiments exhibiting prolonged renal kidney uptake for ^{18}F-rhPSMA-7.3 a late timepoint (300 min) was used for the final experiments.

[0158] The following tissues / fluids were harvested:
Urine, blood, heart, lung, spleen, pancreas, liver, stomach (emptied), small intestine (emptied), large intestine (emptied), kidneys, bladder, testis, fat, muscle (partial, femoral), femur, tail and brain. Urine was collected with a pipette in the CO_2 gas chamber. In case of missing urination in the chamber the bladder was aspirated with an insulin syringe. Blood was withdrawn instantly after sacrifice with an insulin syringe from the heart. All other tissues and organs were dissected and transferred directly in plastic containers.

[0159] The weights of the samples in the plastic containers were measured using an electronic balance. The weights of the empty and pre-labeled plastic containers for the dedicated samples were measured beforehand. The tare weight of the plastic containers was subtracted from the weight of the measurement sample with the plastic container. The thus-calculated weight was designated as the weight of the measurement sample.

[0160] The plastic containers containing the measurement samples were placed in specific racks of an automatic gamma counter (PerkinElmer - Wallac, Waltham, USA) for measuring the counting rate over 60 seconds (counts per minute = cpm). In addition, a 1% (v/v) standard (n=5) with a known amount of radioactivity was measured together with the samples to convert the counting rate of the organ samples into activity.

Data Analysis

[0161] The counting rates of measurement samples were automatically corrected for decay. The radioactivity distribution ratios (unit: percentage of the injected dose (%ID) in the measurement samples were determined using the equation below. The sum of the counting rates from all measurement samples obtained from one mouse was designated as the counting rate for administrated radioactivity.

$$\text{Percentage of injected dose (\%ID)} = \frac{\text{counting rate for measurement sample}}{\text{sum of counting rates for all measurement samples from one mouse}} * 100$$

[0162] The radioactivity distribution ratio per unit weight of the measurement sample (unit: %ID/g) excluding urine and feces samples was determined by using the equation below. The weight of the measurement sample was determined by subtraction of the empty measurement container from the container including the sample.

$$\text{Percentage of injected dose (\%ID/g)} = \frac{\text{Percentage of injected dose (\%ID)}}{\text{weight of measurement sample (g)}}$$

Dosimetry analysis

[0163] For consistency of statistical calculations for each radiotracer the same number of time-points for ^{18}F-rhPSMA-7 and ^{18}F-rhPSMA-7.3 was used. Therefore, for ^{18}F-rhPSMA-7 the 10 min and 20 min time points were combined creating a 15 min endpoint.

[0164] The time-integral of activity for the accumulation in the significant source organs (AUCs) were generated both with numerical integration and physical decay according to J Juan et al., Journal of Pharmaceutical Sciences, 1993, 82:762-763.

[0165] Kirshner et al. established a method that uses linear scaling of the percent injected dose in the animal by the ratio of the organ weights and total body weights of phantoms in both species.

- Kirschner AS, Ice RD, Beierwaltes WH. Radiation Dosimetry of 131I-19-Iodocholesterol. J Nucl Med. 1973 Sep 1;14(9):713-7.
- Kirschner A, Ice R, Beierwaltes W. Letters to the editor. J Nucl Med. (1975):248-9.

[0166] In brief, to calculate a human dosimetry from the biodistribution in the mice, an extrapolation was necessary to account for the differences between the animals and humans. Normal-organ radiation doses were estimated for the 70-kg Standard Adult anatomic model using time-depending organ activity concentrations (in percent of the injected dose per gram, %ID/g) and total-body activities measured in the biodistribution studies in mice.

[0167] Tissue activity concentrations in mice were converted to tissue fractional activities in the 70-kg Standard Adult using the relative fractional organ masses in the Standard Adult and the "standard" 25-gramm mouse. Time-dependent total-body activity was fit to an exponential function and the difference between the injected activity and the total-body activity was assumed to be excreted to the urine because activity concentrations in the liver and GI tracer were low at all time points studied.

[0168] Organ residence time was calculated by numerical integration using the trapezoidal rule and the rest-of-body ^{18}F residence times was calculated as the difference between the total-body residence time and the sum of the organ and urine residence times. The bladder contents residence time was estimated using the dynamic voiding model in the OLINDA/EXM 1.0 dosimetry software. Finally, the Standard Adult mean organ dose equivalents (in mSv/MBq) and effective dose (also in mSv/MBq) were then calculated using OLINDA/EXM 1.0.

[0169] Final calculation of radiation absorbed dose and dosimetry from biodistribution in mice: The tissues or organs in which a significant accumulation of radioactivity occurs (i.e., source organ) were kidney, spleen, lung, liver and heart. With respect to activity accumulation and clearance, a rapid clearance from blood and clearance to urine but relatively slow build-up in kidney was found.

Results

[0170]

Table 14. Dosimetry results for ^{18}F-rhPSMA-7 using a 3.5 h bladder voiding interval.

Target Organ	Alpha	Beta	Photon	Total	EDE Cont.	ED Cont.
Adrenals	0.00E000	1.95E-03	5.85E-03	7.80E-03	0.00E000	3.90E-05
Brain	0.00E000	1.95E-03	2.54E-03	4.49E-03	0.00E000	2.24E-05
Breasts	0.00E000	1.95E-03	2.29E-03	4.24E-03	6.36E-04	2.12E-04
Gallbladder Wall	0.00E000	1.95E-03	5.54E-03	7.49E-03	0.00E000	0.00E000
LLI Wall	0.00E000	1.95E-03	1.41E-02	1.61E-02	9.66E-04	1.93E-03
Small Intestine	0.00E000	1.95E-03	8.40E-03	1.04E-02	0.00E000	5.18E-05
Stomach Wall	0.00E000	1.95E-03	5.05E-03	7.00E-03	0.00E000	8.40E-04
ULI Wall	0.00E000	1.95E-03	7.31E-03	9.26E-03	0.00E000	4.63E-05
Heart Wall	0.00E000	8.82E-04	3.54E-03	4.42E-03	0.00E000	0.00E000
Kidneys	0.00E000	4.70E-02	1.80E-02	6.51E-02	3.91E-03	3.25E-04
Liver	0.00E000	6.35E-04	3.63E-03	4.27E-03	0.00E000	2.13E-04
Lungs	0.00E000	1.25E-03	3.04E-03	4.30E-03	5.16E-04	5.16E-04
Muscle	0.00E000	1.95E-03	5.73E-03	7.68E-03	0.00E000	3.84E-05
Ovaries	0.00E000	1.95E-03	1.35E-02	1.55E-02	3.87E-03	3.09E-03
Pancreas	0.00E000	1.95E-03	6.13E-03	8.08E-03	0.00E000	4.04E-05
Red Marrow	0.00E000	1.39E-03	5.41E-03	6.80E-03	8.16E-04	8.16E-04
Osteogenic Cells	0.00E000	4.18E-03	4.75E-03	8.93E-03	2.68E-04	8.93E-05
Skin	0.00E000	1.95E-03	2.98E-03	4.93E-03	0.00E000	4.93E-05
Spleen	0.00E000	1.59E-02	1.01E-02	2.61E-02	1.56E-03	1.30E-04
Testes	0.00E000	1.95E-03	9.69E-03	1.16E-02	0.00E000	0.00E000
Thymus	0.00E000	1.95E-03	3.24E-03	5.18E-03	0.00E000	2.59E-05
Thyroid	0.00E000	1.95E-03	3.23E-03	5.18E-03	1.55E-04	2.59E-04
Urinary Bladder Wall	0.00E000	2.45E-01	1.08E-01	3.54E-01	2.12E-02	1.77E-02

Target Organ	Alpha	Beta	Photon	Total	EDE Cont.	ED Cont.
Uterus	0.00E000	1.95E-03	2.61E-02	2.80E-02	1.68E-03	1.40E-04
Total Body	0.00E000	2.37E-03	5.39E-03	7.77E-03	0.00E000	0.00E000
Effective Dose Equivalent (mSv/MBq)						**3.56E-02**
Effective Dose (mSv/MBq)						**2.66E-02**

Table 15. Dosimetry results for ^{18}F-rhPSMA-7 using a 1.0 h bladder voiding interval.

Target Organ	Alpha	Beta	Photon	Total	EDE Cont.	ED Cont.
Adrenals	0.00E000	1.95E-03	5.64E-03	7.59E-03	0.00E000	3.79E-05
Brain	0.00E000	1.95E-03	2.54E-03	4.49E-03	0.00E000	2.24E-05
Breasts	0.00E000	1.95E-03	2.25E-03	4.20E-03	6.30E-04	2.10E-04
Gallbladder Wall	0.00E000	1.95E-03	4.96E-03	6.91E-03	0.00E000	0.00E000
LLI Wall	0.00E000	1.95E-03	7.25E-03	9.20E-03	5.52E-04	1.10E-03
Small Intestine	0.00E000	1.95E-03	5.79E-03	7.73E-03	0.00E000	3.87E-05
Stomach Wall	0.00E000	1.95E-03	4.70E-03	6.65E-03	0.00E000	7.98E-04
ULI Wall	0.00E000	1.95E-03	5.33E-03	7.27E-03	0.00E000	3.64E-05
Heart Wall	0.00E000	8.82E-04	3.48E-03	4.36E-03	0.00E000	0.00E000
Kidneys	0.00E000	4.70E-02	1.76E-02	6.47E-02	3.88E-03	3.23E-04
Liver	0.00E000	6.35E-04	3.39E-03	4.02E-03	0.00E000	2.01E-04
Lungs	0.00E000	1.25E-03	3.01E-03	4.26E-03	5.11E-04	5.11E-04
Muscle	0.00E000	1.95E-03	4.01E-03	5.96E-03	0.00E000	2.98E-05
Ovaries	0.00E000	1.95E-03	7.21E-03	9.16E-03	2.29E-03	1.83E-03
Pancreas	0.00E000	1.95E-03	5.86E-03	7.80E-03	0.00E000	3.90E-05
Red Marrow	0.00E000	1.39E-03	4.29E-03	5.68E-03	6.82E-04	6.82E-04
Osteogenic Cells	0.00E000	4.18E-03	4.09E-03	8.27E-03	2.48E-04	8.27E-05
Skin	0.00E000	1.95E-03	2.38E-03	4.32E-03	0.00E000	4.32E-05
Spleen	0.00E000	1.59E-02	9.90E-03	2.58E-02	1.55E-03	1.29E-04
Testes	0.00E000	1.95E-03	5.09E-03	7.03E-03	0.00E000	0.00E000
Thymus	0.00E000	1.95E-03	3.20E-03	5.15E-03	0.00E000	2.57E-05
Thyroid	0.00E000	1.95E-03	3.23E-03	5.17E-03	1.55E-04	2.59E-04
Urinary Bladder Wall	0.00E000	7.87E-02	3.66E-02	1.15 E-01	6.92E-03	5.76E-03
Uterus	0.00E000	1.95E-03	1.12E-02	1.31E-02	7.87E-04	6.56E-05
Total Body	0.00E000	2.27E-03	3.93E-03	6.19E-03	0.00E000	0.00E000
Effective Dose Equivalent (mSv/MBq)						**1.82E-02**

Target Organ	Alpha	Beta	Photon	Total	EDE Cont.	ED Cont.
Effective Dose (mSv/MBq)						**1.22E-02**

Table 16. Dosimetry results for ^{18}F-rhPSMA-7.3 using a 3.5 h bladder voiding interval.

Target Organ	Alpha	Beta	Photon	Total	EDE Cont.	ED Cont.
Adrenals	0.00E000	3.12E-03	7.93E-03	1.10E-02	0.00E000	5.52E-05
Brain	0.00E000	3.12E-03	4.07E-03	7.19E-03	0.00E000	3.59E-05
Breasts	0.00E000	3.12E-03	3.55E-03	6.67E-03	1.00E-03	3.34E-04
Gallbladder Wall	0.00E000	3.12E-03	7.46E-03	1.06E-02	0.00E000	0.00E000
LLI Wall	0.00E000	3.12E-03	1.28E-02	1.59E-02	9.53E-04	1.91E-03
Small Intestine	0.00E000	3.12E-03	9.42E-03	1.25E-02	0.00E000	6.27E-05
Stomach Wall	0.00E000	3.12E-03	7.02E-03	1.01E-02	0.00E000	1.22E-03
ULI Wall	0.00E000	3.12E-03	8.57E-03	1.17E-02	0.00E000	5.85E-05
Heart Wall	0.00E000	1.32E-03	5.39E-03	6.71E-03	0.00E000	0.00E000
Kidneys	0.00E000	5.11E-02	2.07E-02	7.18E-02	4.31E-03	3.59E-04
Liver	0.00E000	9.70E-04	5.02E-03	5.99E-03	0.00E000	3.00E-04
Lungs	0.00E000	1.95E-03	4.66E-03	6.61E-03	7.93E-04	7.93E-04
Muscle	0.00E000	3.12E-03	6.55E-03	9.67E-03	0.00E000	4.83E-05
Ovaries	0.00E000	3.12E-03	1.26E-02	1.57E-02	3.92E-03	3.14E-03
Pancreas	0.00E000	3.12E-03	8.29E-03	1.14E-02	0.00E000	5.70E-05
Red Marrow	0.00E000	2.22E-03	6.79E-03	9.01E-03	1.08E-03	1.08E-03
Osteogenic Cells	0.00E000	6.70E-03	6.52E-03	1.32E-02	3.97E-04	1.32E-04
Skin	0.00E000	3.12E-03	3.83E-03	6.95E-03	0.00E000	6.95E-05

Target Organ	Alpha	Beta	Photon	Total	EDE Cont.	ED Cont.
Spleen	0.00E000	1.52E-02	1.15E-02	2.67E-02	1.60E-03	1.34E-04
Testes	0.00E000	3.12E-03	8.96E-03	1.21E-02	0.00E000	0.00E000
Thymus	0.00E000	3.12E-03	5.08E-03	8.20E-03	0.00E000	4.10E-05
Thyroid	0.00E000	3.12E-03	5.15E-03	8.27E-03	2.48E-04	4.14E-04
Urinary Bladder Wall	0.00E000	1.56E-01	7.14E-02	2.27E-01	1.36E-02	1.14E-02
Uterus	0.00E000	3.12E-03	2.04E-02	2.36E-02	1.41E-03	1.18E-04
Total Body	0.00E000	3.52E-03	6.33E-03	9.86E-03	0.00E000	0.00E000
Effective Dose Equivalent (mSv/MBq)						**2.94E-02**
Effective Dose (mSv/MBq)						**2.17E-02**

Table 17. Dosimetry results for ^{18}F-rhPSMA-7.3 using a 1.0 h bladder voiding interval.

Target Organ	Alpha	Beta	Photon	Total	EDE Cont.	ED Cont.
Adrenals	0.00E000	3.12E-03	7.79E-03	1.09E-02	0.00E000	5.46E-05
Brain	0.00E000	3.12E-03	4.06E-03	7.18E-03	0.00E000	3.59E-05
Breasts	0.00E000	3.12E-03	3.53E-03	6.65E-03	9.97E-04	3.32E-04
Gallbladder Wall	0.00E000	3.12E-03	7.11E-03	1.02E-02	0.00E000	0.00E000
LLI Wall	0.00E000	3.12E-03	8.45E-03	1.16E-02	6.94E-04	1.39E-03
Small Intestine	0.00E000	3.12E-03	7.78E-03	1.09E-02	0.00E000	5.45E-05
Stomach Wall	0.00E000	3.12E-03	6.80E-03	9.92E-03	0.00E000	1.19E-03
ULI Wall	0.00E000	3.12E-03	7.33E-03	1.05E-02	0.00E000	5.23E-05
Heart Wall	0.00E000	1.32E-03	5.36E-03	6.68E-03	0.00E000	0.00E000

Target Organ	Alpha	Beta	Photon	Total	EDE Cont.	ED Cont.
Kidneys	0.00E000	5.11E-02	2.04E-02	7.16E-02	4.29E-03	3.58E-04
Liver	0.00E000	9.70E-04	4.87E-03	5.84E-03	0.00E000	2.92E-04
Lungs	0.00E000	1.95E-03	4.63E-03	6.58E-03	7.90E-04	7.90E-04
Muscle	0.00E000	3.12E-03	5.47E-03	8.59E-03	0.00E000	4.30E-05
Ovaries	0.00E000	3.12E-03	8.61E-03	1.17E-02	2.93E-03	2.35E-03
Pancreas	0.00E000	3.12E-03	8.12E-03	1.12E-02	0.00E000	5.62E-05
Red Marrow	0.00E000	2.22E-03	6.09E-03	8.31E-03	9.97E-04	9.97E-04
Osteogenic Cells	0.00E000	6.70E-03	6.11E-03	1.28E-02	3.84E-04	1.28E-04
Skin	0.00E000	3.12E-03	3.45E-03	6.57E-03	0.00E000	6.57E-05
Spleen	0.00E000	1.52E-02	1.14E-02	2.66E-02	1.59E-03	1.33E-04
Testes	0.00E000	3.12E-03	6.08E-03	9.20E-03	0.00E000	0.00E000
Thymus	0.00E000	3.12E-03	5.06E-03	8.18E-03	0.00E000	4.09E-05
Thyroid	0.00E000	3.12E-03	5.15E-03	8.27E-03	2.48E-04	4.13E-04
Urinary Bladder Wall	0.00E000	5.18E-02	2.66E-02	7.84E-02	4.70E-03	3.92E-03
Uterus	0.00E000	3.12E-03	1.11E-02	1.43E-02	8.55E-04	7.13E-05
Total Body	0.00E000	3.45E-03	5.42E-03	8.87E-03	0.00E000	0.00E000
Effective Dose Equivalent (mSv/MBq)						**1.85E-02**
Effective Dose (mSv/MBq)						**1.28E-02**

Conclusion

[0171] The radioactivity distribution ratios were highest in kidneys after administration of both ^{18}F-rhPSMA-7 and ^{18}F-rhPSMA-7.3 at all examined time points in mice. Moreover, it was high in the spleen and in the bladder for both radiotracers compared to all other assessed tissues, where activity ratios were lower than 8%ID/g.

[0172] Since the majority of ^{18}F-rhPSMA-7/ ^{18}F-rhPSMA-7.3 activity augment in the kidneys and the excretion via bladder reveal high activities, the main excretion route is defined via kidneys and the urinary system.

[0173] Using a 3.5h and 1.0h bladder voiding interval the extrapolated total effective doses were 2.66E-02 and 1.22E-02 mSv/MBq for ^{18}F-rhPSMA-7 and 2.17E-02 and 1.28E-02 mSv/MBq for ^{18}F-rhPSMA-7.3, respectively. An injection of up to 370 MBq (10 mCi) for a clinical scan would result in a favorable radiation exposure of less than 5 mSv for both agents assuming a 1h voiding interval.

[0174] Differences worth to mention between both radiotracers are only evident regarding kidney uptake as ^{18}F-rhPSMA-7.3 tends to accumulate more gradual with longer retention. Yet radiation exposure is comparable between both agents.

***B) H*uman biodistribution and uptake in tumor lesions of 18F-rhPSMA-7 and 18F-rhPSMA-7.3**

[0175] The following sections describe biodistribution of 18F-rhPSMA-7 and 18F-rhPSMA-7.3. Proof-of-concept evaluation was conducted under compassionate use. The agent was applied in compliance with The German Medicinal Products Act, AMG §13 2b, and in accordance with the responsible regulatory body (Government of Oberbayern).

[0176] All subjects were examined on a Biograph mCT scanner (Siemens Medical Solutions, Erlangen, Germany). All PET scans were acquired in 3D-mode with an acquisition time of 2-4 min per bed position. Emission data were corrected for randoms, dead time, scatter, and attenuation and were reconstructed iteratively by an ordered-subsets expectation maximization algorithm (four iterations, eight subsets) followed by a postreconstruction smoothing Gaussian filter (5-mm full width at one-half maximum).

Methods

[0177] Human biodistribution was estimated by analysing clinical ^{18}F-rhPSMA-7- and ^{18}F-rhPSMA-7.3-PET/CT exams in 47 and 32 patients, respectively. Mean injected activities were 324 (range 236-424) MBq vs. 345 (range 235-420) MBq and uptake times were 84 (range 42-

166) min and vs. 76 (range 59-122) min for ^{18}F-rhPSMA-7 vs. ^{18}F-rhPSMA-7.3, respectively.

[0178] The mean and maximum standardized uptake values (SUVmean/SUVmax) were determined for background (gluteal muscle), normal organs (salivary glands, blood pool, lung, liver, spleen, pancreas, duodenum, kidney, bladder, bone) and three representative tumor lesions. Tumor uptake was analyzed in 89 lesions (26 primary tumors/local recurrences, 23 bone, 38 lymph node and 2 visceral metastases) and 63 lesions (14 primary tumors/local recurrences, 30 bone, 18 lymph node and 1 visceral metastases) for ^{18}F-rhPSMA-7 and ^{18}F-rhPSMA-7.3, respectively.

[0179] For calculation of the SUV, circular regions of interest were drawn around areas with focally increased uptake in transaxial slices and automatically adapted to a three-dimensional volume of interest (VOI) at a 50 % isocontour. Organ-background and Tumor-background ratios were calculated.

Results

[0180] Human biodistribution of ^{18}F-rhPSMA-7 and ^{18}F-rhPSMA-7.3 showed the typical pattern known from other PSMA-ligands. Uptake parameters for ^{18}F-rhPSMA-7 and ^{18}F-rhPSMA-7.3 were very similar with a lower activity retention in the bladder and higher uptake in tumor lesions for ^{18}F-rhPSMA-7.3: SUVmean for ^{18}F-rhPSMA-7 vs. ^{18}F-rhPSMA-7.3 were 16.9 vs. 16.0 (parotid gland), 19.6 vs. 19.6 (submandibular gland), 2.0 vs. 1.9 (blood pool), 0.7 vs. 0.7 (lungs), 7.0 vs. 7.3 (liver), 9.1 vs. 8.5 (spleen), 32.4 vs. 35.5 (kidney), 2.5 vs. 2.8 (pancreas), 10.9 vs. 11.0 (duodenum), 1.1 vs. 1.3 (non-diseased bone) and 10.2 vs. 2.0 (bladder) for ^{18}F-rhPSMA-7 vs. ^{18}F-rhPSMA-7.3, respectively. In particular, uptake values of ^{18}F-rhPSMA-7.3 vs. ^{18}F-rhPSMA-7 were significantly lower for retention in the bladder (2.0 ± 0.8 vs. 6.3 ± 21.2, $p < 0.05$) and significantly higher for tumor lesions (32.5 ± 42.7 vs. 20.0 ± 20.2, $p < 0.05$).

Table 18. SUVmax and SUVmean of normal organs and tumor lesions using ^{18}F-rhPSMA-7. Data are shown as mean, minimum and maximum.

	SUVmax			SUVmean		
	mean	min	max	mean	min	max
background	1,0	0,6	1,8	0,6	0,4	1,2
parotic gland	23,8	8,2	42,3	16,9	5,5	32,7
submandibular gland	27,0	10,1	43,8	19,6	7,0	29,7
bloodpool	2,4	1,6	3,9	2,0	1,1	17,0
lungs	1,1	0,5	3,1	0,7	0,3	2,0
liver	9,5	4,5	25,2	7,0	3,2	17,7
spleen	11,8	4,7	21,0	9,1	3,4	17,1

	SUVmax			SUVmean		
	mean	min	max	mean	min	max
kidney	44,8	19,1	75,2	32,4	13,2	54,7
pancreas	3,7	1,8	7,9	2,5	1,3	5,5
duodenum	14,8	2,8	32,7	10,9	1,9	23,9
bone	1,7	0,8	3,1	1,1	0,6	2,1
bladder	8,5	0,5	112,0	6,3	0,3	85,7
tumor	27,6	3,1	167,2	20,0	2,1	115,7

Table 19. SUVmax and SUVmean of normal organs and tumor lesions using ^{18}F-rhPSMA-7.3. Data are shown as mean, minimum and maximum.

	SUVmax			SUVmean		
	mean	min	max	mean	min	max
background	1,0	0,6	1,7	0,7	0,4	1,1
parotic gland	24,6	11,2	38,3	16,0	8,2	25,0
submandibular gland	28,4	14,6	47,4	19,6	10,4	33,4
bloodpool	2,8	1,9	3,9	1,8	1,3	2,5
lungs	1,1	0,7	1,9	0,7	0,4	1,1
liver	9,7	4,6	15,4	7,3	3,2	12,3
spleen	11,4	5,0	22,5	8,5	3,7	17,9
kidney	51,9	30,9	99,9	35,5	20,7	70,6
pancreas	4,2	2,4	7,8	2,8	1,6	5,2
duodenum	16,4	6,1	32,2	11,0	3,0	23,0
bone	2,1	1,1	3,4	1,3	0,7	2,2
bladder	3,1	1,1	6,0	2,0	0,7	4,1
tumor	44,0	2,4	316,0	32,5	1,6	224,1

Table 20. Ratio SUVmax and SUVmean to background of normal organs and tumor lesions using ^{18}F-rhPSMA-7. Data are shown as mean, minimum and maximum.

	ratio SUVmax			ratio SUVmean		
	mean	min	max	mean	min	max
parotid gland	25,2	8,2	45,3	28,3	9,2	54,5
submandibular gland	28,7	10,1	54,7	33,3	11,7	61,8
bloodpool	2,5	1,3	4,8	3,2	1,6	21,3
lungs	1,1	0,4	3,3	1,1	0,4	4,0
liver	10,4	4,7	42,0	11,9	4,6	44,3

	ratio SUVmax			ratio SUVmean		
	mean	min	max	mean	min	max
spleen	12,5	4,7	35,0	15,1	5,7	39,5
kidney	48,1	18,2	98,7	55,2	19,8	109,3
pancreas	3,9	1,5	11,3	4,3	1,9	10,8
duodenum	15,7	2,8	31,3	18,4	3,2	35,3
bone	1,7	0,9	2,9	1,8	1,0	3,2
bladder	8,7	0,6	112,0	10,2	0,5	142,8
tumor	32,0	3,1	278,6	36,0	3,5	289,3

Table 21. Ratio SUVmax and SUVmean to background of normal organs and tumor lesions using ^{18}F-rhPSMA-7.3. Data are shown as mean, minimum and maximum.

	ratio SUVmax			ratio SUVmean		
	mean	min	max	mean	min	max
parotid gland	24,7	11,9	46,2	25,2	12,4	44,6
submandibular gland	28,2	14,0	62,1	30,6	15,7	62,3
bloodpool	2,8	1,5	5,2	2,9	1,7	4,9
lungs	1,0	0,6	1,8	1,0	0,6	1,8
liver	9,7	4,0	19,0	11,4	4,1	20,7
spleen	11,4	3,6	22,4	13,3	3,9	28,6
kidney	51,8	25,7	93,0	55,6	27,6	95,5
pancreas	4,1	2,2	6,9	4,4	2,3	7,8
duodenum	16,2	6,9	34,3	17,1	4,7	39,4
bone	2,0	1,1	3,2	2,1	1,0	3,6
bladder	3,1	0,9	5,5	3,1	0,9	6,8
tumor	43,6	1,7	321,2	50,8	1,8	356,4

Conclusion:

[0181] Human biodistribution is similar between ^{18}F-rhPSMA-7 and ^{18}F-rhPSMA-7.3 for most normal organs. However, tracer retention in the bladder is significantly lower and uptake in tumor lesions significantly higher for ^{18}F-rhPSMA-7.3 posing a clear advantage for clinical imaging. Imaging examples with favorable human biodistribution and high uptake of tumor lesions of ^{18}F-rhPSMA-7.3 are shown in figure 28.

REFERENCES CITED IN THE DESCRIPTION

Cited references

This list of references cited by the applicant is for the reader's convenience only. It does not form part of the European patent document. Even though great care has been taken in compiling the references, errors or omissions cannot be excluded and the EPO disclaims all liability in this regard.

Patent documents cited in the description

- WO2019020831A [0019] [0019]

Non-patent literature cited in the description

- **ZHANG et al.**Journal of the American Chemical Society, 2010, vol. 132, 12711-12716 [0005] [0009]
- **LIU et al.**Bioorganic & medicinal chemistry letters, 2011, vol. 21, 7013-7016 [0005]
- **ROWE et al.**Molecular Imaging and Biology, 2016, 1-9 [0008]
- **DIETLEIN et al.**Molecular Imaging and Biology, 2015, vol. 17, 575-584 [0008]
- **CARDINALE et al.**Journal of nuclear medicine: official publicationSociety of Nuclear Medicine20170000vol. 58, 425-431 [0008]
- **GIESEL et al.**European journal of nuclear medicine and molecular imaging, 2016, vol. 43, 1929-1930 [0008]
- **GIESEL et al.**European journal of nuclear medicine and molecular imaging, 2017, vol. 44, 678-688 [0008]
- **LINDNER et al.**Bioconjugate Chemistry, 2014, vol. 25, 738-749 [0009]
- **SCHIRRMACHER E. et al.**Bioconjugate Chem, 2007, vol. 18, 2085-2089 [0011]
- **WÄNGLER C. et al.**Bioconjugate Chem., 2009, vol. 20, 2317-321 [0012]
- **WÄNGLER C. et al.**Bioconjug Chem., 2010, vol. 21, 122289-96 [0013]
- **BERNARD-GAUTHIER et al.**Biomed Res Int., 2014, vol. 2014, 454503- [0014]
- **LINDNER S. et al.**Bioconjug Chem., 2014, vol. 25, 4738-49 [0015]
- **NIEDERMOSER S. et al.**J Nucl Med., 2015, vol. 56, 71100-5 [0016]
- **S. LITAU et al.**Bioconjugate Chem., 2015, vol. 26, 2350-2359 [0016]

- **SANGSTER**Octanol-water Partition Coefficients: fundamentals and physical chemistryJohn Wiley & Sons19970000 [0034]
- **ROBU et al.**EJNMMI Research, 2018, vol. 8, 30- [0120] [0121]
- **BOUAZIZ H et al.**Fluoride, 2005, vol. 38, 123-31 [0149]
- **POESINA ND et al.**Rom J Morphol Embryol, 2014, vol. 55, 2343-349 [0149]
- **INKIELEWICZ I.**Fluoride, vol. 36, 4263-266 [0149]
- **J JUAN et al.**Journal of Pharmaceutical Sciences, 1993, vol. 82, 762-763 [0164]
- **KIRSCHNER ASICE RDBEIERWALTES WH**Radiation Dosimetry of 131I-19-Iodocholesterol.J Nucl Med., 1973, vol. 14, 9713-7 [0165]
- **KIRSCHNER AICE RBEIERWALTES W**Letters to the editor.J Nucl Med., 1975, 248-9 [0165]

Patentkrav

1. Forbindelse:

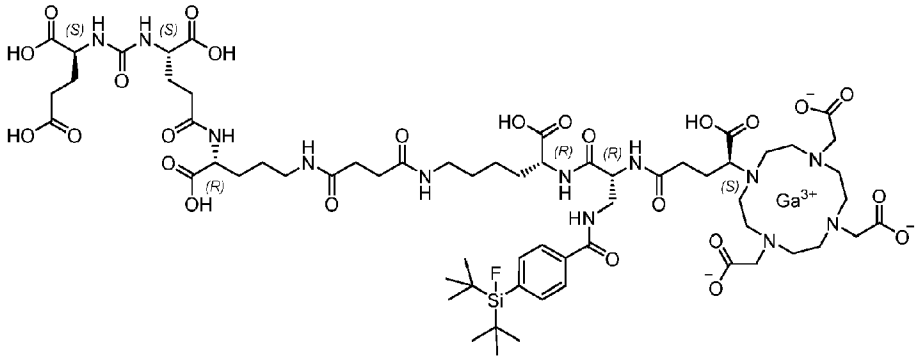

;

eller et farmaceutisk acceptabelt salt deraf, hvor F enten er ^{18}F eller ^{19}F.

2. Forbindelse ifølge krav 1, hvor F er ^{18}F.

3. Forbindelse ifølge krav 1, hvor F er ^{19}F.

4. Forbindelse ifølge et hvilket som helst af kravene 1 til 3, hvor Ga^{3+} er $^{nat}Ga^{3+}$.

5. Forbindelse ifølge krav 1, hvor F er ^{18}F, og Ga^{3+} er $^{nat}Ga^{3+}$.

6. Fremgangsmåde til syntese af en forbindelse ifølge krav 1, som omfatter følgende trin:

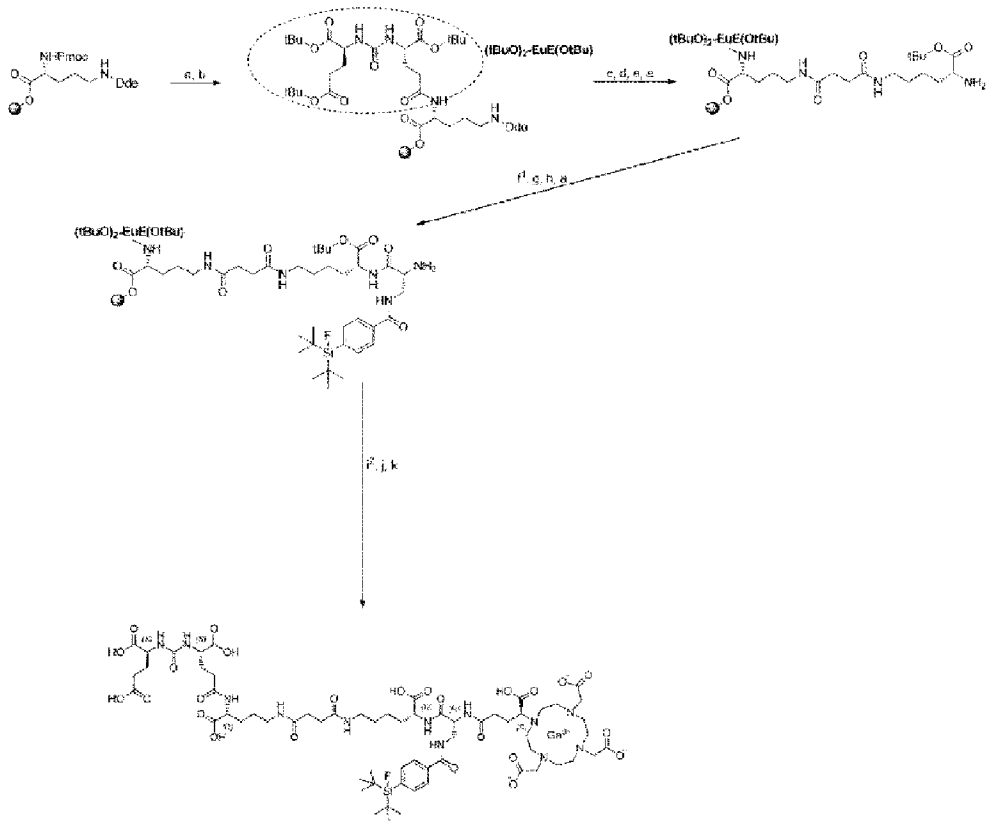

;

hvor procedurerne som vist ved a, b, c, d, e, f^1, g, h, i^2, j og k er som følger:

a) 20 % piperidin, (DMF);

b) (tBuO)EuE(OtBu)$_2$, HOAt, TBTU, DIPEA, (DMF);

c) 2 % hydrazin (DMF);

d) ravsyreanhydrid, DIPEA, (DMF);

e) Fmoc-D-Lys(OtBu)·HCl, HOAt, TBTU, DIPEA, (DMF);

f^1) Fmoc-D-Dap(Dde)-OH, HOAt, TBTU, 2,4,6-collidin, (DMF);

g) imidazol, hydroxylaminhydrochlorid, (NMP, DMF);

h) SiFA-BA, HOAt, TBTU, DIPEA (DMF);

i^2) (S)-DOTA-GA(tBu)4, HOAt, TBTU, 2,4,6-collidin (DMF);

j) spaltning og afbeskyttelse: TFA, TIPS, H_2O;

k) $Ga(NO_3)_3$, (tBuOH, H_2O).

7. Fremgangsmåde ifølge krav 6, som yderligere omfatter et efterfølgende trin med ^{18}F-mærkning.

8. Farmaceutisk eller diagnostisk sammensætning, som omfatter forbindelsen ifølge et hvilket som helst af kravene 1 til 5.

9. Forbindelse ifølge et hvilket som helst af kravene 1 til 5

eller sammensætning ifølge krav 8 til anvendelse som et cancerdiagnostisk eller -billedanalytisk middel.

10. Forbindelse ifølge et hvilket som helst af kravene 1 til 5 eller sammensætning ifølge krav 8 til anvendelse til behandling af cancer.

11. Forbindelse ifølge et hvilket som helst af kravene 1 til 5 eller sammensætning ifølge krav 8 til diagnosticering, billedanalyse eller forebyggelse af neoangiogenese/angiogenese.

12. Forbindelse ifølge et hvilket som helst af kravene 1 til 5 eller sammensætning ifølge krav 8 til anvendelse som et cancerdiagnostisk eller billedanalytisk middel eller til anvendelse til behandling af cancer, hvor canceren er prostata-, bryst-, lunge- eller kolorektal cancer eller renalcellekarcinom.

DRAWINGS

Drawing

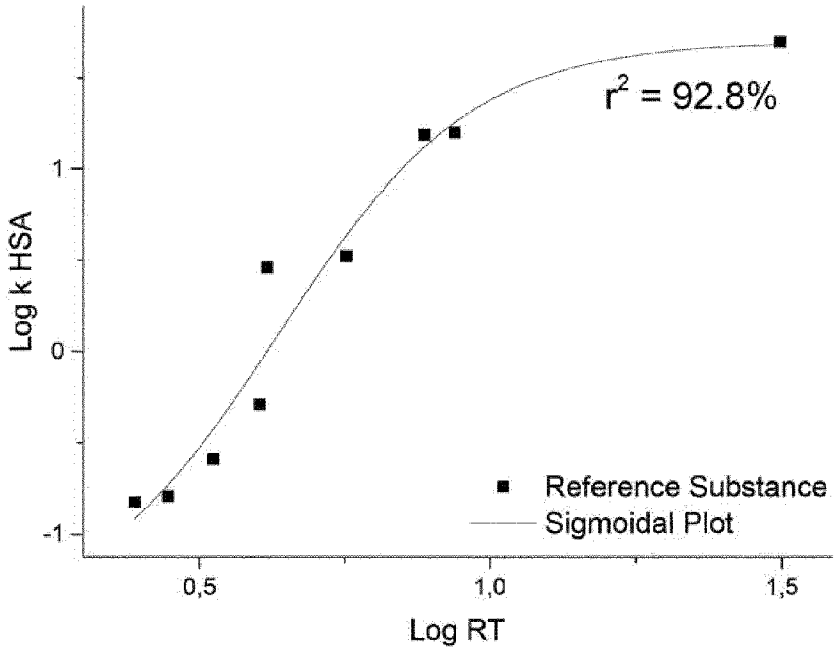

Fig. 1

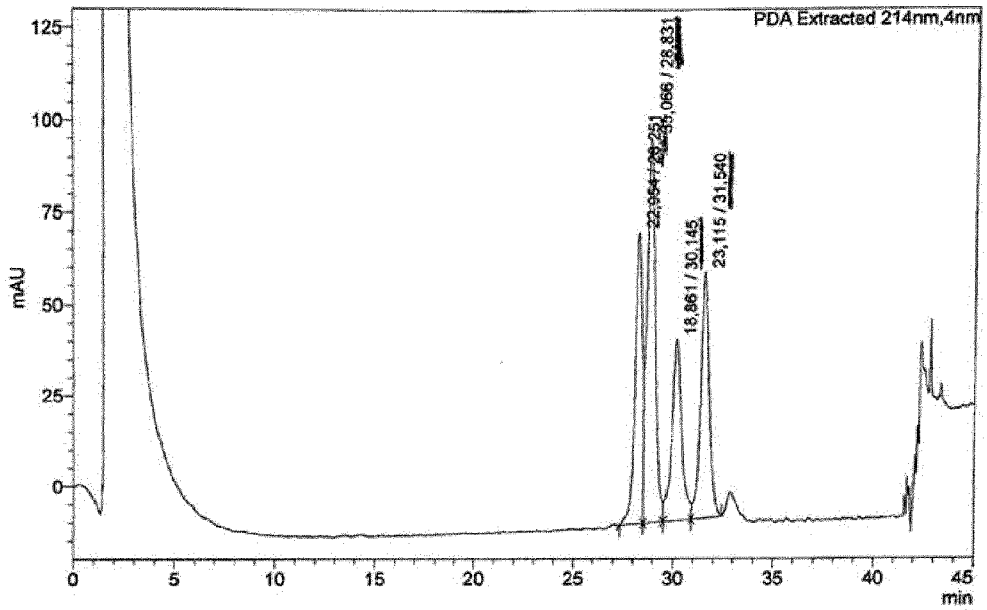

Fig. 2a

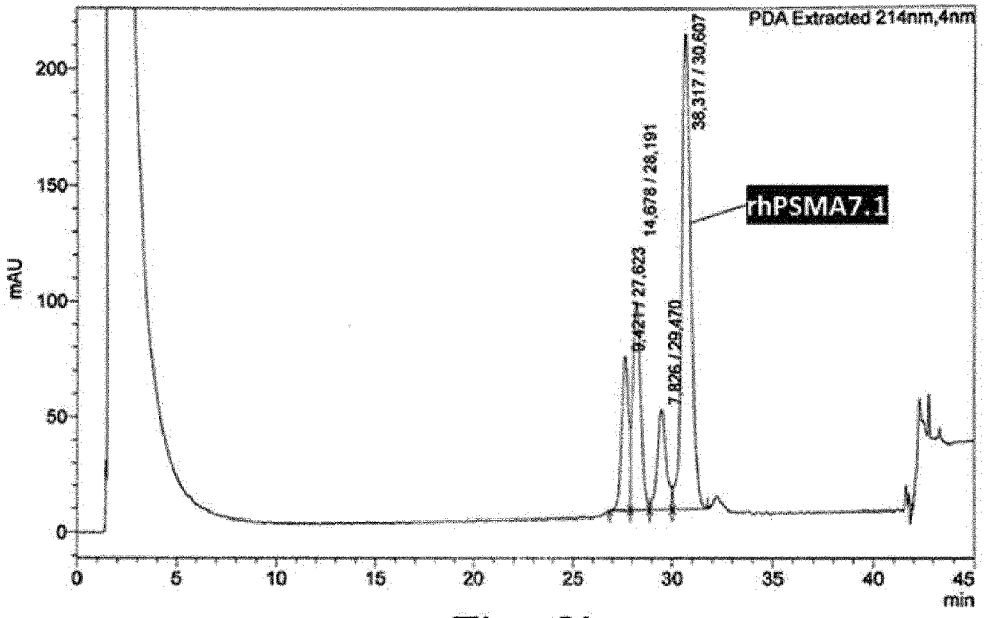
PDA Extracted 214nm,4nm
38,317 / 30,607
14,678 / 28,191
8,421 / 27,623
7,826 / 29,470
rhPSMA7.1
mAU
min

Fig. 2b

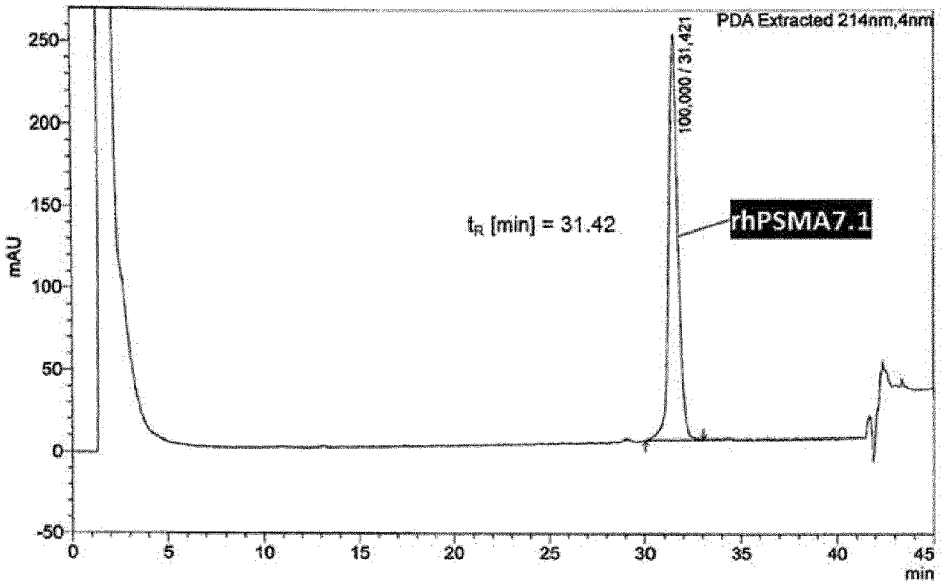
PDA Extracted 214nm,4nm
100,000 / 31,421
t_R [min] = 31.42
rhPSMA7.1
mAU
min

Fig. 2c

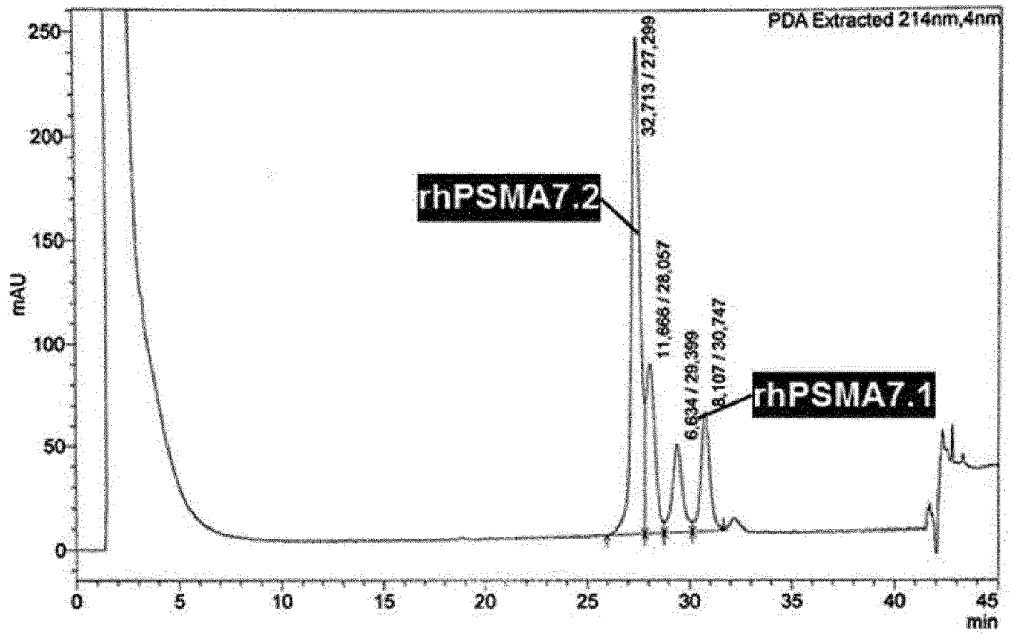
PDA Extracted 214nm,4nm
32,713 / 27,299
11,666 / 28,057
6,634 / 29,399
8,107 / 30,747
rhPSMA7.2
rhPSMA7.1
mAU
min

Fig. 3a

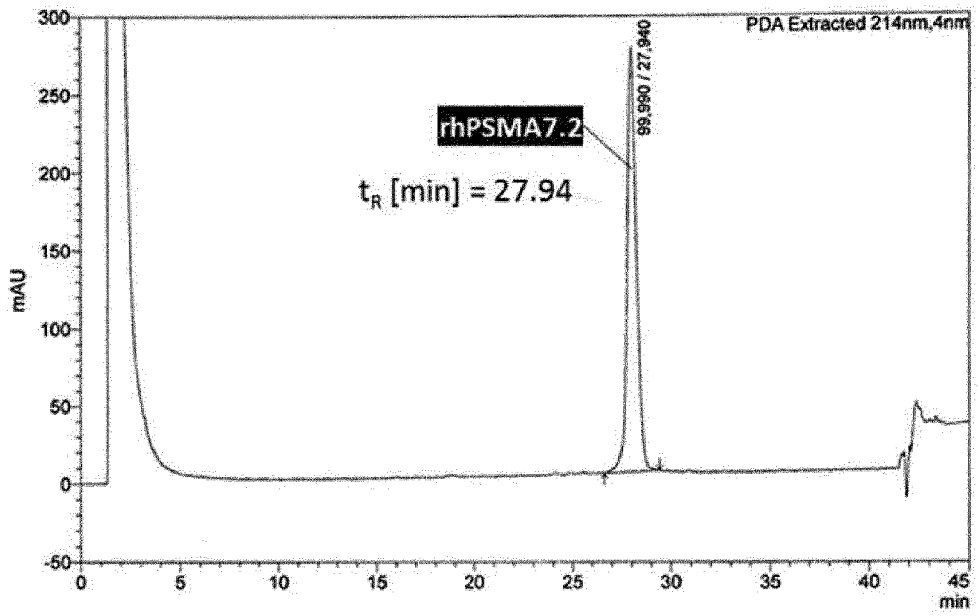
PDA Extracted 214nm,4nm
99,990 / 27,940
rhPSMA7.2
t_R [min] = 27.94
mAU
min

Fig. 3b

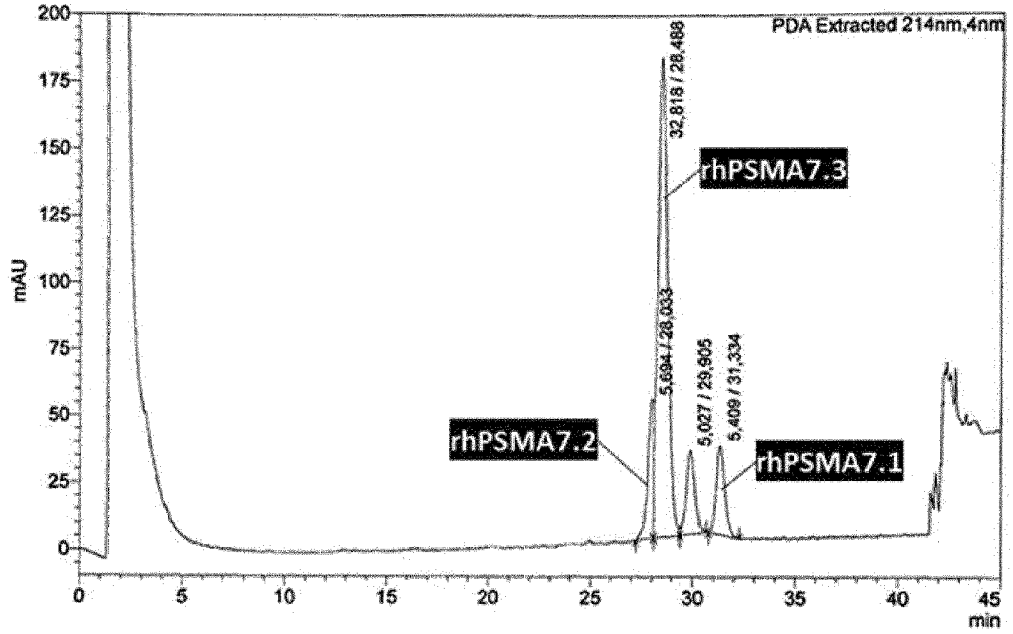
PDA Extracted 214nm,4nm
32,818 / 28,488
5,694 / 28,033
5,027 / 29,905
5,409 / 31,334
rhPSMA7.3
rhPSMA7.2
rhPSMA7.1
mAU
min

Fig. 4a

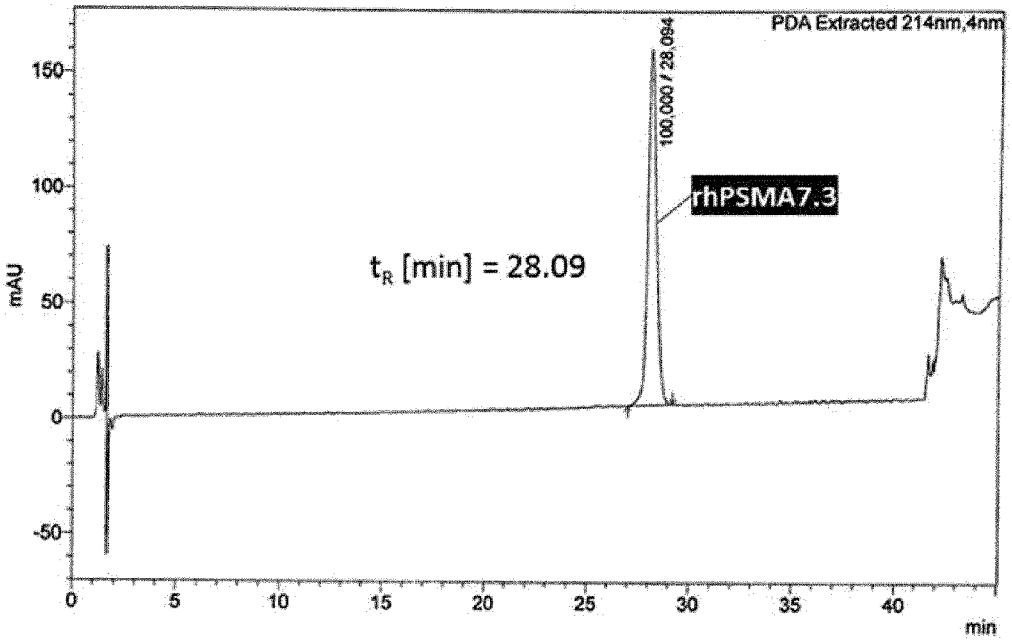
PDA Extracted 214nm,4nm
100,000 / 28,094
rhPSMA7.3
t_R [min] = 28.09
mAU
min

Fig. 4b

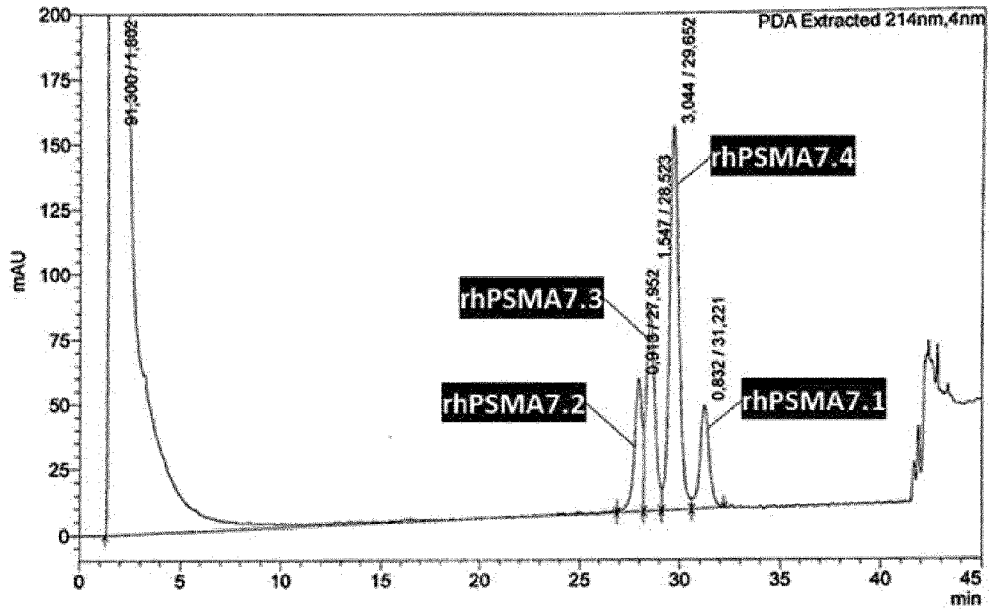
PDA Extracted 214nm,4nm
91,300 / 1,692
3,044 / 29,652
1,547 / 28,523
0,915 / 27,952
0,832 / 31,221
rhPSMA7.4
rhPSMA7.3
rhPSMA7.2
rhPSMA7.1
mAU
min

Fig. 5a

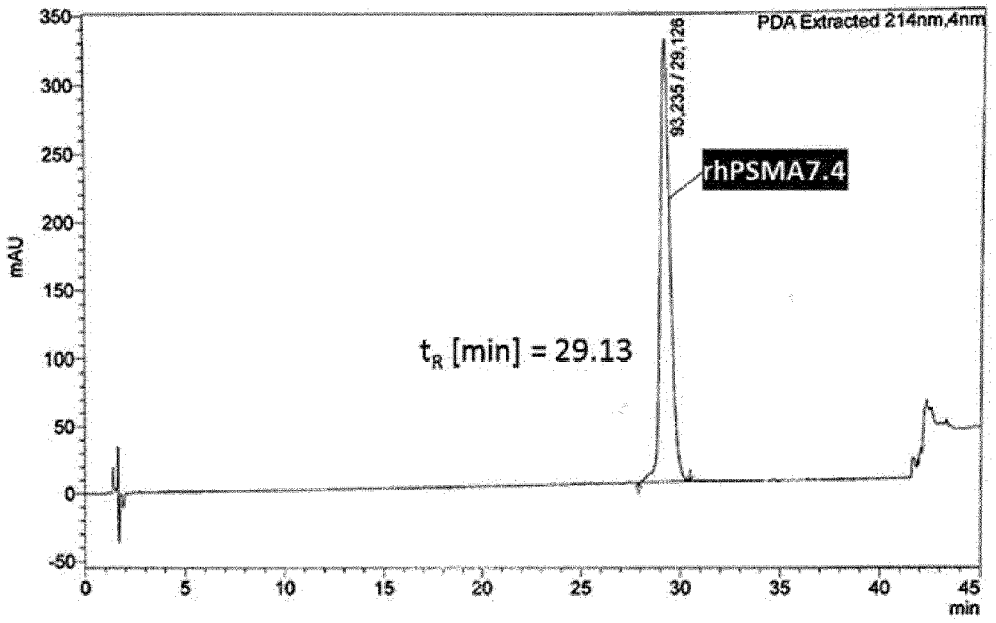
PDA Extracted 214nm,4nm
93,235 / 29,126
rhPSMA7.4
t_R [min] = 29.13
mAU
min

Fig. 5b

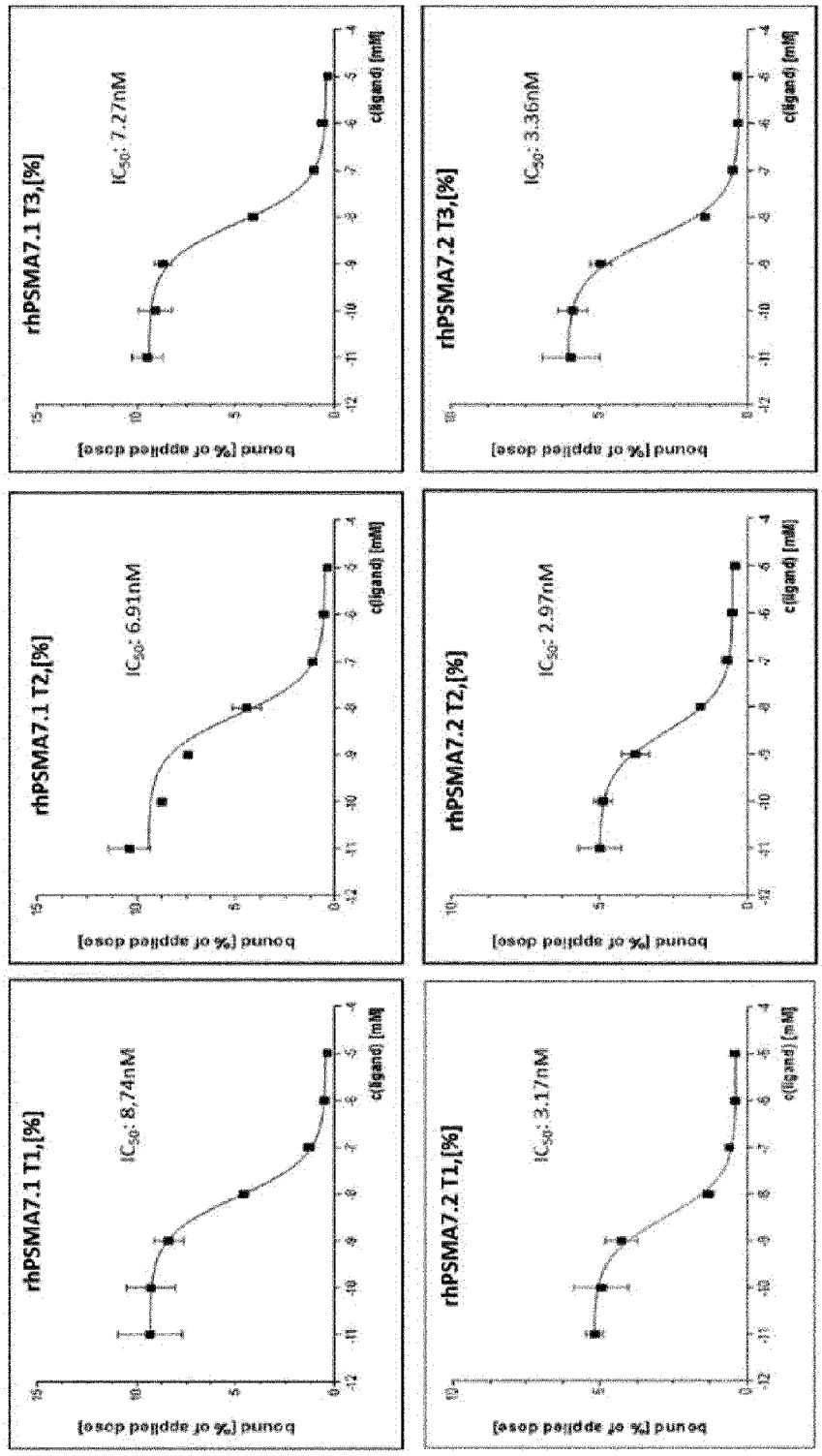
rhPSMA7.1 T1,[%]
IC50: 8.74nM
rhPSMA7.1 T2,[%]
IC50: 6.91nM
rhPSMA7.1 T3,[%]
IC50: 7.27nM
rhPSMA7.2 T1,[%]
IC50: 3.17nM
rhPSMA7.2 T2,[%]
IC50: 2.97nM
rhPSMA7.2 T3,[%]
IC50: 3.36nM
bound [% of applied dose]
c(ligand) [nM]

Fig. 6a

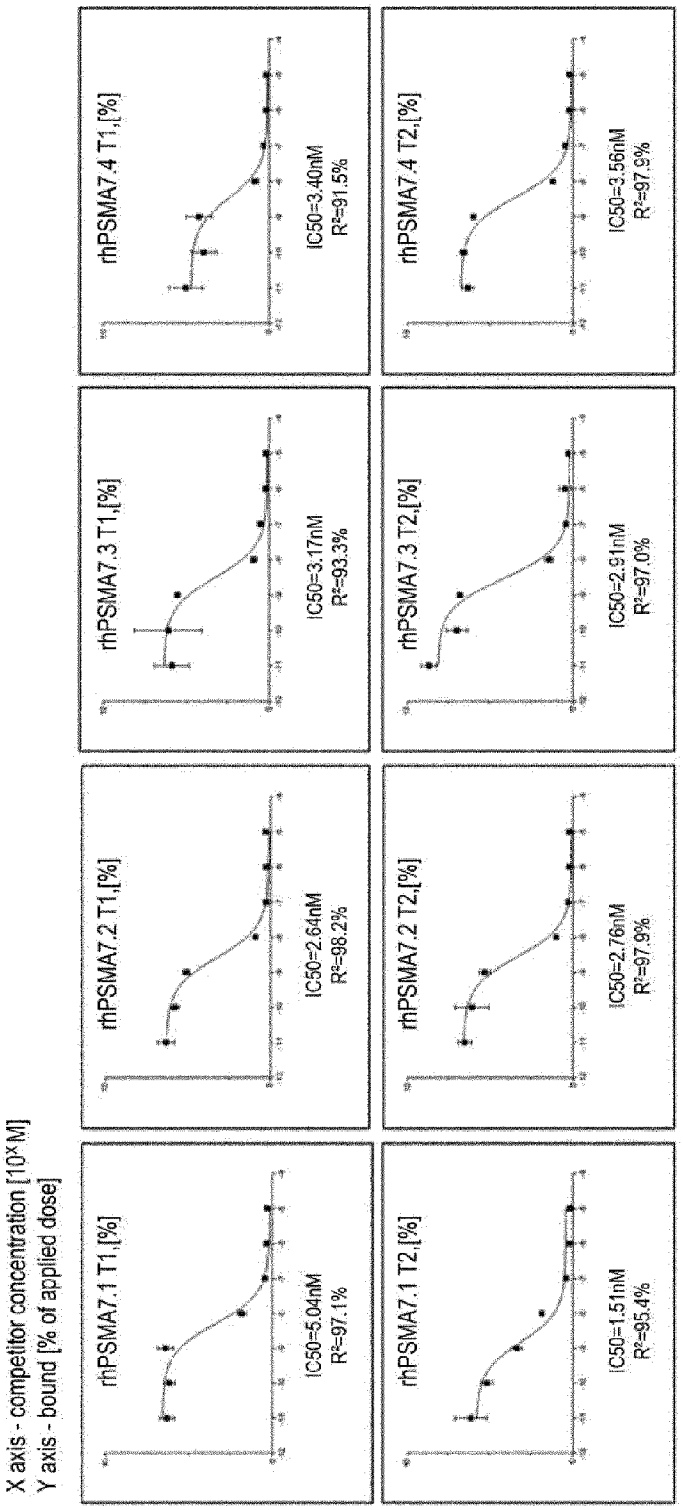
X axis - competitor concentration [10^x M]
Y axis - bound [% of applied dose]
rhPSMA7.1 T1,[%]
IC50=5.04nM
R²=97.1%
rhPSMA7.2 T1,[%]
IC50=2.64nM
R²=98.2%
rhPSMA7.3 T1,[%]
IC50=3.17nM
R²=93.3%
rhPSMA7.4 T1,[%]
IC50=3.40nM
R²=91.5%
rhPSMA7.1 T2,[%]
IC50=1.51nM
R²=95.4%
rhPSMA7.2 T2,[%]
IC50=2.76nM
R²=97.9%
rhPSMA7.3 T2,[%]
IC50=2.91nM
R²=97.0%
rhPSMA7.4 T2,[%]
IC50=3.56nM
R²=97.9%

Fig. 6b

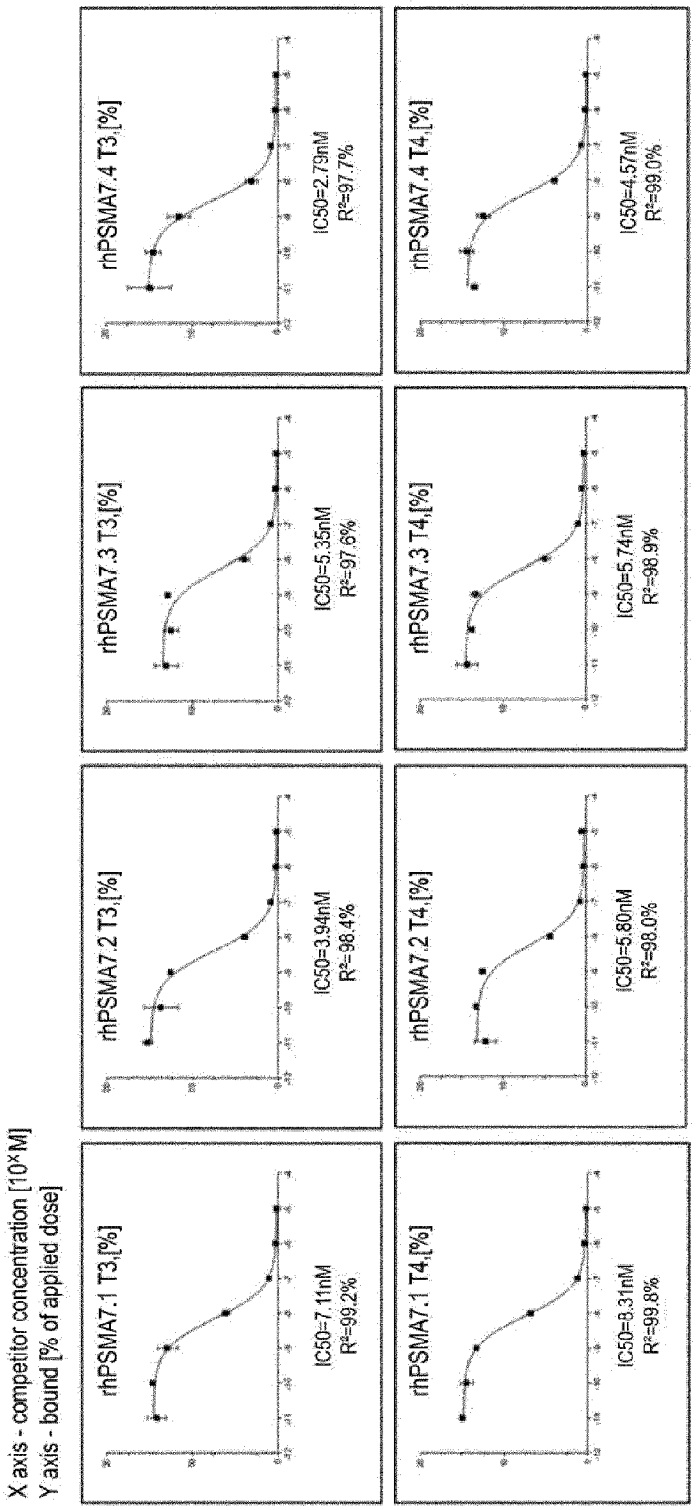

Fig. 6b (continued)

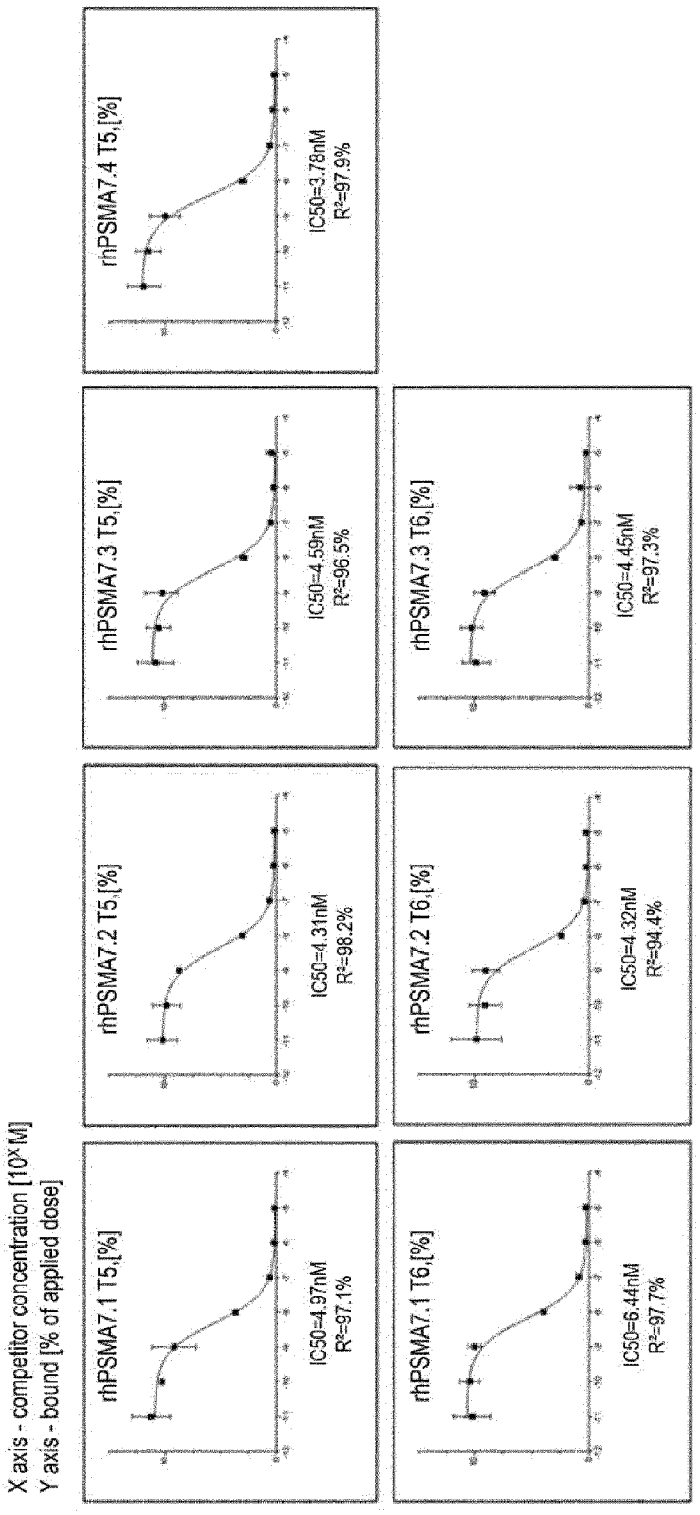

Fig. 6b (continued)

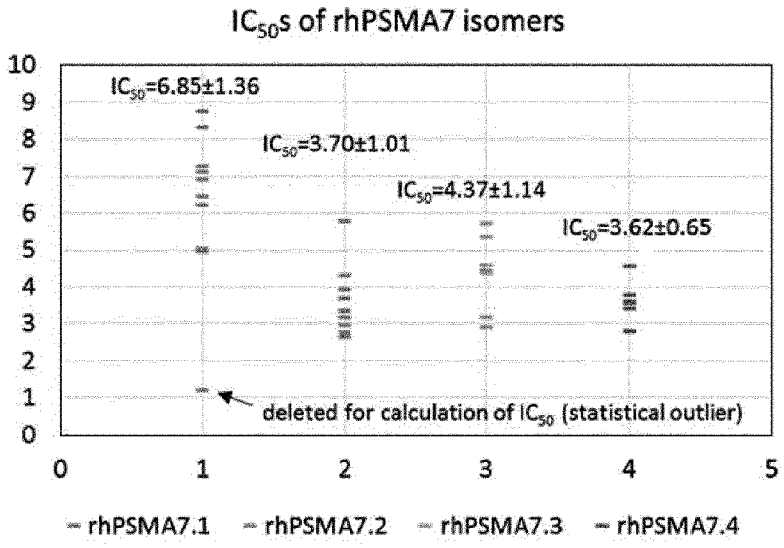
IC50s of rhPSMA7 isomers
IC50=6.85±1.36
IC50=3.70±1.01
IC50=4.37±1.14
IC50=3.62±0.65
deleted for calculation of IC50 (statistical outlier)
rhPSMA7.1
rhPSMA7.2
rhPSMA7.3
rhPSMA7.4

Fig. 7

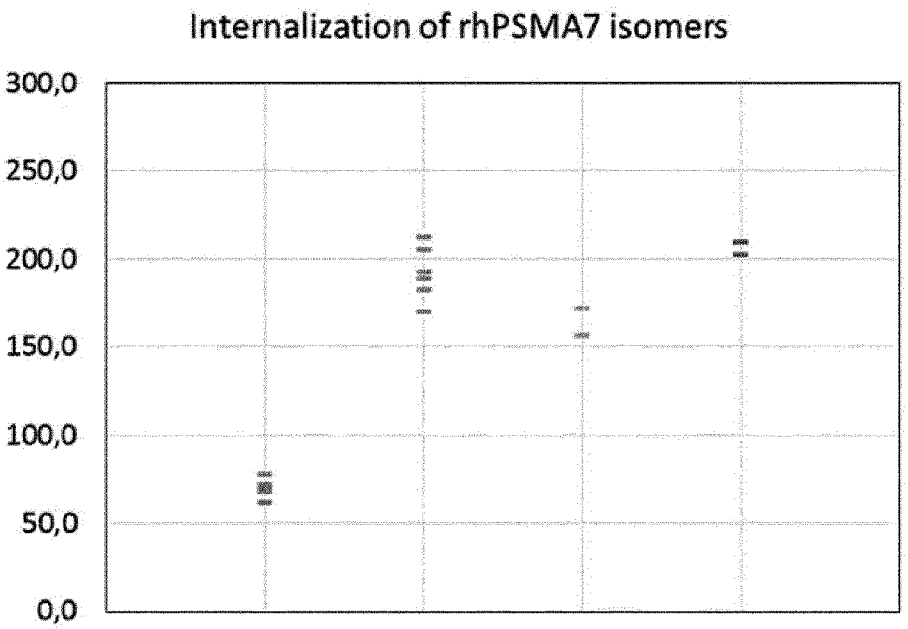
Internalization of rhPSMA7 isomers

Fig. 8

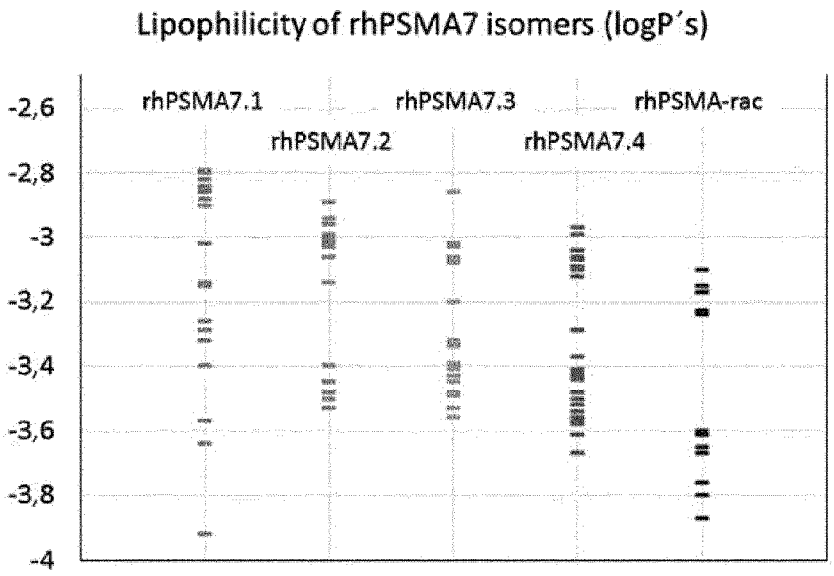
Lipophilicity of rhPSMA7 isomers (logP´s)
rhPSMA7.1
rhPSMA7.2
rhPSMA7.3
rhPSMA7.4
rhPSMA-rac
-2,6
-2,8
-3
-3,2
-3,4
-3,6
-3,8
-4

Fig. 9

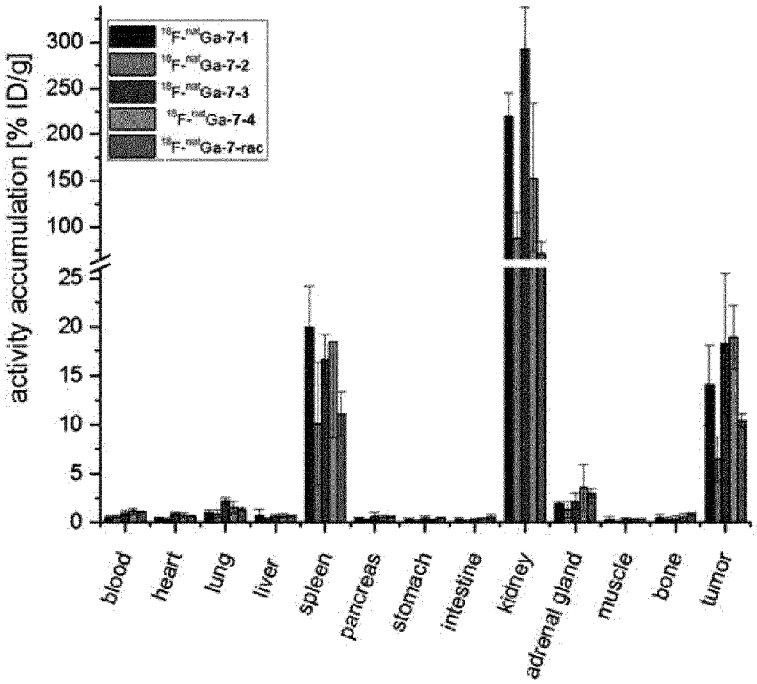
activity accumulation [% ID/g]
300
250
200
150
100
25
20
15
10
5
0
blood
heart
lung
liver
spleen
pancreas
stomach
intestine
kidney
adrenal gland
muscle
bone
tumor

Fig. 10

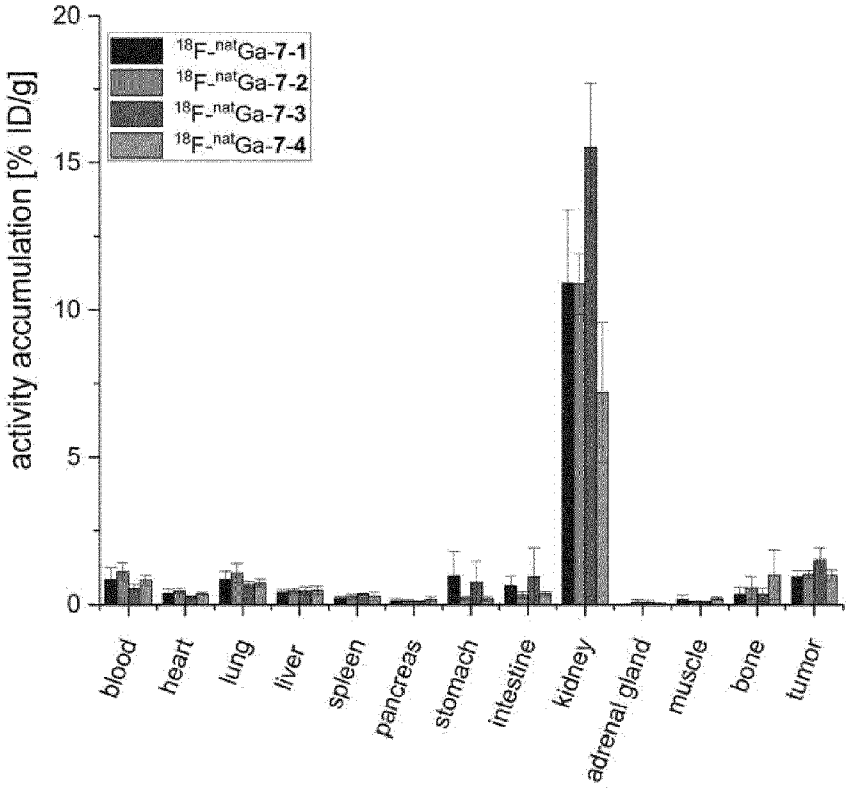
activity accumulation [% ID/g]
20
15
10
5
0
18F-natGa-7-1
18F-natGa-7-2
18F-natGa-7-3
18F-natGa-7-4
blood
heart
lung
liver
spleen
pancreas
stomach
intestine
kidney
adrenal gland
muscle
bone
tumor

Fig. 11

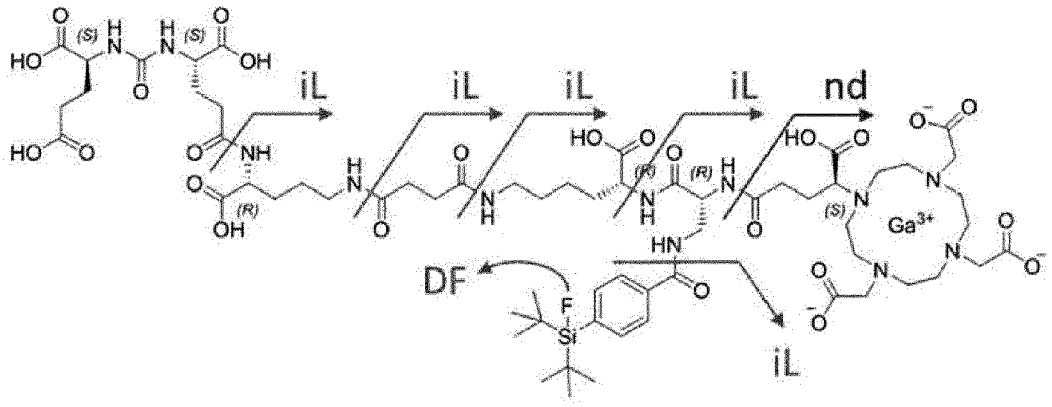
iL
iL
iL
iL
nd
DF
iL
Ga3+

Fig. 12

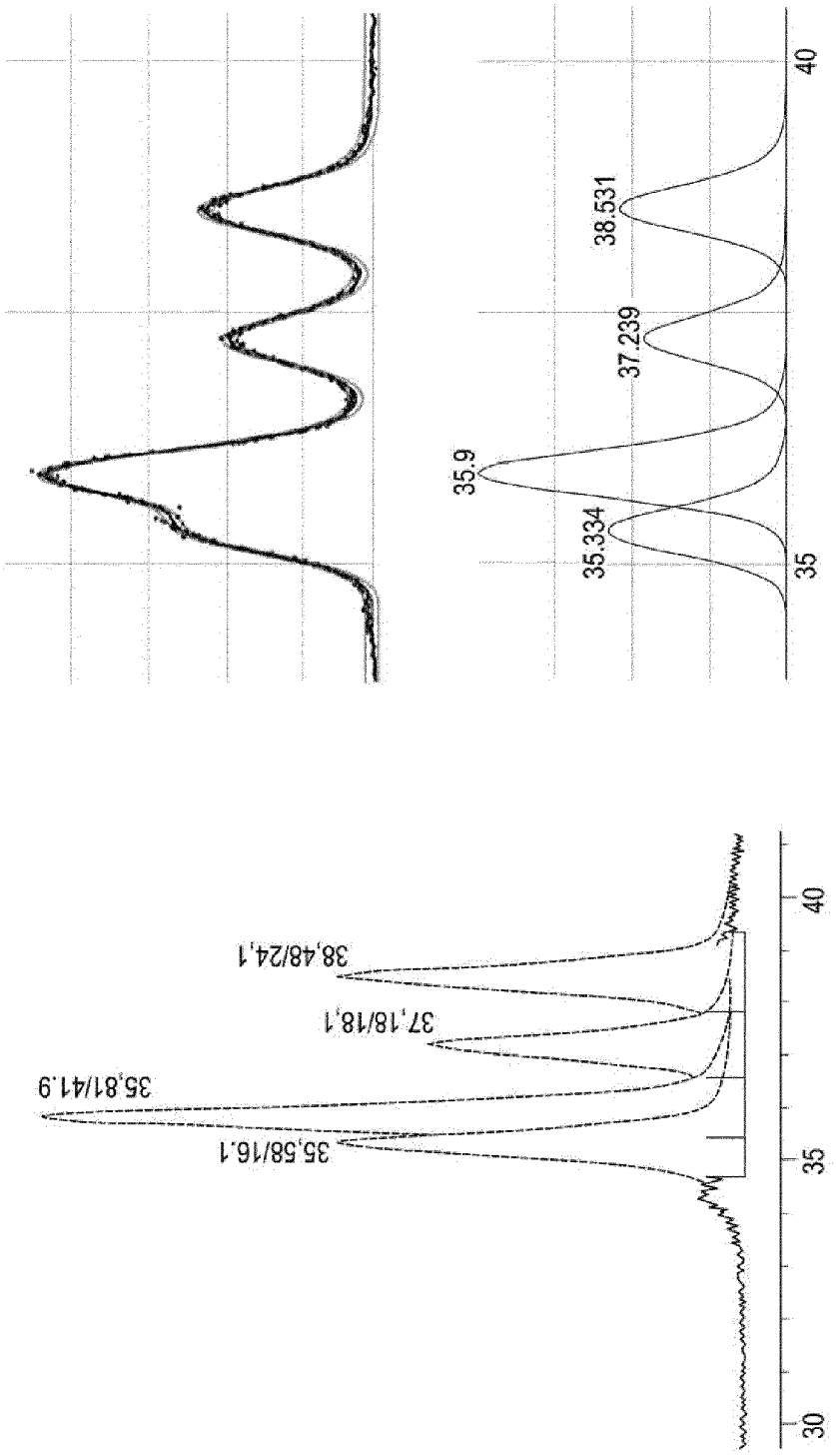
35.9
35.334
37.239
38.531
35
40
35,58/16,1
35,81/41,9
37,18/18,1
38,48/24,1
30
35
40

Fig.13

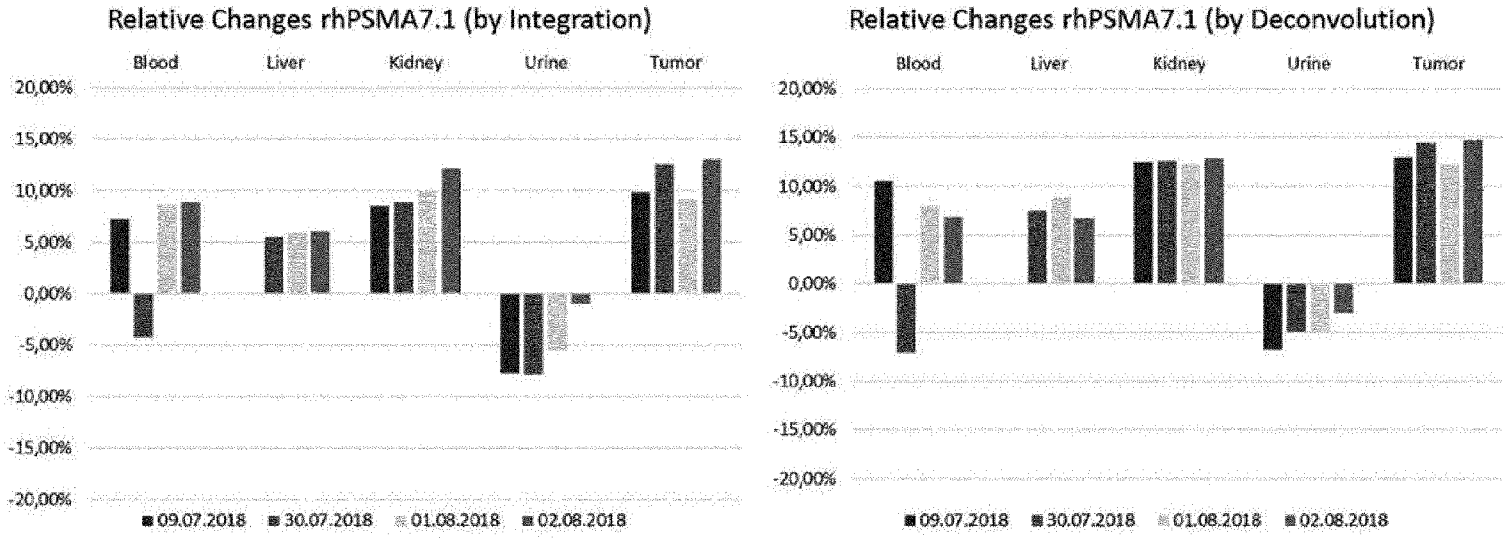

Fig. 14a

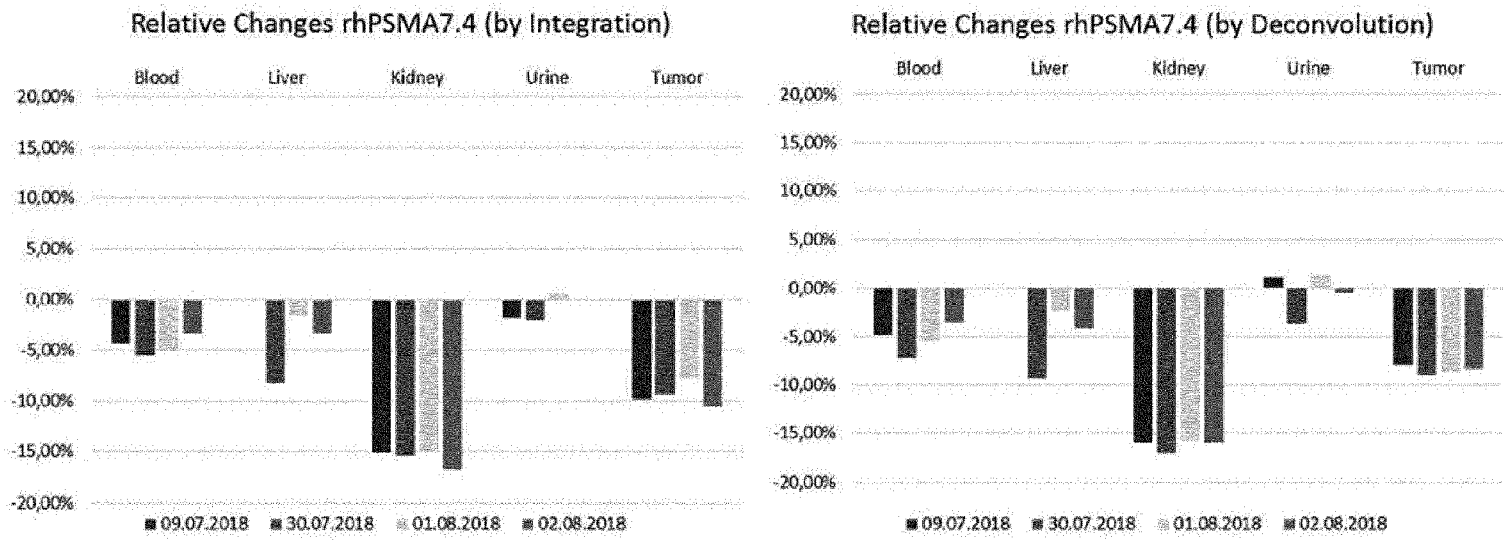

Fig. 14b

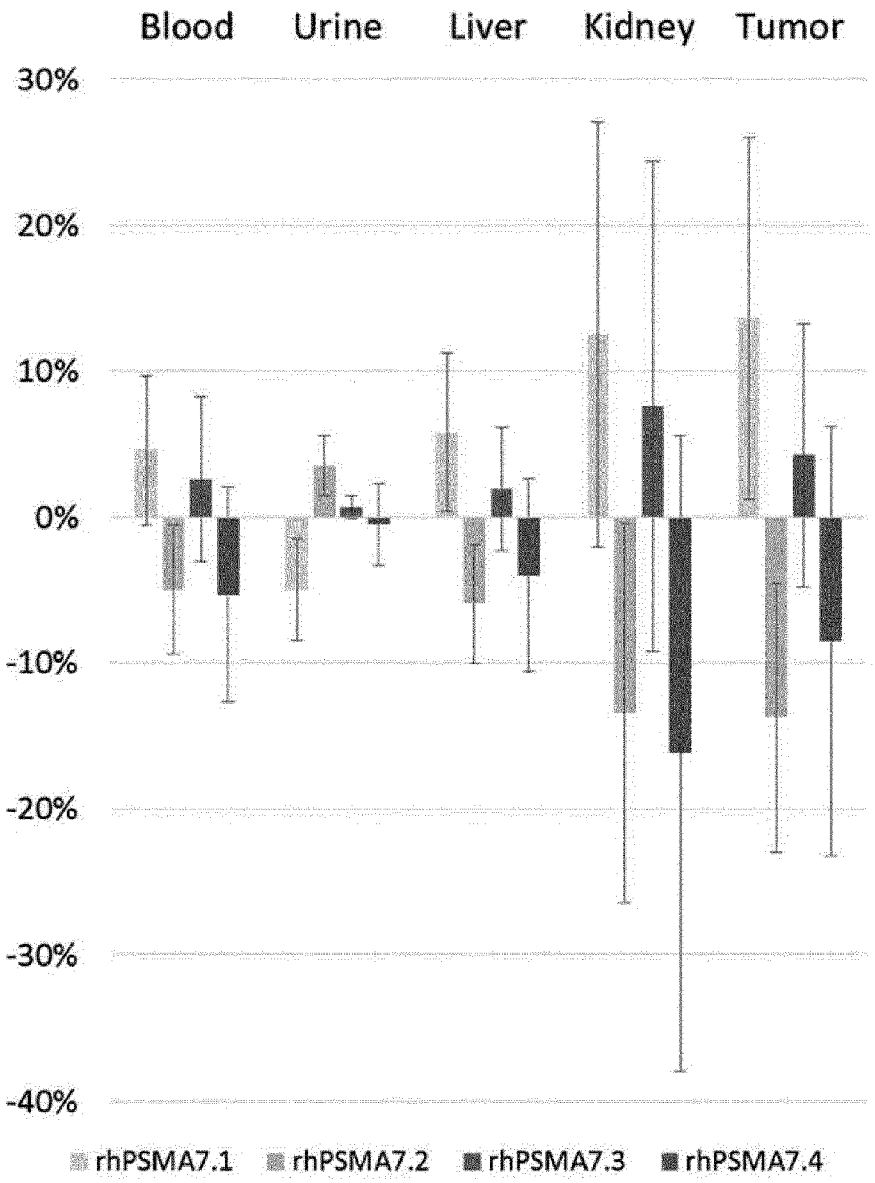
Blood
Urine
Liver
Kidney
Tumor
30%
20%
10%
0%
-10%
-20%
-30%
-40%
rhPSMA7.1
rhPSMA7.2
rhPSMA7.3
rhPSMA7.4

Fig. 15

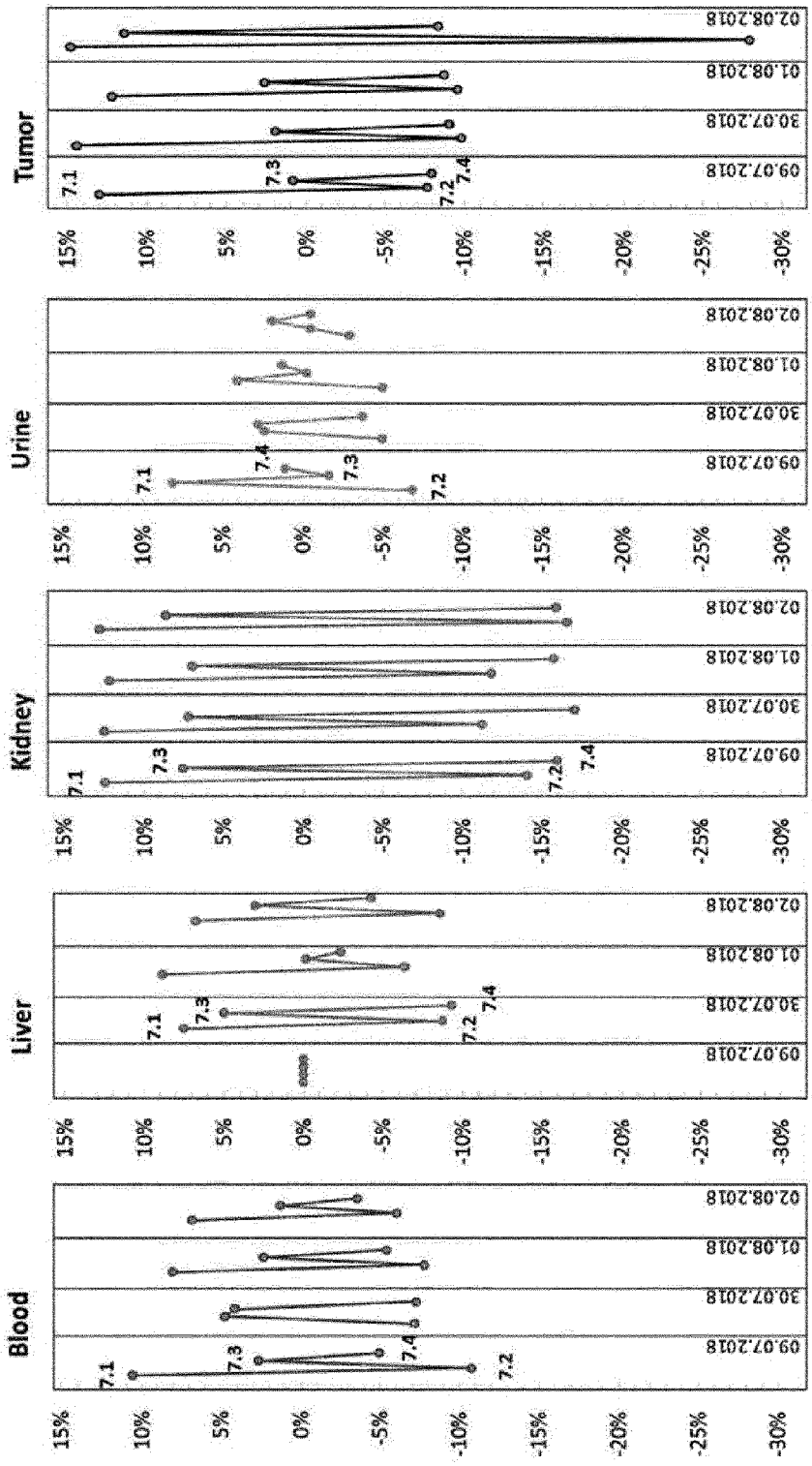
Blood
Liver
Kidney
Urine
Tumor
09.07.2018
30.07.2018
01.08.2018
02.08.2018
7.1
7.2
7.3
7.4
15%
10%
5%
0%
-5%
-10%
-15%
-20%
-25%
-30%

Fig. 16

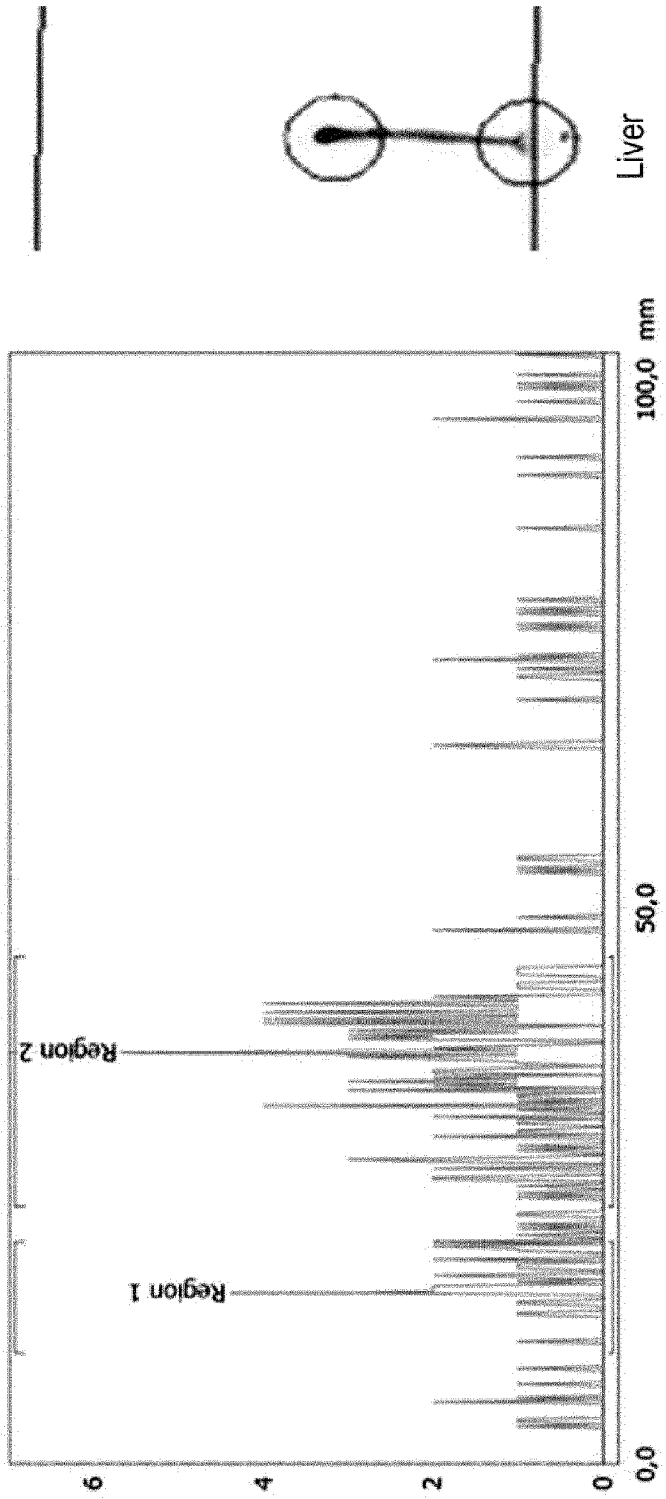

Fig. 17

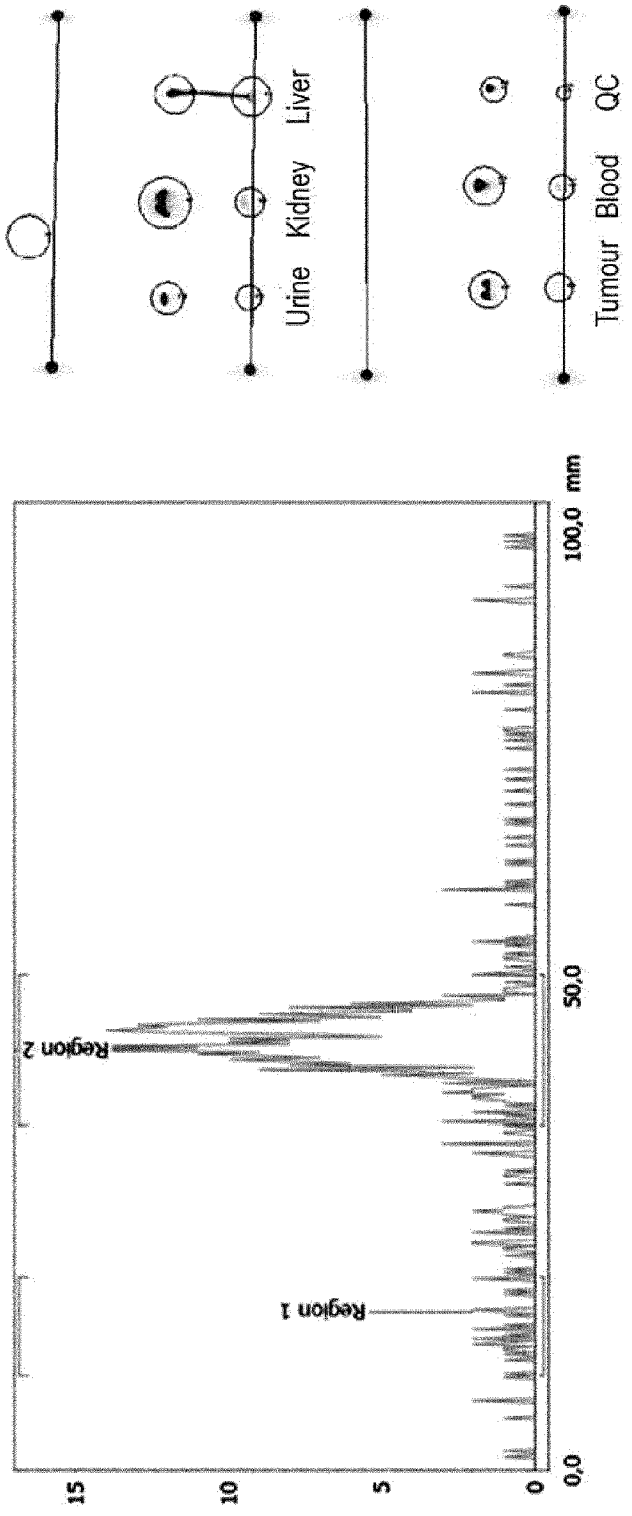
Urine
Kidney
Liver
Tumour
Blood
QC
Region 1
Region 2
0,0
50,0
100,0 mm
0
5
10
15

Fig. 18

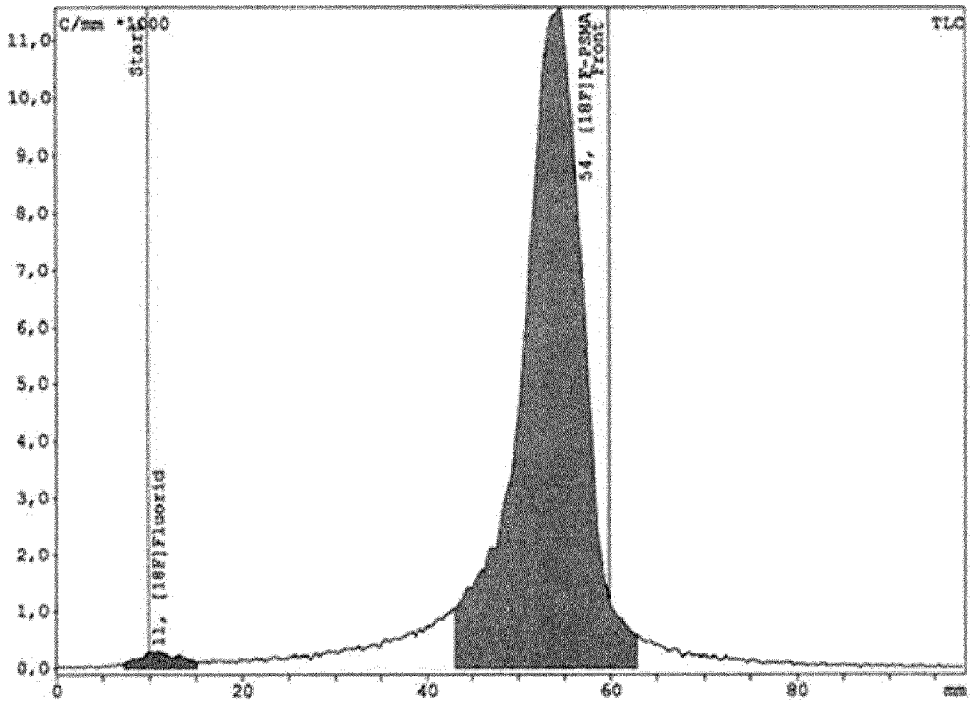

Integration TLC

Substance	RF	%Total %	Typ	Area Counts	%Area %	Instrument	Ret mm	S/N ratio
[18F]Fluoride	0,013	1,50	DD(	1614,00	1,74	TLC	10,52	6,3
[18F]F-PSMA	0,888	84,68	DD(	91023,00	98,26	TLC	54,27	167,5
Total in ROI (region of interest)				92637,00	100,00			
Total Area				107492,00				
Area (Total) RF				99480,00				

Fig. 19

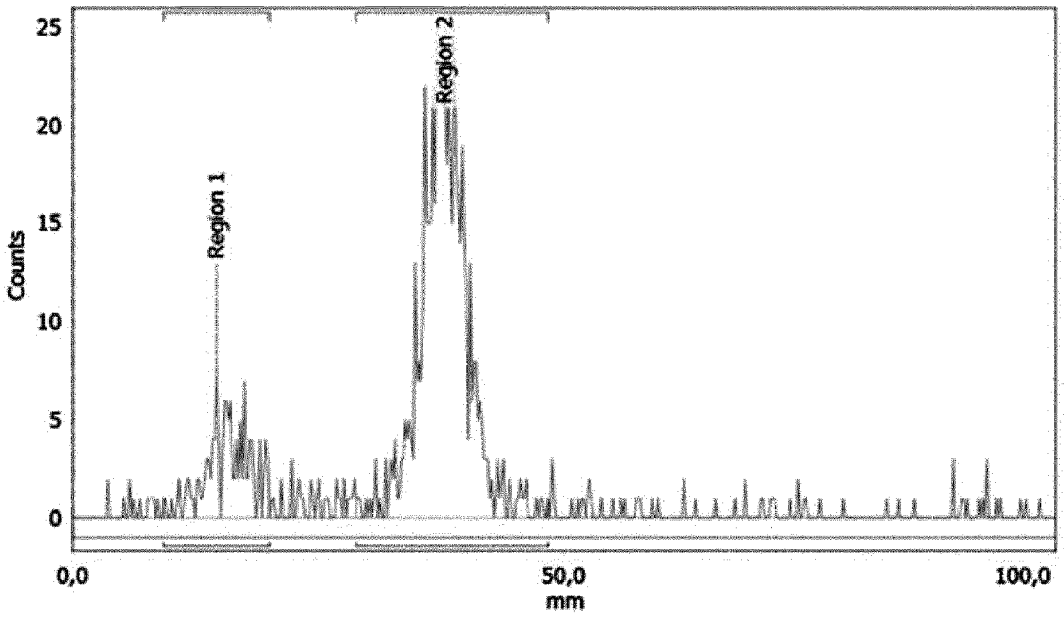

Regions: ^{18}F Detector: PMT

Name	Start (mm)	End (mm)	Retention (RF)	Area (Counts)	%ROI (%)	%Total (%)
Region 1	9,2	20,0	0,073	127	17,49	14,02
Region 2	28,8	48,4	0,189	599	82,51	66,11
2 Peaks				726	100,00	80,13

Fig. 20

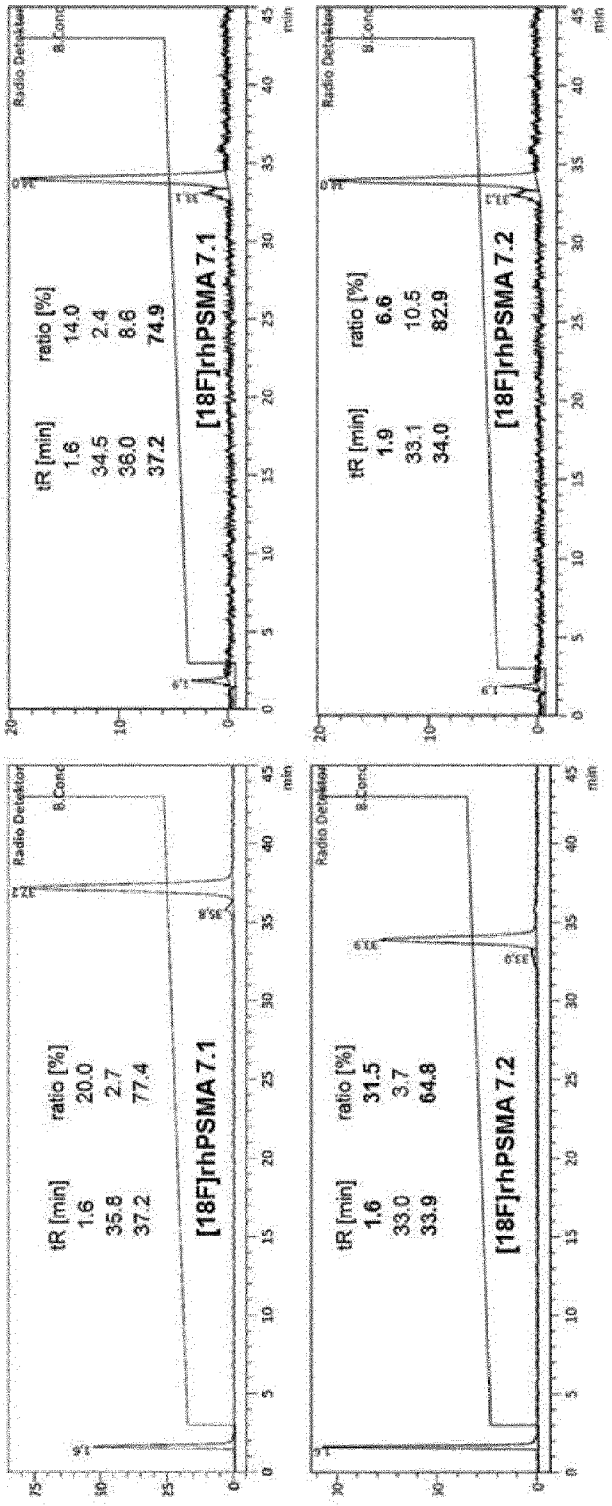
Radio Detektor
B.Conc
tR [min] ratio [%]
1.6 14.0
34.5 2.4
36.0 8.6
37.2 74.9
[18F]rhPSMA 7.1
tR [min] ratio [%]
1.9 6.6
33.1 10.5
34.0 82.9
[18F]rhPSMA 7.2
tR [min] ratio [%]
1.6 20.0
35.8 2.7
37.2 77.4
[18F]rhPSMA 7.1
tR [min] ratio [%]
1.6 31.5
33.0 3.7
33.9 64.8
[18F]rhPSMA 7.2
min

Fig. 21

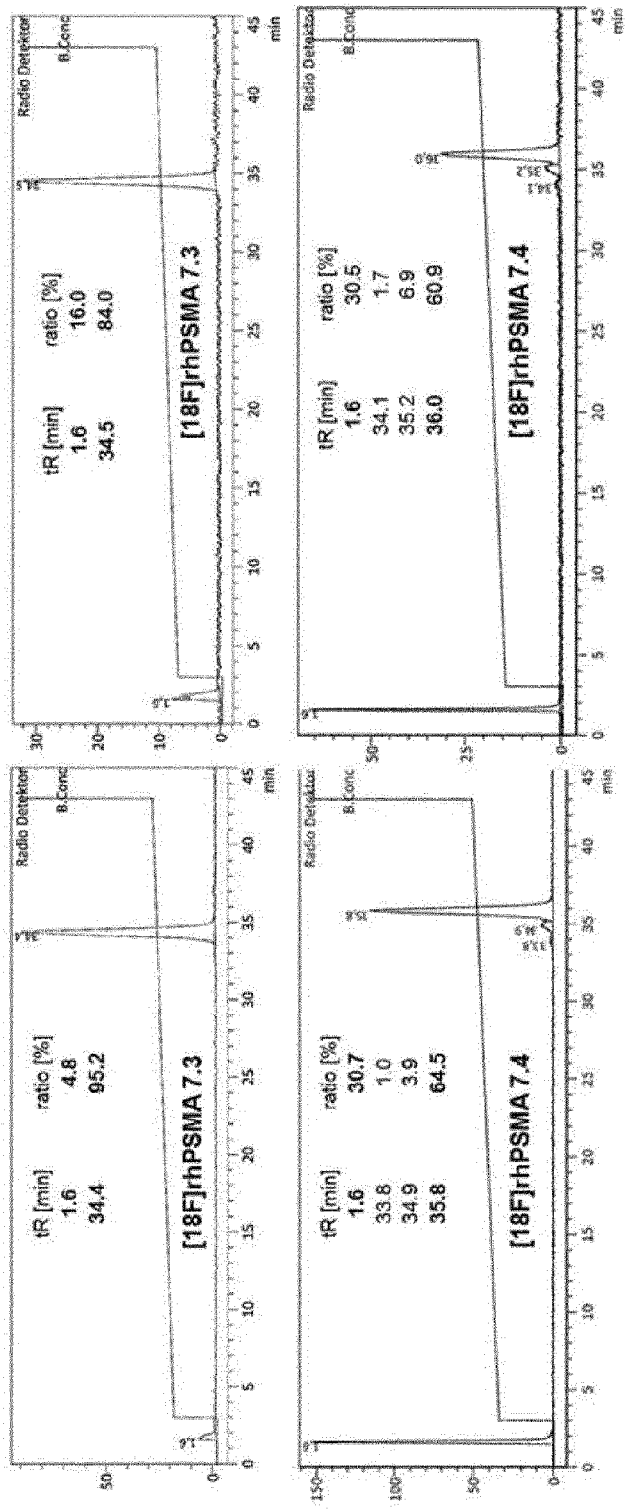

Fig. 21
(continued)

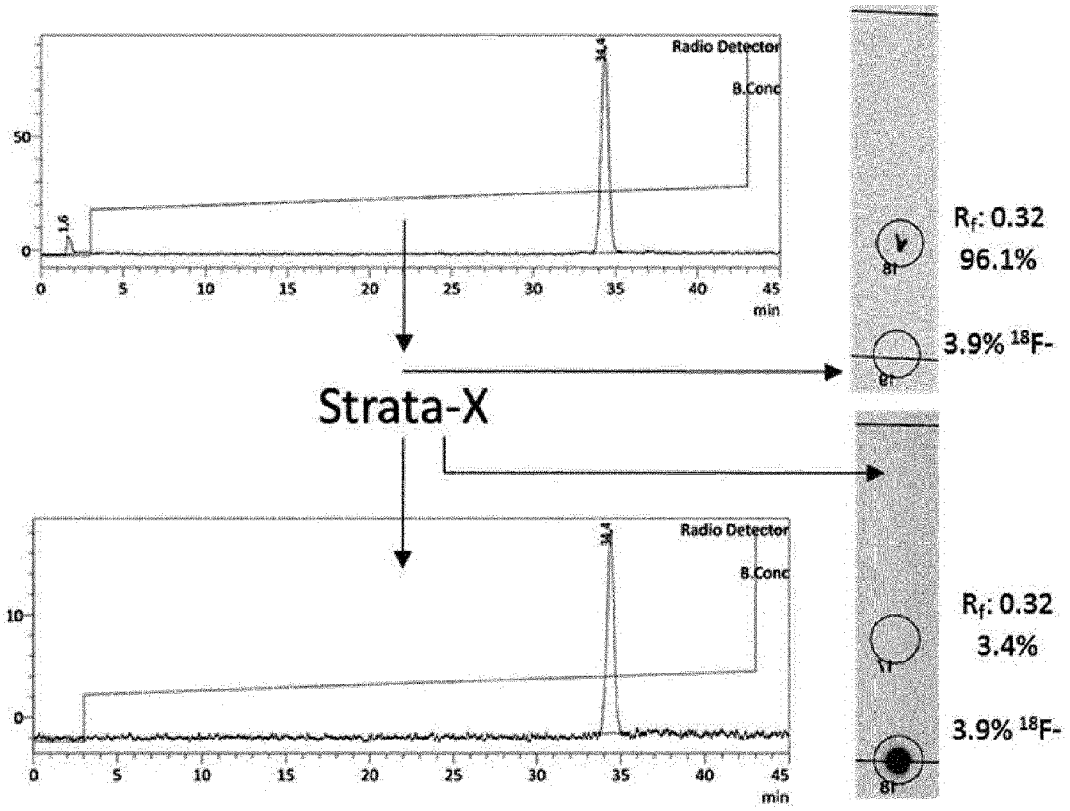
Radio Detector
B.Conc
34.4
1.6
50
0
0 5 10 15 20 25 30 35 40 45
min
Rf: 0.32
96.1%
3.9% 18F-
Strata-X
Radio Detector
B.Conc
34.4
10
0
0 5 10 15 20 25 30 35 40 45
min
Rf: 0.32
3.4%
3.9% 18F-

Fig. 22

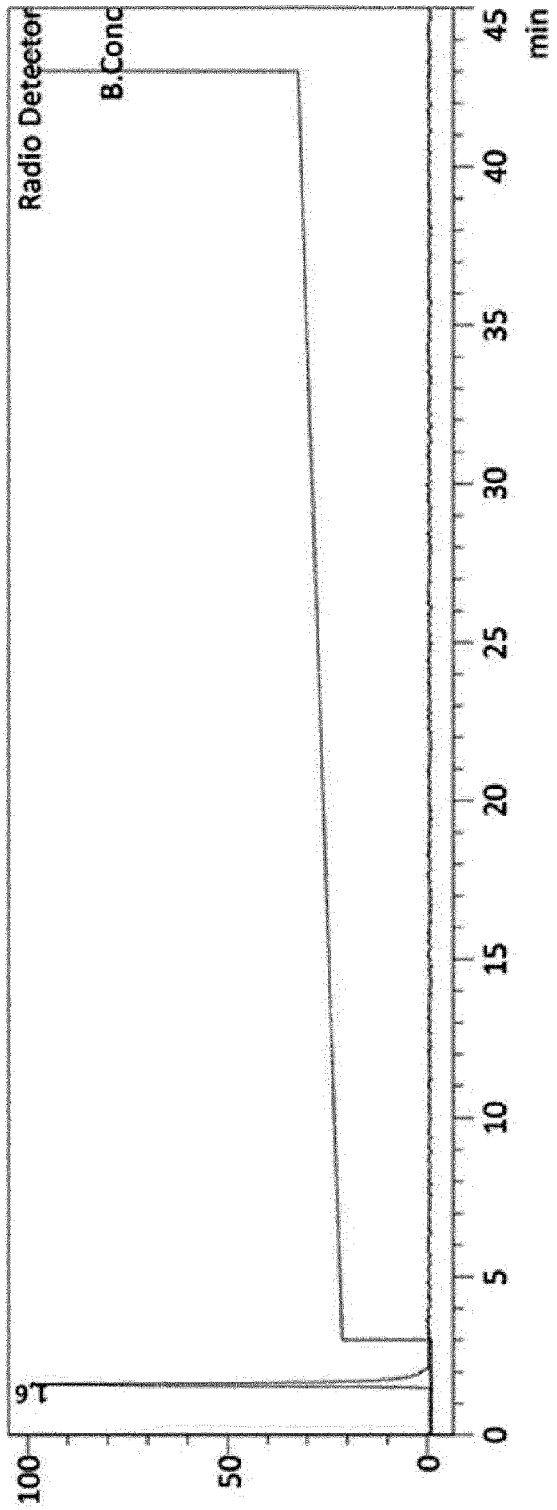

Fig. 23

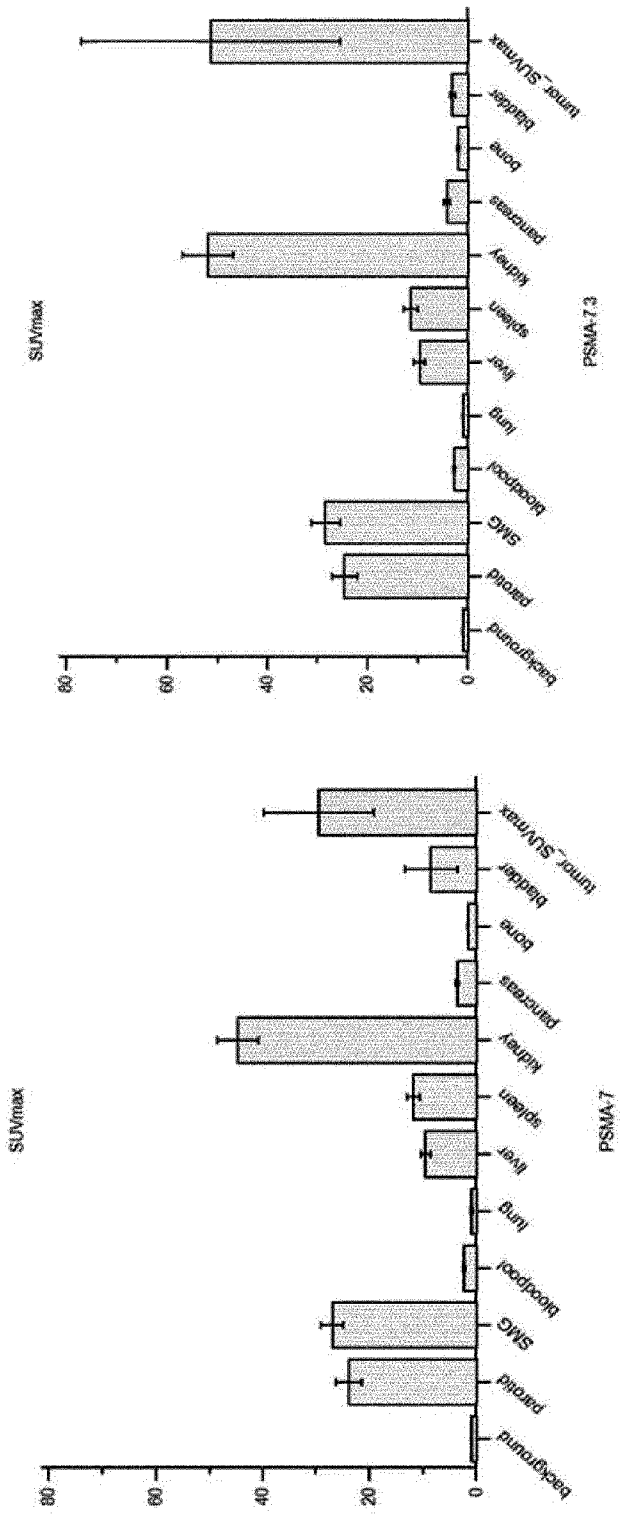
SUVmax
PSMA-7.3
tumor_SUVmax
bladder
bone
pancreas
kidney
spleen
liver
lung
bloodpool
SMG
parotid
background
SUVmax
PSMA-7
tumor_SUVmax
bladder
bone
pancreas
kidney
spleen
liver
lung
bloodpool
SMG
parotid
background

Fig. 24

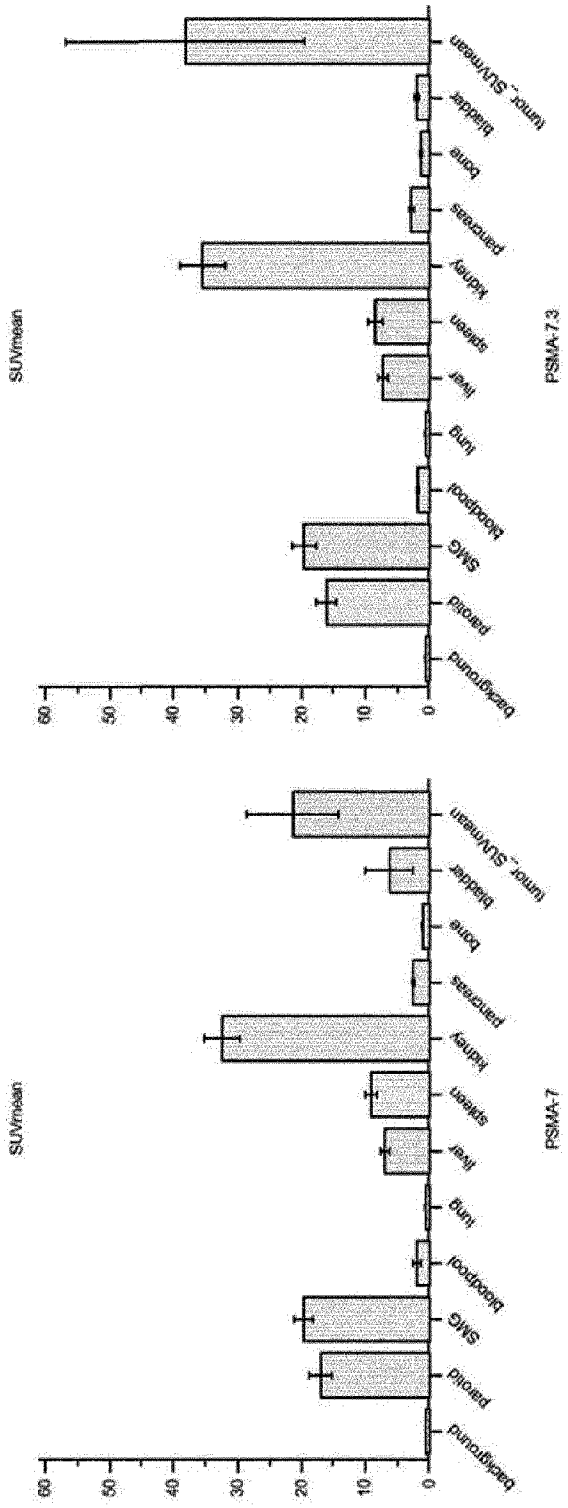
PSMA-7
PSMA-7 3
SUVmean
tumor_SUVmean
bladder
bone
pancreas
kidney
spleen
liver
lung
bloodpool
SMG
parotid
background
0
10
20
30
40
50
60

Fig. 25

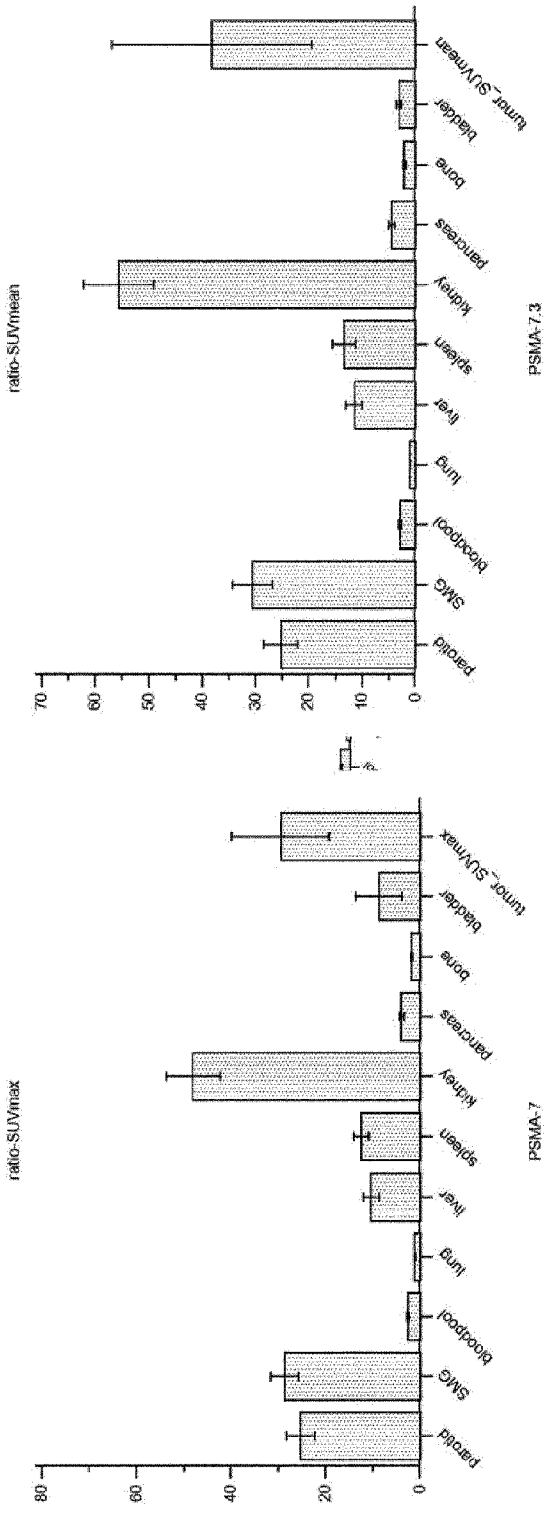
ratio-SUVmean
70
60
50
40
30
20
10
0
parotid
SMG
bloodpool
lung
liver
spleen
kidney
pancreas
bone
bladder
tumor_SUVmean
PSMA-7.3
ratio-SUVmax
80
60
40
20
0
parotid
SMG
bloodpool
lung
liver
spleen
kidney
pancreas
bone
bladder
tumor_SUVmax
PSMA-7

Fig. 26

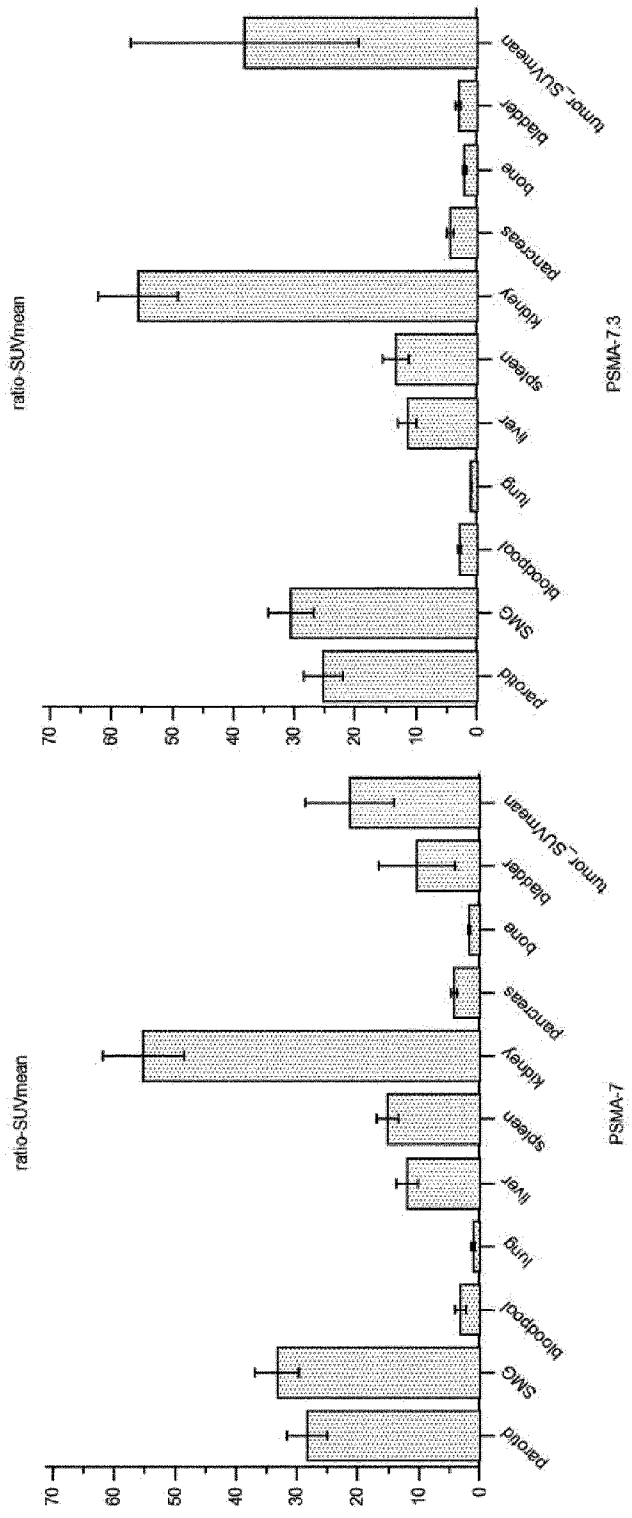
ratio-SUVmean
70
60
50
40
30
20
10
0
parotid
SMG
bloodpool
lung
liver
spleen
kidney
pancreas
bone
bladder
tumor_SUVmean
PSMA-7
PSMA-7.3

Fig. 27

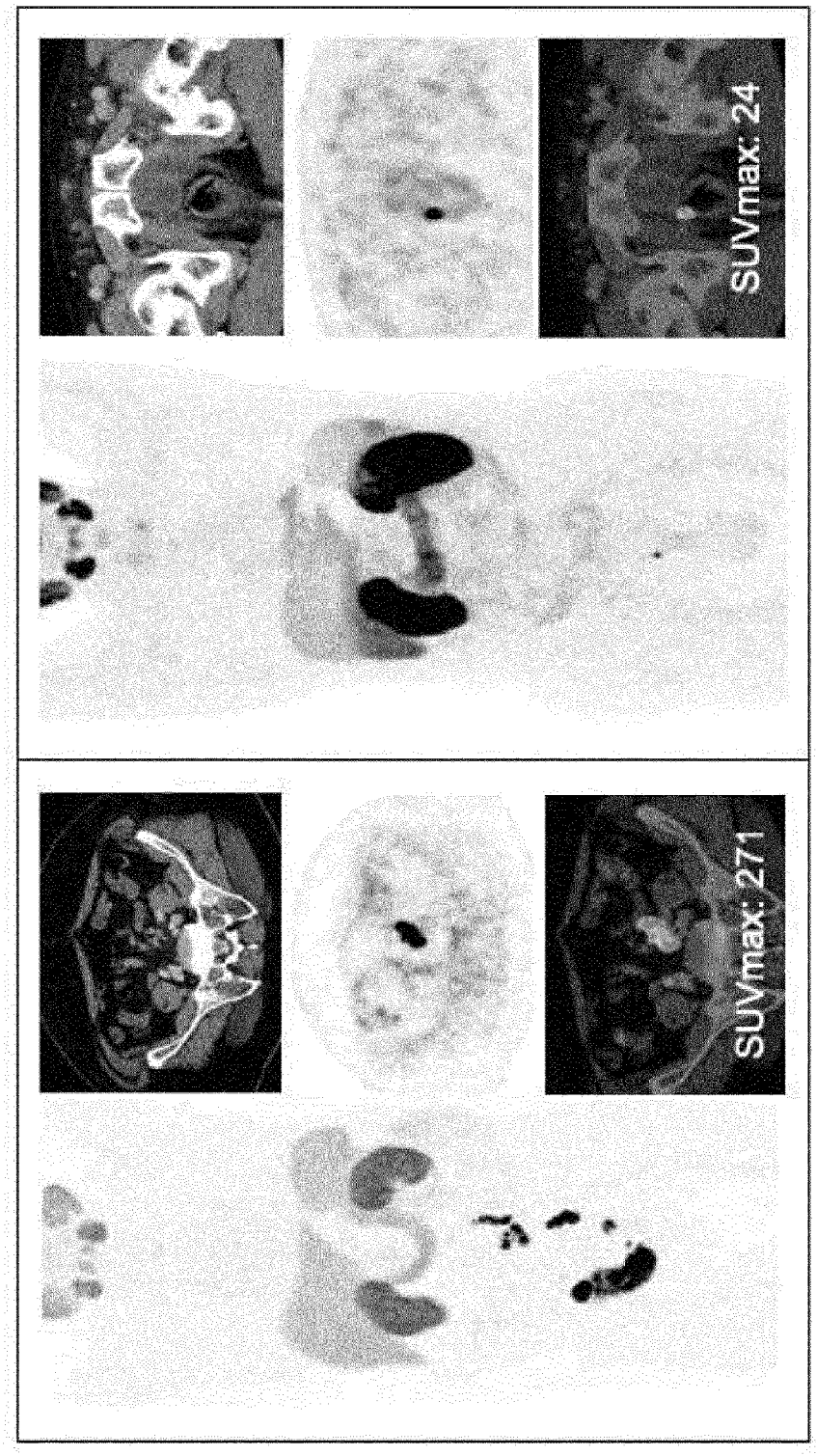

Fig. 28